

FY01 Supplemental Science and Performance Analyses,

Volume 1: Scientific Bases and Analyses
Part 1 of 2



U.S. Department of Energy
Office of Civilian Radioactive Waste Management

June 2001

QA: QA

TDR-MGR-MD-000007 REV 00

June 2001

FY 01 Supplemental Science and Performance Analyses

Volume 1:
Scientific Bases and Analyses

By
BSC

Prepared for:
U.S. Department of Energy
Yucca Mountain Site Characterization Office
P.O. Box 30307
North Las Vegas, Nevada 89036-0307

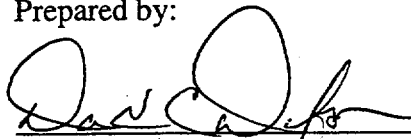
Prepared by:
Bechtel SAIC Company, LLC
1180 Town Center Drive
Las Vegas, Nevada 89144

Under Contract Number
DE-AC08-01RW12101

DISCLAIMER

This report was prepared as an account of work sponsored by an agency of the United States Government. Neither the United States Government nor any agency thereof, nor any of their employees, nor any of their contractors, subcontractors or their employees, makes any warranty, express or implied, or assumes any legal liability or responsibility for the accuracy, completeness, or any third party's use or the results of such use of any information, apparatus, product, or process disclosed, or represents that its use would not infringe privately owned rights. Reference herein to any specific commercial product, process, or service by trade name, trademark, manufacturer, or otherwise, does not necessarily constitute or imply its endorsement, recommendation, or favoring by the United States Government or any agency thereof or its contractors or subcontractors. The views and opinions of authors expressed herein do not necessarily state or reflect those of the United States Government or any agency thereof.

Prepared by:

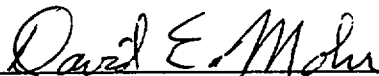


David Dobson et al
Lead Author

6-29-01

Date

Checked by:

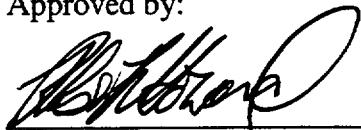


David Mohr et al
Lead Checker

6/30/01

Date

Approved by:



Robert L. Howard
Integration Manager, Science and Analysis Project

30 JUNE 01

Date

ACKNOWLEDGMENTS

The following individuals have contributed to the technical content and preparation of this document: Rob L. Howard, David Dobson, Ahmed M. Monib, Robert W. Andrews, Gudmundur S. Bodvarsson, Karen E. Jenni, Kevin Coppersmith, James A. Blink, Robert MacKinnon, James Nowak, Tammy Summers, Christine Stockman, Mike Gross, Aziz A. Eddebbarh, Anthony J. Smith, Kathy Gaither, Marco W. Lee, David Mohr, James L. Boone, Ardyth Simmons, Gerald Nieder-Westermann, Joe Wang, Andre Unger, MaryAnn Villavert, Stefan Finsterle, Yvonne Tsang, Eric L. Sonnenthal, Dale G. Wilder, Randolph L. Schreiner, Carol J. Passos, Thomas A. Buscheck, James Schreiber, Junghun Leem, Nicholas Francis, Steven Carlson, Alfred Reed, Chin-Fu Tsang, Donna Francis, Hang Yang, Amy R. Loch, Richard C. Metcalf, Darren M. Jolley, Dwayne Kicker, Joon H. Lee, Greg Gdowski, Kevin G. Mon, Bryan B. Bullard, Pasu Pasupathi, Gerald Gordon, John Case, Guy Ragan, Patrick V. Brady, Yueting Chen, Hui-Hai Liu, Patricia VanDillen, Ernest L. Hardin, Bruce Robinson, Stephanie Kuzio, Wesley Wu, Maryla Wasiolek, Jeffery J. Tappen, John F. Schmitt, Richard C. Quittmeyer, Robert Richards, John McCord, William Statham, Richard Aguilar, Greg Valentine, Randy Hedegaard, Jose Archuleta, Robert Youngs, James E. Houseworth, Nicolas Spycher, Paul Reimus, Stephen Blair, Thomas Corbett, Larry Saraka, Kurt R. Rautenstrauch, Bruce E. Kirstein, Thomas W. Doering, Stephen Alcorn, Bill Arnold, Melissa L. Hamner, Alycia N. Kahanaoi, Cecelia Sales, William R. Hunt, Norma E. Biggar, Robert Zimmerman, Amir S. Mobasheran, Terry Steinborn, Holly Miller, Daniel McGregor, Paul Kaplan, Denise R. Myers, Gordon Evans, Janette E. Lloyd, James T. Kam, David Stahl, Ming Zhu, Peter Persoff, Haywood Anderson, Steven H. Swenning, Patrick Rowe, Edward Kwicklis, Claudia Faunt, William Dudley, Pat Tucci, Rick Spengler, Zell Peterman, John Stuckless, Andy Wolfsberg, Arend Meijer, George Zyvoloski, Carl Axness, Leigh Lechel, Diane Hyer, Roger Eckhardt, Kayce Prince, Roseanne Perman, Rick Hyman, Ronda Hyman, Catherine A. Stewart, Sarah Fisher, Penny Meyer, Edna McKlveen, Jacqueline Krogh, Katie Miller, Crissy Cisneros, Linda Grisham, Vicky Obrad, Shelley Royall, Ann Mery, Nick Connerley, Daniel Brenton, Judy Gibes, Richard Danat, Cindy Dodson, Maria Therien, Valerie Kelly, Michelle Prater, Keenan K.N. Fong, Shirley Crawford, and Sandra Martin.

This work was supported by the Yucca Mountain Site Characterization Office as part of the Civilian Radioactive Waste Management Program, which is managed by the U.S. Department of Energy, Yucca Mountain Site Characterization Project.

INTENTIONALLY LEFT BLANK

CONTENTS

	Page
1. INTRODUCTION.....	1-1
1.1 BACKGROUND	1-1
1.2 GOALS AND SCOPE	1-3
1.2.1 Outline of Report.....	1-3
1.3 RATIONALE.....	1-4
1.3.1 Quantification of Uncertainties	1-4
1.3.2 Updated Scientific Bases and Analyses	1-7
1.3.3 Thermal Sensitivity Analyses.....	1-7
1.4 OVERVIEW OF ANALYSIS PROCESS.....	1-9
1.4.1 Quantifying Uncertainties	1-9
1.4.2 Updating Scientific Bases and Analyses	1-10
1.4.3 Evaluating a Range of Thermal Operating Modes.....	1-10
1.5 QUALITY ASSURANCE.....	1-11
1.6 COMPUTER SOFTWARE USAGE.....	1-12
2. METHODS AND APPROACH.....	2-1
2.1 QUANTIFICATION OF UNCERTAINTIES.....	2-1
2.1.1 Identification of Unquantified Uncertainties.....	2-1
2.1.2 Quantification of Unquantified Uncertainties	2-2
2.2 UPDATED SCIENTIFIC BASES AND ANALYSES	2-4
2.3 THERMAL SENSITIVITY ANALYSES.....	2-4
2.3.1 Design and Operating Mode Evolution.....	2-5
2.3.2 Range of Thermal Operating Modes and Bases.....	2-6
2.3.3 Operating Flexibility to Achieve a Range of Thermal Operating Modes	2-7
2.3.4 Assessing the Performance of a Range of Operating Modes	2-8
3. UNSATURATED ZONE FLOW.....	3-1
3.1 INTRODUCTION AND CONCEPTUAL BASIS.....	3-1
3.2 TREATMENT OF UNSATURATED FLOW-RELATED ISSUES IN ANALYSIS AND MODEL REPORTS	3-1
3.2.1 Climate	3-3
3.2.2 Net Infiltration.....	3-3
3.2.3 Lateral Flow in Paintbrush Nonwelded Hydrogeologic Unit.....	3-4
3.2.4 Three-Dimensional Unsaturated Zone Flow Field.....	3-5
3.2.5 Thermal-Hydrologic Effects on Unsaturated Mountain-Scale Flow.....	3-6
3.2.6 Thermal-Hydrologic-Chemical Effects on Mountain-Scale Flow and Geochemistry.....	3-7
3.2.7 Thermal-Hydrologic-Mechanical Effects on Mountain-Scale Flow	3-8
3.3 UNCERTAINTY ANALYSIS	3-9
3.3.1 Climate Model.....	3-9
3.3.2 Net Infiltration Model	3-16
3.3.3 Percolation Redistribution and Flow in the Paintbrush Nonwelded Hydrogeologic Units	3-21

CONTENTS (Continued)

	Page
3.3.4 Three Dimensional Flow Fields	3-29
3.3.5 Thermal-Hydrologic Effects on Unsaturated Zone Mountain-Scale Flow.....	3-45
3.3.6 Thermal-Hydrologic-Chemical Effects on Unsaturated Zone Flow and Geochemistry.....	3-56
3.3.7 Thermal-Hydrologic-Mechanical Effects on Mountain-Scale Permeability.....	3-67
4. SEEPAGE	4-1
4.1 INTRODUCTION AND CONCEPTUAL BASIS	4-1
4.2 TREATMENT OF SEEPAGE-RELATED ISSUES.....	4-4
4.2.1 Spatial and Temporal Flow Focusing.....	4-4
4.2.2 Capillary Barrier Effect.....	4-5
4.2.3 Excavation-Disturbed Zone.....	4-5
4.2.4 Drift Geometry and Drift Surface Effects	4-6
4.2.5 Ventilation and Evaporation-Condensation Effects	4-6
4.2.6 Thermal Effects and Coupled Processes	4-7
4.3 DISCUSSION OF KEY PROCESSES, MODELS, AND RELATED UNCERTAINTIES	4-7
4.3.1 General Seepage Evaluation and Estimation of Seepage-Relevant Parameters	4-7
4.3.2 Flow Focusing and Discrete Flow Paths in the Topopah Spring Welded Hydrogeologic Units.....	4-17
4.3.3 The Effect of Rock Bolts on Seepage.....	4-25
4.3.4 Drift Degradation	4-32
4.3.5 Thermal Effects on Seepage.....	4-40
4.3.6 Thermal-Hydrologic-Chemical Effects on Seepage and Potential Seepage Chemistry	4-59
4.3.7 Thermal-Hydrologic-Mechanical Effects on Seepage	4-80
5. EFFECTS OF DECAY HEAT ON IN-DRIFT THERMAL-HYDROLOGIC CONDITIONS.....	5-1
5.1 INTRODUCTION AND CONCEPTUAL BASIS.....	5-1
5.2 REVIEW OF TOTAL SYSTEM PERFORMANCE ASSESSMENT-SITE RECOMMENDATION TREATMENT	5-5
5.2.1 Overview of Total System Performance Assessment-Site Recommendation Thermal-Hydrologic Results.....	5-8
5.2.2 Information Generated by the Multiscale Thermal-Hydrologic Model	5-9
5.3 UNCERTAINTY ANALYSES	5-9
5.3.1 Multiscale Model of In-Drift Thermal-Hydrologic Conditions	5-11
5.3.2 Ventilation and Convection Modeling of In-Drift Thermal-Hydrologic Conditions	5-54
5.3.3 Quantification of Uncertainty Using Analogues	5-91

CONTENTS (Continued)

	Page	
5.4	SUMMARY AND PARAMETERS PROVIDED TO TOTAL SYSTEM PERFORMANCE ASSESSMENT	5-92
5.4.1	Higher-Temperature Operating Mode Base Case Results	5-93
5.4.2	Lower Temperature Operating Mode Base Case Results.....	5-95
5.4.3	Process Model Results.....	5-98
6.	IN-DRIFT PHYSICAL AND CHEMICAL ENVIRONMENT.....	6-1
6.1	INTRODUCTION	6-1
6.2	REVIEW OF TOTAL SYSTEM PERFORMANCE ASSESSMENT-SITE RECOMMENDATION TREATMENT	6-3
6.2.1	Composition of Liquid and Gas Entering the Drifts (Thermal-Hydrologic-Chemical).....	6-3
6.2.2	Effects of Engineered Materials on the Chemical Environment.....	6-4
6.2.3	Evolution of In-Drift Chemistry.....	6-5
6.2.4	Environment on the Surfaces of the Drip Shield and Waste Package.....	6-6
6.2.5	Rockfall	6-6
6.3	UNCERTAINTY ANALYSES AND NEW MODELS	6-7
6.3.1	Composition of Liquid and Gas Entering the Drifts	6-7
6.3.2	Effects of Engineered Materials on the Chemical Environment.....	6-34
6.3.3	Evolution of the In-Drift Chemical Environment	6-38
6.3.4	Rockfall	6-66
6.4	SUMMARY AND PARAMETERS PROVIDED TO TOTAL SYSTEM PERFORMANCE ASSESSMENT	6-74
6.4.1	Summary of the Total System Performance Assessment Implementation of the Precipitates/Salts Model Lookup Tables	6-74
6.4.2	Summary of the Total System Performance Assessment Implementation of the Acid Neutralizing Capacity/pH Mixing Model	6-74
6.4.3	Incoming Liquid and Gas Abstraction Results.....	6-75
6.4.4	Integration of Water Chemistries in the Drift between Total System Performance Assessment Model Components	6-75
6.4.5	In-Drift Salts and Precipitates Modeling.....	6-76
6.4.6	In-Package Chemistry Models	6-76
6.4.7	Integration of Model Inputs.....	6-77
7.	WASTE PACKAGE AND DRIP SHIELD DEGRADATION	7-1
7.1	INTRODUCTION	7-1
7.2	OVERVIEW OF TOTAL SYSTEM PERFORMANCE ASSESSMENT-SITE RECOMMENDATION REV 00 TREATMENT	7-3
7.2.1	Thermal Aging	7-5
7.2.2	General Corrosion	7-6
7.2.3	Localized Corrosion	7-8
7.2.4	Microbiologically Influenced Corrosion	7-8
7.2.5	Stress Corrosion Cracking.....	7-9
7.2.6	Hydrogen-Induced Cracking	7-12

CONTENTS (Continued)

	Page
7.3	UNCERTAINTY ANALYSES 7-12
7.3.1	Environments on Waste Package and Drip Shield Surfaces 7-13
7.3.2	Aging and Phase Stability 7-21
7.3.3	Stress Corrosion Cracking 7-27
7.3.4	Long-Term Passive Film Stability of Alloy 22 7-42
7.3.5	General Corrosion of Alloy 22 7-52
7.3.6	Early Waste Package Failure: Improper Heat Treatment 7-61
7.3.7	Other Issues 7-64
7.4	EFFECT OF UPDATED UNCERTAINTIES ON WASTE PACKAGE PERFORMANCE 7-69
7.4.1	Baseline Waste Package Degradation Model 7-69
7.4.2	Effect of Updated and/or Quantified Uncertainties in the Stress Corrosion Cracking Model Parameters 7-73
7.4.3	Effect of Updated and Quantified Uncertainties in Alloy 22 General Corrosion 7-75
7.4.4	Recommended Nominal Case for Volume 2 7-81
7.5	SUMMARY AND PARAMETERS PROVIDED TO TOTAL SYSTEM PERFORMANCE ASSESSMENT 7-82
8.	WATER DIVERSION PERFORMANCE 8-1
8.1	INTRODUCTION 8-1
8.2	REVIEW OF TOTAL SYSTEM PERFORMANCE ASSESSMENT-SITE RECOMMENDATION TREATMENT 8-4
8.3	UNCERTAINTY ANALYSES 8-8
8.3.1	Evaporation of Seepage 8-8
8.3.2	Drip Shield Condensation Model 8-11
8.3.3	Drip Shield and Waste Package Flux Models 8-16
8.3.4	Bathtub versus Flow Through Waste Package Model 8-22
8.4	SUMMARY AND ABSTRACTION PROVIDED TO TOTAL SYSTEM PERFORMANCE ASSESSMENT 8-26
9.	WASTE FORM DEGRADATION AND RADIONUCLIDE RELEASE 9-1
9.1	INTRODUCTION AND CONCEPTUAL BASIS 9-1
9.2	REVIEW OF SCIENCE AND ENGINEERING REPORT TREATMENT 9-3
9.3	UNCERTAINTY ANALYSES 9-4
9.3.1	In-Package Chemistry 9-5
9.3.2	Dissolved Concentrations 9-9
9.3.3	Cladding 9-18
9.3.4	Colloids 9-23
9.4	SUMMARY AND PARAMETERS PROVIDED TO TOTAL SYSTEM PERFORMANCE ASSESSMENT FOR SENSITIVITY CALCULATIONS 9-27
9.4.1	In-Package Chemistry 9-27
9.4.2	Dissolved Concentrations 9-28
9.4.3	Cladding 9-28
9.4.4	Colloids 9-28

CONTENTS (Continued)

	Page
10. ENGINEERED BARRIER SYSTEM TRANSPORT	10-1
10.1 INTRODUCTION AND CONCEPTUAL MODEL	10-1
10.1.1 Alternative Conceptual Models	10-4
10.2 REVIEW OF TOTAL SYSTEM PERFORMANCE ASSESSMENT-SITE RECOMMENDATION TREATMENT	10-4
10.2.1 Transport Abstraction	10-5
10.2.2 Conservatism and Uncertainties in the Transport Abstraction	10-7
10.3 UNCERTAINTY ANALYSES	10-8
10.3.1 Diffusion in the Waste Package	10-8
10.3.2 Diffusion from the Waste Package to the Invert	10-38
10.3.3 Diffusion Through the Invert	10-45
10.3.4 Sorption of Dissolved Radionuclides	10-50
10.3.5 Colloidal Transport of Radionuclides	10-62
10.3.6 Microbial Sorption and Transport	10-69
10.4 SUMMARY AND PARAMETERS PROVIDED TO TOTAL SYSTEM PERFORMANCE ASSESSMENT	10-73
10.4.1 Diffusion in the Waste Package	10-73
10.4.2 Transport from the Waste Package to the Invert	10-77
10.4.3 Diffusion Through the Invert	10-77
10.4.4 Sorption of Dissolved Radionuclides	10-78
10.4.5 Colloidal Transport of Radionuclides	10-78
10.4.6 Microbial Sorption and Transport	10-79
11. RADIONUCLIDE TRANSPORT IN THE UNSATURATED ZONE	11-1
11.1 INTRODUCTION	11-1
11.2 TREATMENT OF UNSATURATED ZONE TRANSPORT ISSUES	11-2
11.2.1 Transport in the Drift Shadow	11-2
11.2.2 Matrix Block Discretization Effects	11-4
11.2.3 Calculation Methods for Radionuclide Transport	11-5
11.2.4 Effects of Potential Repository Footprint on Three-Dimensional Transport	11-5
11.2.5 Effects of Thermally-Driven Coupled Processes	11-6
11.3 INTRODUCTION TO UNCERTAINTY ANALYSIS	11-6
11.3.1 Transport in the Drift Shadow Zone	11-6
11.3.2 Matrix Block Discretization and Its Effects on Unsaturated Zone Flow and Transport Simulations	11-19
11.3.3 A Comparison of Radionuclide Transport Calculation Methods	11-26
11.3.4 Effects of Change in Potential Repository Footprint on Three-Dimensional Transport Simulation	11-37
11.3.5 Effects of Thermally-Driven Coupled Processes on Radionuclide Transport in the Unsaturated Zone	11-47

CONTENTS (Continued)

	Page
12. RADIONUCLIDE TRANSPORT IN THE SATURATED ZONE	12-1
12.1 INTRODUCTION	12-1
12.2 REVIEW OF TOTAL SYSTEM PERFORMANCE ASSESSMENT-SITE RECOMMENDATION TREATMENT OF RADIONUCLIDE FLOW AND TRANSPORT IN THE SATURATED ZONE.....	12-6
12.2.1 Hydrogeologic Characterization.....	12-7
12.2.2 Site-Scale Calibrated Flow Field.....	12-8
12.2.3 Abstraction of Saturated Zone Flow and Radionuclide Transport Modeling for Total System Performance Assessment Analyses.....	12-9
12.3 ACCOUNT FOR UNCERTAINTIES AND VARIABILITIES IN PARAMETER VALUES.....	12-11
12.3.1 Groundwater Flow Modeling	12-11
12.3.2 Transport Modeling.....	12-20
12.4 MULTIPLE LINES OF EVIDENCE	12-45
12.4.1 Evidence for Flow Paths Based on Groundwater Hydrochemical and Isotopic Data.....	12-47
12.4.2 Uranium Mill Tailing Analogues	12-48
12.4.3 Preliminary Tracer Testing Results in the Alluvial Testing Complex	12-50
12.4.4 Electric Power Research Institute Flow and Transport Modeling.....	12-52
12.4.5 Transport Studies on Blocks of Intact Tuff	12-53
12.4.6 Analogue Studies.....	12-54
12.4.7 Yucca Mountain Self-Analogue Using Uranium Isotopes.....	12-60
12.4.8 U.S. Nuclear Regulatory Commission Flow and Transport Studies	12-62
12.5 SENSITIVITY ANALYSIS	12-62
12.5.1 Unquantified Uncertainty Sensitivity Analysis for Supplemental Science and Performance Analyses.....	12-62
12.5.2 Additional Sensitivity Analyses for Supplemental Science and Performance Assessment.....	12-63
12.5.3 Evaluation of Boundary to the Accessible Environment	12-67
13. BIOSPHERE	13-1
13.1 INTRODUCTION AND CONCEPTUAL BASIS.....	13-1
13.2 REVIEW OF TOTAL SYSTEM PERFORMANCE ASSESSMENT-SITE RECOMMENDATION TREATMENT AND UPDATES	13-4
13.2.1 Relationship of Biosphere Model Tasks.....	13-4
13.2.2 Identification of Unquantified Uncertainties in the Biosphere Model	13-13
13.2.3 Multiple Lines of Evidence in the Biosphere Model.....	13-17
13.3 UNCERTAINTY, SENSITIVITY, AND NEW ANALYSES	13-18
13.3.1 Receptor of Interest	13-20
13.3.2 Comparison of Dose Assessment Methods	13-33
13.3.3 Uncertainties Associated with Radionuclide Removal from Soil by Leaching	13-36
13.3.4 Uncertainties from Fixed Parameter Values.....	13-39
13.3.5 Uncertainty in Annual Groundwater Usage	13-41

CONTENTS (Continued)

	Page
13.3.6 Inhalation Exposure Pathway.....	13-44
13.3.7 Impacts of Climate Change on Biosphere Dose Conversion Factors.....	13-48
13.3.8 Biosphere Dose Conversion Factors for Selenium-79 and Neptunium-237.....	13-51
13.4 SUMMARY AND PARAMETERS PROVIDED TO TOTAL SYSTEM PERFORMANCE ASSESSMENT	13-54
13.4.1 Biosphere Dose Conversion Factors for the Groundwater Release Exposure Scenario.....	13-54
13.4.2 Groundwater Withdrawal by the Farming Community.....	13-58
13.4.3 Biosphere Dose Conversion Factors for the Volcanic Eruption Exposure Scenarios	13-59
14. VOLCANIC AND SEISMIC DISRUPTIVE EVENTS	14-1
14.1 INTRODUCTION	14-1
14.1.1 Repository Operating Mode Alternatives and Disruptive Events Analyses	14-3
14.1.2 Section Organization	14-3
14.2 PREVIOUS TREATMENT OF DISRUPTIVE EVENTS.....	14-4
14.2.1 Volcanism.....	14-5
14.2.2 Seismic Events	14-5
14.3 VOLCANISM.....	14-6
14.3.1 Treatment of Uncertainty for Volcanism	14-6
14.3.2 Lines of Evidence Supporting the Volcanism Conceptual Model	14-11
14.3.3 New Work for Volcanism Analysis	14-11
14.4 SEISMIC EVENTS: TREATMENT OF UNCERTAINTIES, MULTIPLE LINES OF EVIDENCE, AND NEW WORK.....	14-25
14.4.1 Treatment of Uncertainties.....	14-26
14.4.2 Multiple Lines of Evidence: Implications for Vibratory Ground Motion from Studies of Precarious Rocks at Yucca Mountain.....	14-27
14.4.3 Analyses to Evaluate Seismic Events and Their Effects.....	14-28
14.5 SUMMARY OF DISRUPTIVE EVENTS ANALYSES AND PARAMETERS PROVIDED TO TOTAL SYSTEM PERFORMANCE ASSESSMENT.....	14-29
15. SUMMARY AND CONCLUSIONS.....	15-1
15.1 KEY ATTRIBUTE: LIMITED WATER ENTERING EMPLACEMENT DRIFTS.....	15-3
15.2 KEY ATTRIBUTE: LONG-LIVED WASTE PACKAGE AND DRIP SHIELD.....	15-7
15.3 KEY ATTRIBUTE: LIMITED RELEASE OF RADIONUCLIDES FROM THE ENGINEERED BARRIERS.....	15-15
15.4 KEY ATTRIBUTE: DELAY AND DILUTION OF RADIONUCLIDE CONCENTRATIONS BY THE NATURAL BARRIERS	15-19
15.5 KEY ATTRIBUTE: LOW MEAN ANNUAL DOSE CONSIDERING POTENTIALLY DISRUPTIVE EVENTS.....	15-24

CONTENTS (Continued)

	Page
16. REFERENCES	16-1
16.1 DOCUMENTS CITED.....	16-1
16.2 CODES, STANDARDS, REGULATIONS, AND PROCEDURES.....	16-81
16.3 SOURCE DATA.....	16-82
APPENDIX A - HUMAN INTRUSION SCENARIO.....	A-1

FIGURES

		Page
1-1.	Components of the SSPA Analyses, showing the Relationship of Major Processes Expected to Occur in the Mountain and the Potential Repository System	1F-1
2.3.4-1.	Variables Affecting the Thermal Performance of the Potential Repository.....	2F-1
2.3.4-2.	Footprints Used in the Thermal Hydrology Analyses.....	2F-2
3.1-1.	Main Models Included in the Unsaturated Zone Process Model Report, Interrelations among them, and Connections to Total System Performance Assessment	3F-1
3.3.2-1.	Net Infiltration for the Glacial Stage 6/16-Climate Scenario.....	3F-2
3.3.3-1.	Present-Day Mean Net Infiltration	3F-3
3.3.3-2.	Chloride-Based, Present-Day Mean Net Infiltration.....	3F-4
3.3.3-3.	Vertical Capillary Pressure Gradients	3F-5
3.3.3-4.	Effect of Net Infiltration on Percentage of Flow-Through Faults and Fault Zones	3F-6
3.3.3-5.	Effect of Horizontal Permeability on the Modeled Concentrations of Chloride in the Exploratory Studies Facility.....	3F-7
3.3.3-6.	Effect of Horizontal Permeability on the Modeled Concentrations of Chloride in the Enhanced Characterization Repository Block.....	3F-8
3.3.3-7.	Effect of Horizontal Permeability on the Modeled Concentrations of Chloride in Borehole UZ#16.....	3F-9
3.3.4-1.	Plan View of Total System Performance Assessment Grid and Net Infiltration Distributed Over the Domain of the Unsaturated Zone Model.....	3F-10
3.3.4-2.	Simulated Percolation Flux at the Repository Horizon for the Flow-Through Perched Water Conceptual Model.....	3F-11
3.3.4-3.	Simulated Percolation Flux at the Water Table for the Flow-Through Perched Water Conceptual Model.....	3F-12
3.3.4-4.	Plan View of Net Infiltration Distributed Over the Domain of the Three-Dimensional Unsaturated Zone Total System Performance Assessment Model.....	3F-13
3.3.4-5.	Simulated Percolation Flux at the Potential Repository Horizon under the Full-Glacial, Mean #2 Infiltration Scenario	3F-14
3.3.4-6.	Simulated Percolation Flux at the Water Table under the Full-Glacial, Mean #2 Infiltration Scenario.....	3F-15
3.3.4-7.	Plan View of Unsaturated Zone Model Domains and Potential Repository Layouts	3F-16
3.3.4-8.	Data Locations Characterizing Repository Host Horizon Layers	3F-17
3.3.4-9.	Spatial Distribution of Lithostratigraphic Layers Constituting the Potential Repository Host Horizon.....	3F-18
3.3.4-10.	Section Cut through the Potential Repository Siting Volume.....	3F-19
3.3.4-11.	PTn Occurrence and Thickness	3F-20
3.3.4-12.	Pre-faulted, Pre-eroded Thickness Map of CHn (Ttpv1–Tactb).....	3F-21
3.3.4-13.	Plan View of the Extended Model Grid	3F-22

FIGURES (Continued)

		Page
3.3.4-13a.	Approximate Vertical Distance Between Emplacement Drifts and a Water Table 120 m Above the Current Elevation.....	3F-23
3.3.4-14.	Spatial Distribution of Infiltration in the Domain of the Extended Model	3F-24
3.3.4-15.	Simulated Percolation Flux at the Potential Repository Horizon Using the Extended Model Grid	3F-25
3.3.4-16.	Simulated Percolation Flux at the Water Table Using the Extended Model Grid.....	3F-26
3.3.5-1.	Location of the Potential Repository and Layering of the Hydrogeologic Units	3F-27
3.3.5-2.	Temperature Distribution for the Potential Higher-Temperature Repository at 1,000 Years.....	3F-28
3.3.5-3.	Temperature Distribution for the Potential Lower-Temperature Repository at 1,000 Years.....	3F-29
3.3.5-4.	Temperature Profiles at the Center of the Potential Higher-Temperature Repository, No Lithophysal Cavities	3F-30
3.3.5-5.	Temperature Profiles at the Center of the Potential Higher-Temperature Repository, with Lithophysal Cavities	3F-31
3.3.5-6.	Temperature Profiles at the Center of the Potential Lower-Temperature Repository, No Lithophysal Cavities	3F-32
3.3.5-7.	Fracture Liquid Saturation for the Potential Higher-Temperature Repository at 1,000 Years	3F-33
3.3.5-8.	Fracture Liquid-Flux Profiles at Center of the Potential Repository for the Higher-Temperature Repository, No Lithophysal Cavities	3F-34
3.3.5-9.	Fracture Liquid Flux Profiles at the Center of the Potential Higher-Temperature Repository, With Lithophysal Cavities	3F-35
3.3.5-10.	Fracture Liquid Flux Profiles at the Center of the Potential Lower-Temperature Repository, No Lithophysal Cavities	3F-36
3.3.5-11.	Fracture Liquid-Flux Profiles at the Center of the Potential Lower-Temperature Repository, With Lithophysal Cavities.....	3F-37
3.3.5-12.	Fracture Liquid Flux Profiles at the Center of the Potential Lower-Temperature Repository, No Lithophysal Cavities and Increased Infiltration.....	3F-38
3.3.6-1.	Schematic of Potential Mountain-Scale Thermal-Hydrologic-Chemical Processes and Initial Conditions.....	3F-39
3.3.6-2.	Location of 2-D North-South Cross Section Superimposed on Diagram Showing the 3-D UZ Flow and Transport Model TSPA-SR Grid.....	3F-40
3.3.6-3.	Infiltration Rate Distribution and Simulated Changes in Fracture Porosity, Mineralogy, and Temperature after about 1,400 Years of Heating.....	3F-41
3.3.6-4.	Simulated Changes in Fracture Porosity and Mineralogy after 5,000 Years of Heating	3F-42
3.3.6-5.	Simulated Water and Gas Chemistry after about 1,400 Years of Heating.....	3F-43
3.3.7-1.	Temperature Distribution at 1,000 Years	3F-44
3.3.7-2.	Contour of Horizontal Stress Distribution at 1,000 Years	3F-45
3.3.7-3.	Vertical Permeability Changes due to the Thermal-Hydrologic-Mechanical Effect at 1,000 Years	3F-46

FIGURES (Continued)

		Page
3.3.7-4.	Change in Horizontal Permeability Due to the Thermal-Hydrologic-Mechanical Effect at 1,000 Years.....	3F-47
3.3.7-5.	Correlation Between Permeability and Temperature of Geothermal Reservoirs Worldwide.....	3F-48
4.2-1.	Seepage-Relevant Features and Processes	4F-1
4.3.1-1.	Permeability and Saturation for a Simulated Liquid Release.....	4F-2
4.3.1-2.	Water Supply, Measured Seepage Rates, and Predicted Seepage Rates.....	4F-3
4.3.1-3.	Tomb of Sennefer in the Egyptian Valley of the Kings	4F-4
4.3.2-1.	Distribution of Flux Magnitude within the Two-Dimensional Model Domain	4F-5
4.3.2-2.	Distribution of Vertical Fluxes within the Two-Dimensional Model Domain	4F-6
4.3.2-3.	Comparison of Frequency Distribution of Simulated Fluxes at Different Elevations within the Two-Dimensional Model Domain.....	4F-7
4.3.2-4.	Frequency Distribution of Simulated Fluxes at Different Infiltration Rates within the Two-Dimensional Model Domain	4F-8
4.3.2-5.	Simulated Preferential Flow Pathways.....	4F-9
4.3.2-6.	Distribution and Range of Cumulative Flux as a Function of Percolation Flux for the Bottom of the Model Domain.....	4F-10
4.3.3-1.	Conceptual Model of How a Rock Bolt Hole Might Affect Seepage	4F-11
4.3.3-2.	Grout Parameter Combinations	4F-12
4.3.3-3.	Comparison of Seepage Percentage	4F-13
4.3.4-1.	Drift Degradation Submodel Scenarios.....	4F-14
4.3.4-2.	Seepage Percentage as a Function of Percolation Flux for the Three Set A Drift Degradation Scenarios.....	4F-15
4.3.4-3.	Emplacement Drift Profile for the Ttptmn Unit, Worst Case.....	4F-16
4.3.4-4.	Seepage Percentage as a Function of Percolation Flux for Realization 1 of the Two Set A (Ttptmn) Degradation Scenarios and the Undegraded Base Case	4F-17
4.3.4-5.	Seepage Percentage as a Function of Percolation Flux for Realization 1 of the Two Set B' Degradation Scenarios and the Undegraded Base Case.....	4F-18
4.3.5-1.	Sensitivity of Drift Wall Temperature to Thermal Properties.....	4F-19
4.3.5-2.	Fracture Liquid Fluxes as a Function of Lateral Distance from Drift Center ...	4F-20
4.3.5-3.	Liquid Saturation Contours Around the Drift to Mid-Pillar.....	4F-21
4.3.5-4.	Matrix Liquid Saturations at 1,000 Years after Waste Emplacement.....	4F-22
4.3.5-5.	Fracture Liquid Fluxes as a Function of Lateral Distance from Drift Center ...	4F-23
4.3.5-6.	Comparison of Drift Wall Temperatures for the Higher-Temperature and Lower-Temperature Cases.....	4F-24
4.3.5-7.	Fracture Saturation Contours for the Lower-Temperature Case	4F-25
4.3.5-8.	Fracture Liquid Fluxes as a Function of Lateral Distance from Drift Center for the Lower-Temperature Case.....	4F-26
4.3.5-9.	Liquid-Phase-Flux Histories at Various Locations in the Host Rock	4F-27
4.3.5-10.	Temperature and Relative Humidity History at the Drift Wall.....	4F-28

FIGURES (Continued)

		Page
4.3.5-11.	Cumulative Distribution Function of the Episodicity Factor for Different Weep Widths and Flow Focusing Conditions	4F-29
4.3.5-12.	Cumulative Probability for the Ratio of Penetration Distance to Superheated Distance	4F-30
4.3.5-13.	Cumulative Probability of the Ratio of the Mass Flow Rate at the Drift Wall to the Initial Mass Flow Rate	4F-31
4.3.6-1.	Schematic Diagram of the Relation between Thermal-Hydrologic Processes and Geochemical Processes	4F-32
4.3.6-2.	Comparison of Modeled Carbon Dioxide Concentrations	4F-33
4.3.6-3.	Measured and Modeled Fracture Water Compositions	4F-34
4.3.6-4.	Fracture Liquid Saturations at 600 Years from Thermal-Hydrological Simulations for Three Permeability Realizations	4F-35
4.3.6-5.	Fracture Permeability Ratio After 20,000 Years for Realization #1	4F-36
4.3.6-6.	Chloride Concentrations in Fracture Water After 600 Years	4F-37
4.3.6-7.	Fracture Water pH After 600 Years	4F-38
4.3.6-8.	Schematic of Experiment to Replicate Mineral Dissolution and Precipitation by Condensate-Water in Fractured Tuff	4F-39
4.3.6-9.	Image of a Fracture Opened at the Conclusion of an Experiment to Examine Precipitate Location, Mineralogy, and Morphology	4F-40
4.3.6-10.	Depth Profiles for a Simulated Fracture Plugging Experiment	4F-41
4.3.6-11.	Precipitated Amorphous Silica for Simulated Fracture Plugging Experiment	4F-42
4.3.7-1.	Permeability Ratios at 55 Years for Higher-Temperature Case	4F-43
4.3.7-2.	Histogram of Permeability Ratios at 55 Years for Each Fracture Set for Higher-Temperature Case	4F-44
4.3.7-3.	Histograms of Permeability Ratios at 1,000 Years for Each Fracture Set for the Higher-Temperature Case	4F-45
4.3.7-4.	Histogram of Permeability Ratios at 100,000 Years for Each Fracture Set for the Higher-Temperature Case	4F-46
4.3.7-4a.	Fracture Permeability Multipliers for the Lower-Temperature Operating Mode Case 100 Years after Emplacement	4F-47
4.3.7-4b.	Fracture Permeability Multipliers for the Lower-Temperature Operating Mode Case 400 Years after Emplacement	4F-48
4.3.7-5.	Linking TOUGH2 and FLAC3D Codes	4F-49
4.3.7-6.	Schematic Diagram of the Fracture Rock System Near a Drift and the Conceptual Stress Permeability Model Used	4F-50
4.3.7-7.	Changes in Post- to Pre-Excavation Permeability as a Function of Initial Permeability	4F-51
4.3.7-8.	Contour Plot of Pre- to Post-Excavation Permeability Ratio from the Calibrated Model	4F-52
4.3.7-9.	Model Geometry and Boundary Conditions for a Nuclear Waste Deposition Drift	4F-53
4.3.7-10.	Changes in Horizontal and Vertical Permeabilities Before and After Excavation	4F-54
4.3.7-11.	Temperature Distribution at 10 Years	4F-55

FIGURES (Continued)

		Page
4.3.7-12.	Horizontal Permeability Changes at 10 Years.....	4F-56
4.3.7-13.	Vertical Permeability Changes at 10 Years.....	4F-57
4.3.7-14.	Temperature Distributions After 1,000 Years.....	4F-58
4.3.7-15.	Horizontal Permeability Changes at 1,000 Years.....	4F-59
4.3.7-16.	Vertical Permeability Changes at 1,000 Years.....	4F-60
4.3.7-17.	Distribution of Saturation and Percolation Flux for Thermal-Hydrologic-Mechanical and Thermal-Hydrologic Processes for the Higher-Temperature Case.....	4F-61
4.3.7-18.	Distribution of Saturation (S_1) and Percolation Flux (Q_1) for Thermal-Hydrologic-Mechanical and Thermal-Hydrologic Processes for the Lower-Temperature Case.....	4F-62
4.3.7-19.	Correlation Between Permeability and Temperature for Worldwide Geothermal Reservoir.....	4F-63
5.2-1.	Relationship of the Multiscale Thermal-Hydrologic Model to Other Models.....	5F-1
5.2-2.	Illustration of the Multiscale Thermal-Hydrologic Model.....	5F-2
5.2-3.	Locations at Which Thermal-Hydrologic Parameters are Calculated by the Multiscale Thermal-Hydrologic Model.....	5F-3
5.2-4.	Waste Package Temperature Histories.....	5F-4
5.2-5.	Waste Package Relative Humidity Histories.....	5F-5
5.2-6.	Histories of Percolation Flux 5 m Above the Drift Crown.....	5F-6
5.3.1.4.4-1.	Liquid Phase Flux 5 m above Drift Wall as a Function of Permeability for the Higher-Temperature Operating Mode.....	5F-7
5.3.1.4.4-2.	Postclosure Liquid Phase Flux 5 m above Drift Wall as a Function of Permeability for the Lower-Temperature Operating Mode.....	5F-8
5.3.1.4.4-3.	Liquid Phase Flux 1 m above Drift Wall as a Function of Permeability for the Higher-Temperature Operating Mode.....	5F-9
5.3.1.4.4-4.	Postclosure Liquid Phase Flux 1 m above Drift Wall as a Function of Permeability for the Lower-Temperature Operating Mode.....	5F-10
5.3.1.4.6-1.	Simulations of the Large Block Test.....	5F-11
5.3.1.4.6-2.	Comparison of Simulated and Observed Deformation for Borehole WM-2 in the Large Block Test.....	5F-12
5.3.1.4.7-1.	Drift Wall and Drip Shield Temperatures and Relative Humidities as a Function of Bulk Permeability for the Higher-Temperature Operating Mode (Page 1 of 2).....	5F-13
5.3.1.4.7-1.	Drift Wall and Drip Shield Temperatures and Relative Humidities as a Function of Bulk Permeability for the Higher-Temperature Operating Mode (Page 2 of 2).....	5F-14
5.3.1.4.7-2.	Invert Liquid Saturations as a Function of Bulk-Permeability for the Higher-Temperature Operating Mode.....	5F-15
5.3.1.4.7-3.	Drift Wall and Drip Shield Temperatures and Relative Humidities as a Function of Bulk Permeability for the Lower-Temperature Operating Mode (Page 1 of 2).....	5F-16

FIGURES (Continued)

	Page
5.3.1.4.7-3. Drift Wall and Drip Shield Temperatures and Relative Humidities as a Function of Bulk Permeability for the Lower-Temperature Operating Mode (Page 2 of 2).....	5F-17
5.3.1.4.7-4. Invert Liquid-Saturations as a Function of Bulk Permeability for the Lower-Temperature Operating Mode.....	5F-18
5.3.1.4.8-1. Temperature and Relative Humidity at the Drift Wall and Drip Shield as a Function of Host-Rock Thermal Conductivity for the Central Repository (L5C3) Location of the Higher-Temperature Operating Mode and the Mean Infiltration-Flux Scenario.....	5F-19
5.3.1.4.8-2. Liquid-Saturation in the Invert as a Function of Host-Rock Thermal Conductivity for the Central Repository (L5C3) Location of the Higher-Temperature Operating Mode and the Mean Infiltration-Flux Scenario.....	5F-20
5.3.1.4.8-3. Temperature and Relative Humidity at the Drift Wall and Drip Shield as a Function of Host-Rock Thermal Conductivity for the Central Repository (L5C3) Location of the Lower-Temperature Operating Mode and the Mean Infiltration-Flux Scenario.....	5F-21
5.3.1.4.8-4. Liquid-saturation in the Invert as a Function of Host-Rock Thermal Conductivity for the Central Repository (L5C3) Location of the Lower-Temperature Operating Mode and the Mean Infiltration-Flux Scenario.....	5F-22
5.3.1.4.9-1. Higher-Temperature Operating Mode as a Function of Mean, High, and Low Lithophysal Porosity (f_{lith}) for the Mean Infiltration-Flux Scenario.....	5F-23
5.3.1.4.9-2. Higher-Temperature Operating Mode Invert Liquid-Saturations as a Function of Mean, High, and Low Lithophysal Porosity (f_{lith}) for the Mean Infiltration-Flux Scenario.....	5F-24
5.3.1.4.9-3. Lower-Temperature Operating Mode Drift Wall and Drip Shield Temperatures and Relative Humidities as a Function of Mean, High, and Low Lithophysal Porosity (f_{lith}) for the Mean Infiltration-Flux Scenario.....	5F-25
5.3.1.4.9-4. Lower-Temperature Operating Mode Invert Saturation for the Central Repository Location (Location L5C3) as a Function of Mean, High and Low Lithophysal Porosity (f_{lith}) Associated with Appropriate Thermal Conductivity (K_{th}) for the Mean Infiltration-Flux Scenario.....	5F-26
5.3.1.4.10-1. Drift Wall (Crown) Temperature Sensitivity to Invert Thermal Conductivity for the Higher-Temperature Operating Mode.....	5F-27
5.3.1.4.10-2. Invert (Lower-Center) Temperature Sensitivity to Invert Thermal Conductivity for the Higher-Temperature Operating Mode.....	5F-28
5.3.1.4.10-3. Drift Wall (Crown) Liquid Saturation Sensitivity to Invert Thermal Conductivity for the Higher-Temperature Operating Mode.....	5F-29
5.3.1.4.10-4. Invert (Lower-Center) Liquid Saturation Sensitivity to Invert Thermal Conductivity for the Higher-Temperature Operating Mode.....	5F-30
5.3.1.4.10-5. Drip Shield (Top) Relative Humidity Sensitivity to Invert Thermal Conductivity for the Higher-Temperature Operating Mode.....	5F-31
5.3.1.4.11-1. Design and Operating Mode Parameters Used to Meet Peak Waste Package Temperature Goals.....	5F-32
5.3.1.4.11-2. Waste Package Temperatures and Relative Humidity for Two Methods of Archiving the Lower-Temperature Operating Mode.....	5F-33

FIGURES (Continued)

		Page
5.3.2-1.	Air Flow Pattern in a Prediction of a Quarter-Scale Test of In-Drift Convection.....	5F-35
5.3.2-2.	Three-Dimensional Air Flow in a Closed Emplacement Drift.....	5F-36
5.3.2.3-1.	Numerical Mesh Used in the Line-Source Drift-Scale Thermal-Hydrologic Submodels	5F-37
5.3.2.4.1-1.	Wall Temperature During Continuous Ventilation at 10 m ³ /s.....	5F-38
5.3.2.4.1-2.	Wall Temperature During Continuous Ventilation at 15 m ³ /s.....	5F-39
5.3.2.4.1-3.	Air Temperature During Continuous Ventilation at 10 m ³ /s	5F-40
5.3.2.4.1-4.	Air Temperature During Continuous Ventilation at 15 m ³ /s	5F-40
5.3.2.4.1-5.	Heat Removed During Continuous Ventilation at 10 m ³ /s	5F-41
5.3.2.4.1-6.	Heat Removed During Continuous Ventilation at 15 m ³ /s	5F-41
5.3.2.4.1-7.	Wall Temperature During Continuous Ventilation of 10 m ³ /s.....	5F-42
5.3.2.4.1-8.	Wall Temperature During Continuous Ventilation of 15 m ³ /s.....	5F-43
5.3.2.4.1-9.	Airflow Temperature During Continuous Ventilation of 10 m ³ /s.....	5F-44
5.3.2.4.1-10.	Airflow Temperature During Continuous Ventilation of 15 m ³ /s.....	5F-45
5.3.2.4.1-11.	Heat Removed During Continuous Ventilation of 10 m ³ /s.....	5F-46
5.3.2.4.1-12.	Heat Removed During Continuous Ventilation of 15 m ³ /s.....	5F-47
5.3.2.4.1-13.	Relative Humidity During Continuous Ventilation of 10 m ³ /s	5F-48
5.3.2.4.1-14.	Relative Humidity During Continuous Ventilation of 15 m ³ /s	5F-49
5.3.2.4.2-1.	Time-Dependent Ventilation Efficiencies for the Higher- and Lower-Temperature Operating Modes.....	5F-50
5.3.2.4.2-2.	Time History of Heat Available to Enter the Near-Field Rock for the Higher-Temperature Operating Mode Ventilation Cases.....	5F-51
5.3.2.4.2-3.	Drip Shield Top Temperature Histories for the Higher-Temperature Operating Mode.....	5F-52
5.3.2.4.2-4.	Drift Wall Crown Temperature Histories for the Higher-Temperature Operating Mode.....	5F-53
5.3.2.4.2-5.	Drip Shield Top Relative Humidity Histories for the Higher-Temperature Operating Mode.....	5F-54
5.3.2.4.2-6.	Drift Wall Crown Relative Humidity Histories for the Higher-Temperature Operating Mode.....	5F-55
5.3.2.4.2-7.	Invert (Lower Center) Saturation Histories for the Higher-Temperature Operating Mode.....	5F-56
5.3.2.4.2-8.	Time History of Heat Available to Enter the Near-Field Rock for the Lower-Temperature Operating Mode Ventilation Cases	5F-57
5.3.2.4.2-9.	Drip Shield Top Temperature Histories for the Lower-Temperature Operating Mode.....	5F-58
5.3.2.4.2-10.	Drift Wall Crown Temperature Histories for the Lower-Temperature Operating Mode.....	5F-59
5.3.2.4.2-11.	Drip Shield Crown Relative Humidity Histories for the Lower-Temperature Operating Mode	5F-60
5.3.2.4.2-12.	Invert (Lower Center) Saturation Histories for the Lower-Temperature Operating Mode.....	5F-61
5.3.2.4.3-1.	Temperature Histories at the Top of the Drip Shield for the Lower-Temperature Operating Mode.....	5F-62

FIGURES (Continued)

	Page
5.3.2.4.3-2. Temperature Histories at the Drift Wall Crown for the Lower-Temperature Operating Mode.....	5F-63
5.3.2.4.3-3. Relative Humidity Histories at the Top of the Drip Shield for the Lower-Temperature Operating Mode.....	5F-64
5.3.2.4.3-4. Saturation Histories at the Lower-Center of the Invert for the Lower-Temperature Operating Mode.....	5F-65
5.3.2.4.4-1. Lateral Extent of Host-Rock Dryout Due to Ventilation for Case 1 for the Higher- and Lower-Temperature Operating Modes.....	5F-66
5.3.2.4.4-2. Temperature of the Drift Wall and the Drip Shield, Relative Humidity on the Drip Shield, and Liquid Saturation at the Drift Wall and in the Invert for Case 1 of the Higher-Temperature-Operating Mode.....	5F-67
5.3.2.4.4-3. Temperature of the Drift Wall and the Drip Shield, Relative Humidity on the Drip Shield, and Liquid Saturation at the Drift Wall and in the Invert for Case 1 of the Lower-Temperature-Operating Mode.....	5F-68
5.3.2.4.4-4. Lateral Extent of Host-rock Dryout Due to Ventilation for Cases 1, 2, 3, and 4 for the Higher- and Lower-Temperature Operating Modes.....	5F-69
5.3.2.4.4-5. Temperature of the Drift Wall and the Drip Shield, Relative Humidity on the Drip shield, and Liquid Saturation at the Drift Wall and in the Invert for Cases 1, 2, 3, and 4 of the Higher-Temperature Operating Mode.....	5F-70
5.3.2.4.4-6. Temperature of the Drift Wall and the Drip Shield, Relative Humidity on the Drip Shield, and Liquid Saturation at the Drift Wall and in the Invert for Cases 1, 2, 3, and 4 of the Lower-Temperature Operating Mode.....	5F-71
5.3.2.4.4-7. Temperature (a) and Relative Humidity (b) Histories at the Drip Shield for 0 Percent, 3 Percent, and 30 Percent of the Percolation Flux Seeping into the Drift.....	5F-72
5.3.2.4.5-1. Comparison of Thermal Conductivities.....	5F-73
5.3.2.4.5-2. Comparison of Preclosure Temperature Differences at In-Drift Locations.....	5F-74
5.3.2.4.5-3. Comparison of Postclosure Temperature Differences at In-Drift Locations.....	5F-75
5.3.2.4.5-4. Comparison of the Effective Thermal Conductivities Developed Using the TSPA-SR Rev 00 Design and Using Four Areal Mass Loadings.....	5F-76
5.3.2.4.5-5. Temperature at the Drip Shield for Explicit and Approximated Thermal Radiation and Natural Convection.....	5F-77
5.3.2.4.5-5a. Temperature Comparison at the Drift Wall for Explicit and Approximated Thermal Radiation and Natural Convection.....	5F-78
5.3.2.4.5-6. Temperature Histories at the Base of the Drip Shield.....	5F-79
5.3.2.4.5-7. Temperature Histories at the Crown of the Drift Wall.....	5F-80
5.3.2.4.5-8. Temperature Histories at the Bottom-Center of the Invert.....	5F-81
5.3.2.4.5-9. Relative Humidity Histories at the Base of the Drip Shield.....	5F-82
5.3.2.4.5-10. Air Mass Fraction Differences Between the High Permeability and Base Cases at the Base of the Drip Shield.....	5F-83
5.3.2.4.5-11. Saturation History of Near-Field Rock at the Crown of the Drift Wall.....	5F-84
5.3.2.4.5-12. Saturation History of the Bottom-Center of the Invert.....	5F-85
5.3.2.4.5-13. Temperature Histories at the Top of the Drip Shield.....	5F-86
5.3.2.4.5-14. Temperature Histories at the Crown of the Drift Wall.....	5F-87

FIGURES (Continued)

		Page
5.3.2.4.5-15.	Nondimensional Temperature Versus Nondimensional Horizontal Distance for the Horizontal Midplane Through the In-Drift Air.....	5F-88
5.3.2.4.5-16.	Nondimensional Vertical Velocity Versus Nondimensional Horizontal Distance for the Horizontal Midplane Through the In-Drift Air.....	5F-89
5.3.2.4.5-17.	Nondimensional Heat Flux on the Cool (Outer) Cylinder Versus Nondimensional Distance Along the Cylinder Perimeter	5F-90
5.3.2.4.5-18.	Natural Convection Flow Velocities Calculated Using ANSYS	5F-91
5.3.2.4.5-19.	Effective Thermal Conductivity for Natural Convection for the Higher-Temperature Operating Mode	5F-92
5.3.2.4.5-20.	Effective Thermal Conductivity for Natural Convection for the Lower-Temperature Operating Mode	5F-93
5.4.1-1.	Location of Seven Sites Used in Analyses of the Higher-Temperature Operating Mode Repository	5F-94
5.4.1-2.	Temperature and Relative Humidity Histories on the Drift Wall and the Waste Package for Seven Locations in the Higher-Temperature Operating Mode Repository	5F-95
5.4.1-3.	Liquid Saturation and Evaporation Rate Histories for Seven Locations in the Higher-Temperature Operating Mode Repository.....	5F-96
5.4.1-4.	Contour Plots of Waste-Package Temperature for Six Times in the Higher-Temperature Operating Mode Repository.....	5F-97
5.4.1-5.	Contour Plots of Waste-Package Relative Humidity at Six Times for the Higher-Temperature Operating Mode Repository	5F-98
5.4.1-6.	Complementary Cumulative Distribution Function of Temperature and Relative Humidity Conditions on the Drift Wall and Waste Package for the Higher-Temperature Operating Mode Repository	5F-99
5.4.1-7.	Temperature and Relative Humidity Histories for the Higher-Temperature Operating Mode Predicted by the Multiscale Thermal-Hydrologic Model	5F-100
5.4.2-1.	Location of Eight Sites Used in Analyses of the Potential Lower-Temperature Operating Mode Repository.....	5F-101
5.4.2-2.	Temperature and Relative Humidity Histories on the Drift Wall and on the Waste Package for Eight Locations in the Potential Lower-Temperature Operating Mode Repository	5F-102
5.4.2-3.	Liquid Saturation and Evaporation Rate Histories in the Invert for Eight Locations in the Potential Lower-Temperature Operating Mode Repository.....	5F-103
5.4.2-4.	Contour Plots of Waste-Package Temperature for Six Times in the Lower-Temperature Operating Mode Repository.....	5F-104
5.4.2-5.	Contour Plots of Waste-Package Relative Humidity at Six Times for the Lower-Temperature Operating Mode Repository	5F-105
5.4.2-6.	Complementary Cumulative Distribution Function of Temperature and Relative Humidity Conditions on the Waste Package for the Potential Lower-Temperature Operating Mode Repository	5F-106
5.4.2-7.	Temperature and Relative Humidity for the Lower-Temperature Operating Mode, Histories Predicted by the Multiscale Thermal-Hydrologic Model.....	5F-107

FIGURES (Continued)

		Page
5.4.2-8.	Thermal-Hydrologic Parameter Evolution for the Higher- and Lower-Temperature Operating Modes.....	5F-108
6.3.1.2-1.	Example of Thermal-Hydrologic-Chemical Seepage Model Mesh with Drift in the Topopah Spring Tuff Lower Lithophysal Geologic Unit (Tptpll).....	6F-1
6.3.1.4-1.	Time Profiles for Thermal-Hydrologic-Chemical Simulations of Carbon Dioxide (Pore Gas) Concentration and pH (Pore Water) in Fractures at the Drift Crown	6F-2
6.3.1.4-2.	Time Profiles for Thermal-Hydrologic-Chemical Simulations of Aqueous Calcium and Sodium Concentrations in Fractures at the Drift Crown.....	6F-3
6.3.1.4-3.	Time Profiles for Thermal-Hydrologic-Chemical Simulations of Total Aqueous Fluoride Concentrations in Fractures at the Drift Crown for the Tptpll and Tptpmn Hydrogeologic Units	6F-4
6.3.1.5-1.	Time Profiles of Thermal-Hydrologic-Chemical Simulations of Modeled Carbon Dioxide Concentrations (Pore Gas), Temperature, and Liquid Saturation in Fractures at the Drift Crown	6F-5
6.3.1.5-2.	Time Profiles for Thermal-Hydrologic-Chemical Simulations of Modeled pH, Total Aqueous Chloride, and Total Aqueous Fluoride Concentrations in Fractures at the Drift Crown.....	6F-6
6.3.1.5-3.	Time Profiles for Thermal-Hydrologic-Chemical Simulations for Modeled Total Aqueous Sodium, Calcium, and Magnesium Concentrations in Fractures at the Drift Crown.....	6F-7
6.3.1.5-4.	Time Profiles for Thermal-Hydrologic-Chemical Simulations of Modeled Carbon Dioxide Concentrations (Pore Gas) in Fractures at the Drift Crown.....	6F-8
6.3.1.5-5.	Time Profiles for Thermal-Hydrologic-Chemical Simulations of Modeled pH in Fractures at the Drift Crown.....	6F-9
6.3.1.5-6.	Piper Diagram for the Compositions of Selected Pore Water and Other Water	6F-10
6.3.1.5-7.	Piper Diagram of the Modeled Evolution of Water Compositions for Two Initial Water Compositions Under Ambient Conditions	6F-11
6.3.1.5-8.	Piper Diagram of the Modeled Evolution of Water Compositions for the Lower-Temperature Case and Two Initial Water Compositions	6F-12
6.3.1.5-9.	Piper Diagram of the Modeled Evolution of Water Compositions for the Higher-Temperature Case and Two Initial Water Compositions.....	6F-13
6.3.3-1.	Ionic Strength, pH, and Chloride Model Predictions versus Well J-13 Evaporation Data.....	6F-14
6.3.3-2.	Ionic Strength, pH, and Chloride Model Predictions versus 100 x Well J-13 Evaporation Data	6F-15
6.3.3-3.	Ionic Strength, pH, and Chloride Model Predictions versus Topopah Spring Tuff Pore Water Evaporation Data	6F-16
6.3.3-4.	Aqueous Evaporative Evolution of In Situ J-13 Well Water at f_{CO_2} of 10^{-3}	6F-17
6.3.3-5.	Aqueous Evaporative Evolution of Topopah Spring Tuff Pore Water at f_{CO_2} of 10^{-3}	6F-18

FIGURES (Continued)

		Page
6.3.4-1.	Cumulative Key-Block Size Distribution for Various Sizes of Joint Planes in the Tptpmn Unit	6F-19
6.3.4-2.	Cumulative Key-Block Size Distribution for Various Sizes of Joint Planes in the Tptpll Unit	6F-20
6.3.4-3.	Cumulative Block Size Distributions for Various Monte Carlo Simulations in the Tptpmn Unit	6F-21
6.3.4-4.	Predicted Number of Key-Blocks for Various Monte Carlo Simulations in the Tptpmn Unit	6F-22
6.3.4-5.	Predicted Maximum Block Size for Various Monte Carlo Simulations in the Tptpmn Unit	6F-23
6.3.4-6.	Block Size Distributions for Various Monte Carlo Simulations in the Tptpll Unit	6F-24
6.3.4-7.	Predicted Number of Key Blocks for Various Monte Carlo Simulations in the Tptpll Unit	6F-25
6.3.4-8.	Predicted Maximum Block Size for Various Monte Carlo Simulations in the Tptpll Unit	6F-26
6.3.4-9.	Histogram and Cumulative Frequency Distribution of Fracture Spacing	6F-27
6.3.4-10.	Histogram and Cumulative Frequency Distribution of Fracture Spacing	6F-28
6.3.4-11.	Cumulative Key-Block Size Distribution using Original and Modified Terzaghi Corrections	6F-29
7.1-1.	Arrangements for Different Types of Waste Packages and the Drip Shield in an Emplacement Drift	7F-1
7.1-2.	Typical Waste Package Designed for 21-PWR Fuel Assemblies	7F-2
7.3.2-1.	Graphical Extrapolation of the Kinetic Data for Long-Range Ordering in Alloy 22 Base Metal	7F-3
7.3.2-2.	Phase Fraction Predicted for Alloy 22 as a Function of Temperature	7F-4
7.3.2-3.	Isothermal Time-Temperature-Transformation Diagrams for an FCC-Based Matrix of a Binary Nickel-Chromium Alloy and a Ternary Nickel-Chromium-Molybdenum Alloy	7F-5
7.3.2-4.	Extrapolation of Volume Fraction Data from Half-Inch Thick, Alloy 22, Double-V, Gas-Tungsten-Arc Welds	7F-6
7.3.2-5.	Extrapolation of Mechanical (Charpy Impact Toughness) and Electrochemical (Corrosion Resistance) Behavior of Alloy 22	7F-7
7.3.3-1.	Fractile Plot of Measured Surface Residual Stress Values for Shot Peened-Incoloy 908 Samples	7F-8
7.3.3-2.	Probability Plot of Measured Surface Residual Stress Values for Shot Peened Incoloy 908 Samples	7F-9
7.3.3-3.	Constant Load (Uniaxial Tension) Stress Corrosion Crack Initiation Test No. 1	7F-10
7.3.3-4.	Constant Load (Uniaxial Tension) Stress Corrosion Crack Initiation Test No. 2	7F-11
7.3.4-1.	Elementary Interfacial Reactions Postulated in the Point Defect Model to Generate or Annihilate Point Defects in the Barrier Layer of a Passive Film	7F-12

FIGURES (Continued)

		Page
7.3.4-2.	Dependence of Electrochemical Corrosion Potential on the Partial Pressure of Oxygen and on Temperature	7F-13
7.3.4-3.	Corrosion Current Density as a Function of the Partial Pressure of Oxygen and Temperature.....	7F-14
7.3.4-4.	Calculated Electrochemical Corrosion Potential Versus Thickness of the Electrolyte Film on the Metal Surface.....	7F-15
7.3.4-5.	Calculated Electrochemical Corrosion Potential Versus pH of the Thin Electrolyte Film on the Alloy Surface.....	7F-16
7.3.4-6.	Calculated Corrosion Current Density Versus pH of the Thin Electrolyte Film on the Alloy Surface	7F-17
7.3.4-7.	Mineral Variations Shown in a Scanning Electron Microscope Micrograph of a Cross Section of a Josephinite Sample.....	7F-18
7.3.5-1.	Data Fit for Temperature Dependence of Alloy 22 General Corrosion Model I Using the Entire Data Set	7F-19
7.3.5-2.	Cumulative Distribution Functions of General Corrosion Rate of the Waste Package Outer Barrier at 25, 60, and 125°C Calculated with Temperature-Dependent Alloy 22 General Corrosion Model I	7F-20
7.3.5-3.	Data Fit for Temperature Dependence of Alloy 22 General Corrosion Model II with the Outer Excluded.....	7F-21
7.3.5-4.	Cumulative Distribution Functions of General Corrosion Rate of the Waste Package Outer Barrier at 25°, 60°, and 125°C Calculated with Temperature-Dependent Alloy 22 General Corrosion Model II	7F-22
7.3.5-5.	Cumulative Distribution Functions of General Corrosion Rate of the Waste Package Outer Barrier at 25, 60, and 125°C Calculated with Temperature-Dependent Alloy 22 General Corrosion Model III.....	7F-23
7.3.5-6.	Mean General Corrosion Rate of Alloy 22 Versus Exposure Time for Weight Loss Specimens from the Long-Term Corrosion Testing Facility	7F-24
7.3.5-7.	FIGURE REMOVED.....	7F-25
7.3.5-8.	Cumulative Distribution Functions of General Corrosion Rate of the Alloy 22 Waste Package Outer Barrier	7F-26
7.3.5-9.	Waste Package Failure Profile with Time Incorporating the Temperature-Dependent Alloy 22 General Corrosion Model II.....	7F-27
7.3.5-10.	Waste Package First Patch Breach Profile with Time Incorporating the Temperature-Dependent Alloy 22 General Corrosion Model II	7F-28
7.4-1.	Waste Package Failure over Time for the Baseline WAPDEG Model	7F-29
7.4-2.	Drip Shield Failure over Time for the Baseline WAPDEG Model.....	7F-30
7.4-3.	Average Number of Drip Shield Patch Breaches per Failed Drip Shield for the Baseline WAPDEG Model.....	7F-31
7.4-4.	Waste Package First Crack Failure for the Baseline WAPDEG Model.....	7F-32
7.4-5.	Waste Package First Patch Failure for the Baseline WAPDEG Model	7F-33
7.4-6.	Average Number of Crack Breaches per Failed Waste Package for the Baseline WAPDEG Model.....	7F-34
7.4-7.	Average Number of Patch Breaches per Failed Waste Package for the Baseline WAPDEG Model.....	7F-35

FIGURES (Continued)

		Page
7.4-8.	Waste Package Failure with Time Incorporating the Updated Uncertainty for Weld Flaw Orientation	7F-36
7.4-9.	Waste Package Failure with Time Incorporating the Updated Stress Uncertainty Bounds for the Outer and Inner Closure-Lids of the Waste Package Outer Barrier	7F-37
7.4-10.	Waste Package Failure with Time Incorporating the Updated Stress Threshold Uncertainty for Crack Initiation by Stress Corrosion Cracking	7F-38
7.4-11.	Hoop Stress versus Depth for Outer Closure-Lid Weld Region of Waste package Outer Barrier.....	7F-39
7.4-12.	Hoop Stress versus Depth for Inner Closure-Lid Weld Region of Waste Package Outer Barrier for Crack Initiation by Stress Corrosion Cracking	7F-40
7.4-13.	Average Number of Crack Breaches per Failed Waste Package with Time Incorporating the Updated Stress Threshold Uncertainty for Crack Initiation by Stress Corrosion Cracking	7F-41
7.4-14.	Drip Shield Failure with Time Assuming 100 Percent Uncertainty in the General Corrosion Rates	7F-42
7.4-15.	Waste Package First Failure with Time Assuming 100 Percent Uncertainty in the General Corrosion Rates	7F-43
7.4-16.	Waste Package Failure with Time Incorporating the Temperature-Dependent Alloy 22 General Corrosion Model I	7F-44
7.4-17.	Waste Package First Patch Failure for the Update Case Incorporating the Temperature-Dependent Alloy 22 General Corrosion Model II	7F-45
7.4-18.	Waste Package Failure Profile with Time Incorporating the Temperature-Dependent Alloy 22 General Corrosion Model I	7F-46
7.4-19.	Waste Package First Patch Breach Profile with Time Incorporating the Temperature-Dependent Alloy 22 General Corrosion Model I	7F-47
7.4-20.	Waste Package Failure Profile with Time for the Integrated Model I	7F-48
7.4-21.	Waste Packages First Crack Breach Profile with Time for the Integrated Model I	7F-49
7.4-22.	Waste Package Failure Profile with Time Incorporating the Temperature-Dependent Alloy 22 General Corrosion Model II	7F-50
7.4-23.	Waste Package First Patch Breach Profile with Time Incorporating the Temperature-Dependent Alloy 22 General Corrosion Model II	7F-51
7.4-24.	Waste Package Failure Profile with Time for the Integrated Model II	7F-52
7.4-25.	Waste Packages First Crack Breach Profile with Time for the Integrated Model II	7F-53
8.2-1.	Schematic Diagram of Engineered Barrier System Flow Pathways	8F-1
8.3.1-1.	Average High Level Radioactive Waste Drip Shield Evaporation Rate	8F-2
8.3.1-2.	Average Non-Commercial Drip Shield Evaporation Rate	8F-3
8.3.2.3-1.	Conceptual Model for EBS Sensible and Latent Heat Flow Paths and Drip Shield Condensation.....	8F-4
8.3.2.3.1-1.	Main Convection Cells within the EBS	8F-5
8.3.3-1.	Conceptual Drip Shield Flux Model	8F-6
8.3.3-2.	Event Tree for the Drip Shield Flux Model	8F-7

FIGURES (Continued)

		Page
8.3.3-2b	Event Tree for the Waste Package Flux Model.....	8F-8
8.3.3-3.	Geometric Factors in the Assignment of Probabilities.....	8F-9
8.3.3-4.	Relationship of Moisture Potential to Relative Humidity	8F-10
8.3.4-1.	Schematic of the Bathtub Geometry for the Waste Package.....	8F-11
8.3.4-2.	Cumulative Distribution Function for the Bathtub Delay Time for a Single WAPDEG Realization with 400 Packages.....	8F-12
8.3.4-3.	Cumulative Distribution Function for the Bathtub Delay Time for 100 WAPDEG Realizations. Each Curve is Based on the Results for 400 Waste Packages	8F-13
9-1.	Updated Expected Case Model pH-Time Trajectories for Commercial Spent Nuclear Fuel Packages	9F-1
9-2.	Updated Expected Case Model pH-Time Trajectories for Codisposal Packages	9F-2
9-3.	Sensitivity Model pH-Time Trajectories for Commercial Spent Nuclear Fuel Packages	9F-3
9-4.	Sensitivity Model pH-Time Trajectories for Codisposal Packages	9F-4
9-5.	Thorium Solubility versus pH with Different Controlling Minerals.....	9F-5
9-6.	Concentrating Factors of Neptunium in Drip Tests	9F-6
9-6b.	Neptunium Dissolved Concentration Limit Models and Data	9F-7
9-7.	Plutonium Dissolved Concentration Limit Estimations and Data.....	9F-8
9-7b.	Plutonium Dissolved Concentration Limit Abstraction and Data.....	9F-9
9-8.	Experimentally Measured pH and Dissolved Uranium of Leachates	9F-10
9-9.	Temporal Variations in the Molar Concentrations of Neptunium and Uranium.....	9F-11
10.2-1.	Conceptualization of an Emplacement Drift after the Drip Shield and Waste Package are Breached and Radionuclides can Transport through the Engineered Barrier System.....	10F-1
10.3.1-1.	Comparison of Adsorption Isotherms for Water Vapor on Fe ₂ O ₃ , NiO, and ZrO ₂	10F-2
10.3.1-2.	Adsorption Isotherm for Water Vapor on α-Fe ₂ O ₃	10F-3
10.3.1-3.	Adsorption Isotherm for Water on Nickel.....	10F-4
10.3.1-4.	Regression Fit to Adsorption Isotherm Data for Water Vapor on ZrO ₂	10F-5
10.3.2-1.	Film Thickness Data and Predictive Relationships from the Literature.....	10F-6
10.3.2-2.	Average Film Flow Velocity versus Film Thickness	10F-7
10.3.3-1.	Measured Diffusivity for Various Granular Media as a Function of Volumetric Moisture Content.....	10F-8
10.3.3-2.	Uncertainty in the Statistical Fit for the Diffusion Coefficient	10F-9
10.3.3-3.	Limiting Diffusion Coefficients for Anions and Simple (Non-Complexed) Cations.....	10F-10
10.3.3-4.	Grid for NUFT Calculation of Invert Saturation.....	10F-11
10.3.3-5.	Liquid Saturation in the Engineered Barrier System at 10,000 Years	10F-12
10.3.3-6.	Liquid Saturation in the Invert at 10,000 Years	10F-13

FIGURES (Continued)

		Page
10.3.4-1.	Comparison of Log-Normal and Log-Uniform Distributions for the Partition Coefficient of Americium.....	10F-14
11.3.1-1.	Model Grid with Waste Emplacement Drift used for Dual-Permeability Model.....	11F-1
11.3.1-2.	Vertical Flow Velocity Contours for Flow in Drift Shadow	11F-2
11.3.1-3.	Vertical Flow Velocity Contours for Flow around a Drift in the tsw35 Fracture Continuum.....	11F-3
11.3.1-4.	Water Saturation Contours for Flow around a Drift in the tsw35 Fracture Continuum.....	11F-4
11.3.1-5.	Vertical Flow Velocity Contours for Flow around a Drift in the tsw35 Matrix Continuum	11F-5
11.3.1-6.	Water Saturation Contours for Flow around a Drift in the tsw35 Matrix Continuum.....	11F-6
11.3.1-7.	Technetium (a) and Neptunium (b) Transport with a Total Percolation Rate of 10 mm/yr.....	11F-7
11.3.1-8.	Technetium (a) and Neptunium (b) Transport with a Total Percolation Rate of 100 mm/yr.....	11F-8
11.3.2-1.	Schematic Diagram of a One-Dimensional Column of Gridblocks and Four Models of Flow	11F-9
11.3.2-2.	Matrix Discretization for the Multiple Interacting Continua Model Scheme .	11F-10
11.3.2-3.	Plan View of the Unsaturated Zone Model Domain and the East-West Cross Section.....	11F-11
11.3.2-4.	Two-Dimensional Numerical Grids for the East West (A-A') Cross Section	11F-12
11.3.2-5.	Comparison of (a) Saturation and (b) Fracture-Flux Output from Two Simulation Models for Vertical Column a14	11F-13
11.3.2-6.	Comparison of (a) Matrix-Saturation and (b) Fracture-Flux Output from Two Simulation Models for Vertical Column a23	11F-14
11.3.2-7.	Distribution of Capillary Pressures Within a Matrix Block	11F-15
11.3.2-8.	Normalized Tracer Cumulative Flux at Water Table as a Function of Time..	11F-16
11.3.3-1.	Schematic of the Propagation of a Pulse in Fracture-Matrix System with Time.....	11F-17
11.3.3-2.	Schematic of a Parallel Fracture System without Water Flow between the Fractures and the Matrix.....	11F-18
11.3.3-3.	Predicted Breakthrough of the Current Model, a More-Refined Model, and the Analytical Solution using 1 m Fracture Spacing	11F-19
11.3.3-4.	Predicted Breakthrough by the Current Model, a More-Refined Model, and the Analytical Solution using 10 m Fracture Spacing	11F-20
11.3.3-5.	Effect of Fracture Spacing on Breakthrough as a Function of Time.....	11F-21
11.3.3-6.	Predicted Cumulative Breakthrough Curves for the Base Case of the Unsaturated Zone Transport System, the Current Model, and the More-Refined Model	11F-22
11.3.4-1.	Correlations of Average Infiltration Rates and Groundwater Travel or Tracer Transport Times	11F-23

FIGURES (Continued)

		Page
11.3.4-2.	Simulated Breakthrough Curves of Cumulative Tracer and Radionuclide Mass Arriving at the Water Table	11F-24
11.3.4-3.	Uranium Activity Ratios in Peña Blanca Waters	11F-25
11.3.5-1.	Liquid Saturation Distributions in the Fracture Continuum for the Higher-Temperature Case	11F-26
11.3.5-2.	Liquid Saturation Distributions in the Matrix Continuum for the Higher-Temperature Case	11F-27
11.3.5-3.	Changes in the Depth of the Dryout Zone over Time for the Higher-Temperature Case	11F-28
11.3.5-4.	Liquid Saturation Distributions in the Fracture Continuum for the Lower-Temperature Case	11F-29
12.1-1.	Flow Paths Predicted by the Site-Scale Saturated Zone Flow and Transport Model.....	12F-1
12.2-1.	Boundary of the Numerical Model for the Site-Scale Saturated Zone Flow and Transport Model	12F-2
12.2-2.	Borehole Locations, Water-Level Altitudes, Potentiometric Surface Contours, and Location of Tertiary Faults in the Site-Scale Saturated Zone Model Area.....	12F-3
12.3.1.2-1.	Locations of Nye County Early Warning Drilling Program Wells	12F-4
12.3.1.3-1.	Features in the Newer Saturated Zone Model	12F-5
12.3.1.2-2.	Potentiometric Surface Map in the Saturated Zone Site-Scale Model Area	12F-6
12.3.1.3-2.	Flow Paths Simulated with the Original Site-Scale Saturated Zone Flow and Transport Model	12F-7
12.3.1.3-3.	Flow Paths Simulated with the New Saturated Zone Model (Excluding the Northwest Trending Fault Zone)	12F-8
12.3.1.3-4.	Flow Paths Simulated with the New Saturated Zone Model (Including the Northwest Trending Fault Zone)	12F-9
12.3.2.3-1.	Preliminary 70,000 MTHM Layout for the Lower-Temperature Operating Mode.....	12F-10
12.3.2.3-2.	Locations of Particle Tracking Points Associated with Differing Potential Repository Footprints	12F-11
12.3.2.3-3a.	Plan View of Particle Pathlines the Higher-Temperature Operating Mode for the Potential Repository.....	12F-12
12.3.2.3-3b.	Plan View of Particle Pathlines from the Potential Repository with Pathlines from an Increased Repository Footprint	12F-13
12.3.2.3-3c.	Plan View of Particle Pathlines from the Potential Repository with Pathlines from the Southern Lobe of an Increased Repository Footprint	12F-14
12.3.2.3-4.	Breakthrough Curves to the 20-km Compliance Boundary for the Case of No Matrix Diffusion and Distributed Release Over the Entire Potential Repository Footprint.....	12F-15
12.3.2.3-5.	Breakthrough Curves at the 20-km Point of Compliance Using Two Dispersion Coefficient Tensors and Two Radionuclides	12F-16
12.3.2.3-6.	Effective Simulated Longitudinal Dispersivity Versus Specified Longitudinal Dispersivity.....	12F-17

FIGURES (Continued)

		Page
12.3.2.3-7.	Schematic Diagram of the Matrix Diffusion Model	12F-18
12.3.2.3-8.	Matrix Diffusion Models for Carbon-14 (Conservative) and Neptunium-237 (Weakly Sorbing) Radionuclides	12F-19
12.3.2.4-1.	Neptunium Sorption Coefficients results from Batch Sorption Tests	12F-20
12.3.2.4-2.	Cumulative Distribution Function for Neptunium Sorption Coefficients (K_{ds}) used for Unquantified Uncertainty Calculations	12F-21
12.3.2.4-3.	Distribution of Simulated and Measured Dry Bulk Density for Alluvium	12F-22
12.3.2.4-5.	Matrix Diffusion Coefficients as a Function of Matrix Porosity	12F-24
12.3.2.4-6.	Matrix Diffusion Mass Transfer Coefficients as a Function of Mean Tracer Residence Time	12F-24
12.3.2.4-7.	Histogram of Mass Transfer Coefficient Values	12F-25
12.4-1.	Groundwater Flow Paths Determined from Hydrochemical and Isotopic Data	12F-26
12.4-2.	Groundwater Flow Paths Determined from Simulated Particle Pathlines	12F-27
12.4-3.	Normalized Tracer Concentration Versus Gallons Pumped in Three Single-Well Tracer Tests Conducted in the Uppermost Screened Interval of Well NC-EWDP-19D1	12F-28
12.4-4.	Normalized Microsphere Concentrations Versus Time During the Second and Third Single-Well Tests in the Uppermost Screened Interval in Well NC-EWDP-19D1	12F-29
12.4-5.	Chloride Concentration in Groundwater	12F-30
12.4-6.	Uranium Activity Ratios in Saturated Zone Waters	12F-31
12.5.1-1.	Simulated Median Transport Times of Neptunium for the Supplemental Science and Performance Analysis and the Unquantified Uncertainty Cases	12F-32
12.5.2-1.	Simulated Median Transport Times of Uranium for the Supplemental Science and Performance Analysis and the No-Matrix-Diffusion Cases	12F-33
12.5.2-2.	Simulated Median Transport Times of Neptunium for the Supplemental Science and Performance Analysis and Enhanced Matrix Diffusion Cases ...	12F-34
12.5.2-3.	Simulated Median Transport Times of Neptunium for the Supplemental Science and Performance Analysis and the Minimum Alluvium Cases	12F-35
12.5.2-4.	Simulated Median Transport Times of Plutonium Reversibly Sorbed onto Colloids (K_c Model)	12F-36
12.5.3-1	Southernmost Boundary of the Controlled Area and the Accessible Environment	12F-37
12.5.3-2.	Frequency of Breakthrough for Simulated Median Transport Times of Neptunium-237	12F-38
12.5.3-3.	Frequency of Breakthrough for Simulated Median Transport Times of Carbon-14	12F-39
13.3-1.	Distribution of Annual Doses at 25,000 years for a Hypothetical Group of Farmers Based on Amargosa Valley Population	13F-1
13.3-2.	Dependence of the Average Annual Dose to the Members of the Exposed Group at 25,000 years on the Group Size	13F-2

FIGURES (Continued)

	Page
13.3-3. Pathway Biosphere Dose Conversion Factor Ratios for Plutonium-239 for Groundwater Release of Evolved and Current Climates.....	13F-3
13.4-1. Contributions of Major Exposure Pathways to Biosphere Dose Conversion Factors for Plutonium-239 for Groundwater Release at Different Irrigation Periods	13F-4
14.1-1a. Repository Layout Used in Disruptive Events Analyses: Enhanced Design Alternative II Higher-Temperature Operating Mode	14F-1
14.1-1b. Repository Layout Used in Disruptive Events Analyses: Higher-Temperature Operating Mode Addressed in the Yucca Mountain Science and Engineering Report.....	14F-2
14.1-1c. Repository Layout Used in Disruptive Events Analyses: Lower-Temperature Operating Mode	14F-3
14.2-1. Location and Age of Post-Miocene Volcanoes in the Yucca Mountain Region	14F-4
14.2-2a. Known or Suspected Quaternary Faults and Potentially Important Local Faults within 100 km of Yucca Mountain.....	14F-5
14.2-2b. Known or Suspected Quaternary Faults and Potentially Important Local Faults in the Vicinity of the Yucca Mountain Site.....	14F-6
14.3.3.5-1. Desert Rock Airstrip Wind Speed Cumulative Probability Distribution	14F-7

TABLES

		Page
1-1.	Summary of Supplemental Models and Analyses.....	1T-1
1-2.	Computer Software.....	1T-8
2-1.	Comparison of Higher-Temperature and Lower-Temperature Operating Modes Evaluated in the Fiscal Year 2001 Supplemental Science and Performance Analyses with the Design Analyzed in the Yucca Mountain Science and Engineering Report	2T-1
3-1.	Summary of Supplemental Models and Analyses.....	3-2
3.3.1-1.	Mean Annual Precipitation for Analogues for the Lower and Upper Bound of the Three Climate Scenarios Adjusted for the Topography of the UZ Flow and Transport Model Area	3T-1
3.3.1-2.	Mean Annual Temperature for Analogues for the Lower and Upper Bound of the Three Climate Scenarios Adjusted for the Topography of the UZ Flow and Transport Model Area	3T-1
3.3.1-3.	Climate Sequence from 10,000 to 1 Million Years.....	3T-1
3.3.1-4.	Summary of Uncertainty Issues Related to the Development of the Climate Model.....	3T-3
3.3.1-5.	Mean Annual Precipitation for the Lower and Upper Bound of the Three Glacial Climate Scenarios Adjusted for the Topography of the UZ Flow and Transport Model Area.....	3T-4
3.3.1-6.	Mean Annual Temperature for the Lower and Upper Bound of the Three Glacial Climate Scenarios Adjusted for the Topography of the UZ Flow and Transport Model Area.....	3T-5
3.3.2-1.	Average Net Infiltration Rates over the Unsaturated Zone Flow and Transport Model Domain for the Modern, Monsoon, and Glacial Transition Climate States	3T-5
3.3.2-2.	Summary of Uncertainty Issues Related to the Development of the Net Infiltration Model	3T-6
3.3.2-3.	Average Net Infiltration Rates over the Unsaturated Zone Flow and Transport Model Domain for Full Glacial Climate States	3T-7
3.3.3-1.	Net Infiltration Data by Region.....	3T-7
3.3.3-2.	Summary of Uncertainty Issues Related to Percolation Redistribution and Flow in PTn.....	3T-8
3.3.4-1.	Average Percolation Fluxes (mm/yr) Simulated Within the Potential Repository Footprint for Thirteen Infiltration Scenarios.....	3T-9
3.3.4-2.	Summary of Uncertainty Issues Related to Three-Dimensional Flow Fields ...	3T-10
3.3.5-1.	Summary of Numerical Model Cases for Mountain-Scale Thermal Hydrologic.....	3T-11
3.3.5-2.	Recent Applications of TOUGH2 in Modeling Geothermal Systems	3T-12
3.3.5-3.	Summary of Uncertainty Issues Related to Thermal Hydrologic Effects on Mountain-Scale Flow	3T-13
3.3.6-1.	Minerals, Aqueous Species, and Gaseous Species in the Mountain-Scale Thermal-Hydrologic-Chemical Model.....	3T-14

TABLES (Continued)

		Page
3.3.6-2.	Summary of Uncertainty Issues Related to the Prediction of Thermal Hydrologic-Chemical Effects on Mountain-Scale Unsaturated Zone Flow and Geochemistry	3T-15
3.3.7-1.	Thermal-Hydrologic-Mechanical Parameter Data Used in Current Simulation	3T-16
3.3.7-2.	Changes In Permeability for Hydrostratigraphic Layers at the Mid-Repository Symmetry Boundary on the Left Side of the Model.....	3T-17
3.3.7-3.	Summary of Uncertainty Issues Related to Thermal-Hydrologic-Mechanical Effects on Mountain-Scale Flow.....	3T-17
4-1.	Summary of Supplemental Models and Analyses.....	4-2
4.3.1-1.	Triangular Distributions of Seepage Fraction, Seep Flow Rate, and Standard Deviation of Seep Flow Rate as a Function of Percolation Flux	4T-1
4.3.1-2.	Summary of Uncertainty Issues Related to the Determination of Seepage-Relevant Parameters	4T-1
4.3.2-1.	Cases Considered in Flow Focusing Sensitivity Studies.....	4T-3
4.3.2-2.	Summary of Uncertainty Issues Related to Flow Focusing and Discrete Flow Paths in the TSw Hydrogeologic Unit.....	4T-3
4.3.3-1.	Summary of Uncertainty Issues Related to Rock Bolts	4T-4
4.3.4-1.	Seepage Percentage for Alternative Drift-Degradation Scenarios for Qp = 500 mm/yr and Set A	4T-4
4.3.4-2.	Seepage Percentage for Set A Drift Degradation Scenarios	4T-5
4.3.4-3.	Seepage Percentage for Set B' Drift Degradation Scenarios	4T-5
4.3.4-4.	Summary of Uncertainty Issues Related to Determining Seepage-Relevant Parameters	4T-6
4.3.5-1.	Analysis Model Report Revision 00 and Post-Analysis Model Report Lithophysae Thermal Property Values.....	4T-6
4.3.5-2.	Statistical Parameters Used in the Three-Dimensional Heterogeneous Line-Averaged-Heat-Source, Drift-Scale Thermohydrologic Model Realizations	4T-6
4.3.5-3.	Input Parameters for Application of Asperity-Induced Episodic Infiltration at Yucca Mountain	4T-7
4.3.5-4.	Summary of Uncertainty Issues Related to Thermohydrologic Effects on Seepage.....	4T-8
4.3.6-1.	Comparison of Experimental and Potential Yucca Mountain Repository Conditions	4T-9
4.3.6-2.	Summary of Uncertainty Issues Related to the Prediction of Thermal-Hydrologic-Chemical Effects on Seepage and Potential Seepage Chemistry	4T-9
4.3.7-1.	Input Parameters and Data Tracking Numbers for Distinct Element Analysis.....	4T-11
4.3.7-2.	Permeability Ratio Distribution for Horizontal Fractures.....	4T-12
4.3.7-3.	Permeability Ratio Distribution for Vertical Fractures	4T-12
4.3.7-4.	Thermal-Hydrologic-Mechanical Property Parameters Used in Simulations.....	4T-12

TABLES (Continued)

		Page
4.3.7-5.	Summary of Uncertainty Issues Related to Thermal-Hydrologic-Mechanical Effects on Seepage	4T-13
5.1-1.	Design Parameters Used in Sensitivity Studies to Address Three Operational Modes	5-1
5.2-1.	Near Field Environment and Engineered Barrier System Thermal-Hydrologic Variables Calculated with the Multiscale Thermal-Hydrologic Model at 610 Repository Locations for No-Backfill Realizations	5T-1
5.3.1.2-1.	Key Thermal-Hydrologic Uncertainties	5T-2
5.3.1.4.2-1.	Statistical Parameters Used in the Three-Dimensional, Heterogeneous Line-Averaged-Heat-Source, Drift-Scale Thermal-Hydrologic Model Realizations	5T-3
5.3.1.4.2-2.	Summary of Seepage Conditions When TH Conditions Have Returned to Near-Ambient (Glacial Climate)	5T-3
5.3.1.4.6-1.	Input Parameters and Data Tracking Numbers for Distinct Element Analysis	5T-4
5.3.1.4.6-2.	Comparison of Range of Bulk (Fracture) Permeability Values for Geologic Units Considered in Multiscale Thermal-Hydrologic Model Sensitivity Studies to Potential Range from THM Effects.....	5T-4
5.3.1.4.6-3.	Summary of Thermal-Hydrologic-Mechanical Simulations of the Large Block Test.....	5T-5
5.3.1.4.7-1.	Bulk (Fracture) Permeability Values for Geologic Units used in the Multiscale Thermal-Hydrologic Model Analyses, Along with the Assumed Value of Sigma used in the Sensitivity Study of k_b	5T-5
5.3.1.4.8-1.	Lithophysal Unit Thermal Conductivity Values Used in the MSTH Model Sensitivity Analyses	5T-5
5.3.1.4.8-2.	Comparison of Relative Humidity Conditions on Drift Wall as Function of K_{th} for the Higher-Thermal Operating Mode Case.....	5T-6
5.3.1.4.9-1.	Lithophysal Porosity Values used in MSTH Model Sensitivity Analyses.....	5T-6
5.3.1.4.10-1.	Thermal Conductivity in the Upper Half of the Invert for the Sensitivity Calculation.....	5T-6
5.3.1.4.10-2.	Calculated Peak Temperatures for Each Invert Conductivity	5T-6
5.3.1.4.11-1.	Waste Package Peak Temperatures for the Three Lower-Temperature Operating Mode Sensitivity Cases	5T-7
5.3.2.4.1-1.	Preclosure Temperatures and Ventilation Efficiencies Calculated with Two Models.....	5T-7
5.3.2.4.1-2.	Fraction of Total Heat Removal via Ventilation Due to Latent Heat of Water Vaporized from the Near-Field Rock	5T-7
5.3.2.4.2-1.	Summary of HTOM Thermal-Hydrologic Parameter Sensitivity to Ventilation Efficiency	5T-8
5.3.2.4.2-2.	Summary of Lower-Temperature Operating Mode Thermal-Hydrologic Parameter Sensitivity to Ventilation Efficiency	5T-8
5.3.2.4.3-1.	Summary of Lower-Temperature Operating Mode Thermal-Hydrologic Parameter Sensitivity to Ventilation Duration	5T-8

TABLES (Continued)

		Page
5.3.2.4.5-1.	Bulk Permeabilities for In-Drift Air.....	5T-9
5.3.2.4.6-1.	In-Drift Temperatures for the Higher-Temperature Operating Mode.....	5T-9
5.3.2.4.6-2.	In-Drift Temperatures for the Lower-Temperature Operating Mode (Page 1 of 2)	5T-11
5.4-1.	Sequence of Steps to Combine Submodel Results in the Multiscale Thermal-Hydrologic Model (Page 1 of 2).....	5T-13
5.4.3-1.	Sensitivity of In-Drift Thermal-Hydrologic Performance to Uncertainties and Parameters (Page 1 of 3).....	5T-15
6-1.	Summary of Supplemental Models and Analyses.....	6-2
6.3.1.5-1.	Thermal-Hydrologic-Chemical Seepage Simulations.....	6T-1
6.3.1.5-2.	Composition of Selected Pore Water and Other Waters from Yucca Mountain	6T-2
6.3.1.6-1.	Abstraction Results for High Temperature and Low Carbon Dioxide Partial Pressure in the Tptpl Lithology for Seepage at the Crown of the Drift	6T-3
6.3.1.6-2.	Abstraction Results for High Temperature and High Carbon Dioxide Partial Pressure in the Tptpl Lithology for Seepage at the Crown of the Drift	6T-4
6.3.1.6-3.	Abstraction Results for Low Temperature and Low Carbon Dioxide Partial Pressure in the Tptpl Lithology for Seepage at the Crown of the Drift	6T-5
6.3.1.6-4.	Abstraction Results for Low Temperature and High Carbon Dioxide Partial Pressure in the Tptpl Lithology for Seepage at the Crown of the Drift	6T-6
6.3.1.6-5.	Abstraction Results for High Temperature and Low Carbon Dioxide Partial Pressure in the Tptpl Lithology for Matrix Imbibition into the Invert	6T-7
6.3.1.6-6.	Abstraction Results for High Temperature and High Carbon Dioxide Partial Pressure in the Tptpl Lithology for Matrix Imbibition at the Base of the Invert	6T-8
6.3.1.6-7.	Abstraction Results for Low Temperature and Low Carbon Dioxide Partial Pressure in the Tptpl Lithology for Matrix Imbibition into the Invert	6T-9
6.3.1.6-8.	Abstraction Results for Low Temperature and High Carbon Dioxide Partial Pressure in the Tptpl Lithology for Matrix Imbibition at the Base of the Invert	6T-10
6.3.1.8-1.	Summary of Uncertainty Issues Related to Predicted Composition of Fluids Entering Drifts	6T-11
6.3.2-1.	Summary of Uncertainties on the Effects of Engineered Materials in the In-Drift Chemical Environment and any Associated Model Improvements.....	6T-14
6.3.3-1.	Example Precipitates/Salts Model Lookup Table for Selected Outputs	6T-15
6.3.3.5.2-1.	Sensitivity Analysis of the In-Drift ANC/pH Model	6T-16
6.3.3.5.2-2.	Validation Analyses of In-Drift ANC/pH Model Showing Agreement Between Mixing Model Results and Literature Mixing Examples.....	6T-16

TABLES (Continued)

		Page
6.3.4-1.	Block Volume Corresponding to Various Levels of Predicted Cumulative Frequency of Occurrence, Emplacement Drift in Tptpmn Unit, Static Condition	6T-17
6.3.4-2.	Block Volume Corresponding to Various Levels of Predicted Cumulative Frequency of Occurrence, Emplacement Drift in Tptpll Unit, Static Condition	6T-17
6.3.4-3.	Predicted Number of Key Blocks per Unit Length along Emplacement Drift, Static Condition	6T-17
6.3.4-4.	Beta Distribution Parameters for Spacing of the Subhorizontal Joint Set of the Tptpmn Unit	6T-17
6.3.4-5.	Block Volume Corresponding to Various Levels of Predicted Cumulative Frequency of Occurrence, Emplacement Drift in Tptpmn Unit, Static Condition with Modified Terzaghi Correction.....	6T-18
7-1.	Summary of Supplemental Models and Analyses.....	7-4
7.3.1-1.	Compositions of Brines from Saline Lakes in Western North America	7T-1
7.3.1-2.	Compositions of Yucca Mountain Waters	7T-1
7.3.1-2b.	Deliquescence Point Data of Pure Salts of MgCl ₂ , NaCl, and NaNO ₃	7T-2
7.3.1-3.	National Atmospheric Deposition Program/National Trends Network Deposition Data for Site NV00, Red Rock Canyon, Clark County, Nevada	7T-3
7.3.2-1.	Preliminary Measurements of Time to Give Precipitate Volume Fractions of 0.05 and 0.10 in Aged Alloy 22 Welds.....	7T-3
7.3.3-1.	Descriptive Statistics of Surface Residual Stress Data of Shot-Peened Samples	7T-4
7.3.3-2.	Cumulative Density Function Values of Fractional Uncertainty	7T-4
7.3.3-3.	Slow Strain Rate Test Results for Alloy 22.....	7T-5
7.3.5-1.	Passive Current Density Data from Potentiostatic Polarization Experiments for Alloy 22.....	7T-6
7.3.5-2.	Calculations for the Temperature Dependence Term for the Alloy 22 General Corrosion Rate Model.....	7T-6
7.3.5-3.	Passive Current Density Data from Potentiostatic Polarization Experiments and Calculated Passive Dissolution Rate for Alloy 22	7T-7
7.3.6-1.	Poisson Probabilities for Improper Heat Treatment of Waste Packages.....	7T-7
7.3.7-1	Critical Crevice Temperatures for Alloy 22.....	7T-8
8-1.	Summary of Supplemental Models and Analyses.....	8-2
9-1.	Summary of Supplemental Models and Analyses.....	9-2
9-2.	Important Input Parameters for the Impact of Glass and Steel Degradation Unquantified Uncertainties on In-package pH Calculations	9T-1
9-3.	Total System Performance Assessment Model Results for pH Ranges	9T-1
9-4.	Model Results for Commercial Spent Fuel Package pH Ranges	9T-2
9-5.	Model Results for Codisposal Fuel Package pH Ranges	9T-2
9-6.	Primary Cladding Uncertainties Considered.....	9T-3

TABLES (Continued)

		Page
9-7.	Complementary Cumulative Distribution Function for Fraction of Rods Failed per m ³ of Seepage.....	9T-3
9-8.	Complementary Cumulative Distribution Function for Frequency of Seismic Cladding Failure	9T-4
9-9.	Complementary Cumulative Distribution Function for Unzipping Velocity Multiplier.....	9T-4
10-1.	Summary of Supplemental Models and Analyses.....	10-2
10.3.1-1.	Comparison of the Adsorption of Water on Various Metals.....	10T-1
10.3.1-2.	Least Squares Analysis of Adsorption of Water on ZrO ₂	10T-1
10.3.1-3.	Specific Surface Area of Oxide Samples Reported in Literature.....	10T-1
10.3.1-4.	Characteristics of a 21-PWR Waste Package.....	10T-2
10.3.1-5.	Porosity Calculation for a 21-PWR Waste Package (Density, Mass, and Sources Listed in Table 10.3.1-4).....	10T-3
10.3.1-6.	Masses and Materials for the Three Types of Waste Packages That Will Comprise the Bulk of Waste in the Repository	10T-4
10.3.1-7.	Elemental Composition of Each Waste Package Material	10T-5
10.3.1-8.	Surface Area Available for Adsorption of Water Inside a 21-PWR Waste Package.....	10T-5
10.3.1-9.	Effective Water Saturation in Waste Package Resulting from Adsorption of Water Vapor	10T-5
10.3.1-10.	Values of Diffusion Coefficient Normalized to the Diffusion Coefficient in Water for Various Waste Package Surface Areas and Relative Humidities	10T-6
10.3.1-11.	Summary of Cross-Sectional Areas for Diffusion for Various Configurations at a Relative Humidity of 95 Percent	10T-6
10.3.1-12.	Parameters to be Sampled for In-Package Diffusion Model.....	10T-8
10.3.4-1.	Summary of Partition Coefficient Ranges on Corrosion Products, Sand, and Loam.....	10T-8
10.3.4-2.	Expected Material Lifetimes of Invert, Pallet, and Waste Package Components in the Drift	10T-10
10.3.4-3.	Calculated Mass of Sorbing Material in the Waste Package.....	10T-10
10.3.4-4.	Summary of Tolerance Interval Calculations for Sand, Loam, and Clay Data Sets.....	10T-11
10.3.4-5.	Fraction of Contaminant Metal Irreversibly Sorbed	10T-11
10.3.5-1.	Summary of Uncertainties Considered for Engineered Barrier System Colloids	10T-11
10.3.5-2.	Summary of Recommended Parameter Changes for Total System Performance Assessment.....	10T-12
10.3.6-1.	Distribution of Uranium Uptake for Microbial Transport.....	10T-12
10.4.4-1.	Recommended Ranges and Distribution Type for the Partition Coefficients (K _d s) of Dissolved Radionuclides.....	10T-12

TABLES (Continued)

		Page
11-1.	Summary of Supplemental Models and Analyses.....	11-3
11.3.1-1.	Summary of Uncertainty Issues Related to the Drift Shadow Transport Model.....	11T-1
11.3.2-1.	Summary of Key Uncertainty Issues Related to Calculating Flow and Transport between Fractures and the Matrix.....	11T-2
11.3.3-1.	Parameters Used for the Transport Problem in a Parallel Fracture System	11T-3
11.3.3-2.	Summary of Key Uncertainty Issues.....	11T-3
11.3.4-1.	Stable Uranium and Stable Isotope Data from Peña Blanca.....	11T-4
11.3.4-2.	Summary of Key Uncertainty Issues.....	11T-4
11.3.5-1.	Summary of Uncertainty Issues Related to the Effects of Thermally-Driven Coupled Processes on Transport in the Unsaturated Zone.....	11T-5
12-1.	Summary of Supplemental Models and Analyses.....	12-2
12.3.2.1.1-1.	Identification and Treatment of Unquantified Uncertainties Based on the Total System Performance Assessment-Site Recommendation.....	12T-1
12.3.2.3-1.	Bounding Nevada State Plane Coordinates for the Emplacement Area for the Potential Lower-Temperature Operating Mode Repository Footprint.....	12T-2
12.3.2.4-1.	Zeolitic Rock Volume	12T-6
12.3.2.4-2.	Comparison of Sorption Coefficients for Uranium and Neptunium	12T-6
12.3.2.4-3.	Measured Saturated Density, Computed Porosity, and Computed Dry Bulk Density for Depths from 402 to 776 Feet Below the Surface at the Nye County EWDP-19D1 Well.....	12T-7
12.3.2.4-4.	Parameters for Retardation Factor Calculations and Uncertainty Range Distributions	12T-7
12.5.1-1.	Identification and Treatment of Unquantified Uncertainties Based on the Total System Performance Assessment-Site Recommendation.....	12T-8
13-1.	Summary of Supplemental Models and Analyses.....	13-3
13.2-1.	Comparison of the Assessment Context for the Yucca Mountain Project and BIOMASS Biosphere Models	13T-1
13.2-2.	Comparison of the Pathways and Methodologies Used in the Yucca Mountain Project Groundwater Release and BIOMASS Biosphere Models....	13T-2
13.3-1.	Pathway Factors	13T-3
13.3-2.	Annual Pathway Exposure Levels for the Current Receptor and Alternative Receptors	13T-4
13.3-3.	Average Annual Doses to the Current Receptor and to Alternative Receptors at 25,000 Years Postclosure	13T-4
13.3-4.	Average Annual Doses to the Current Receptor and to Alternative Receptors at 100,000 Years Postclosure	13T-5
13.3-5.	Comparison of International Commission on Radiological Protection Tissue Weighting Factors.....	13T-6
13.3-6.	Comparison of Biosphere Dose Conversion Factors for the Groundwater Release Scenario.....	13T-7

TABLES (Continued)

		Page
13.3-7.	Comparison of Biosphere Dose Conversion Factors for the Volcanic Eruption Scenario (Transition Phase, 1-cm Ash Layer, Annual Average Mass Loading).....	13T-8
13.3-8.	Parameters Used to Characterize the Leaching Process for Sandy Soils	13T-9
13.3-9.	Impact of Leaching Factor Changes on Biosphere Dose Conversion Factor Mean Values.....	13T-9
13.3-10.	Pathway Contribution (Percent) to Biosphere Dose Conversion Factors	13T-10
13.3-11.	Mean Biosphere Dose Conversion Factor Values (rem/(pCi/L)).....	13T-10
13.3-12.	Lower and Upper Limit of the Multiplying Factor to be Applied to Groundwater Release Biosphere Dose Conversion Factors to Reflect Additional Uncertainty in Input Parameter Uncertainty	13T-10
13.3-13.	Parameters Forming a Basis for Alfalfa Irrigation for the Present and Future Climate.....	13T-10
13.3-14.	Annual Average Meteorological Parameters for Potential Future Climate States at Yucca Mountain and the Analogue Sites for the Climate Change Analysis	13T-11
13.3-15.	Comparison of the Biosphere Dose Conversion Factors (rem per pCi/L) and Buildup Factors for the Current and Evolved Climate ^a	13T-12
13.3-16.	Recommended Transfer Parameter Values for Selenium	13T-12
13.3-17.	Removal Constants and Prior Irrigation Time Periods for Selenium-79	13T-13
13.3-18.	Dose Coefficients for Exposure to Soil Contaminated with Selenium-79.....	13T-13
13.3-19.	Selenium-79 Biosphere Dose Conversion Factors for the Three Volcanic Eruption Exposure Scenarios	13T-14
13.3-20.	Neptunium-237 Biosphere Dose Conversion Factors for the Three Volcanic Eruption Exposure Scenarios	13T-15
13.3-21.	Biosphere Dose Conversion Factors for Selenium-79, Groundwater Release Scenario, for the Current Climate and the Evolved Climate.....	13T-15
13.3-22.	Biosphere Dose Conversion Factors for Selenium-79, Groundwater Release Scenario, for the Current Climate	13T-16
13.4-1.	Summary of the Biosphere Dose Conversion Factors for the Groundwater Release Scenario for the Current Climate and the Corresponding Buildup Factors	13T-16
13.4-2.	The Biosphere Dose Conversion Factor Distribution for Carbon-14 Given as an Empirical Percentile Table	13T-17
13.4-3.	Distributions and Parameters for Abstracted Biosphere Dose Conversion Factors for those Radionuclides Exhibiting Less than a 15 Percent Build-Up Due to Continuing Irrigation	13T-18
13.4-4.	Asymptotic Buildup Factors for Those Radionuclides Showing Significant Buildup Before and After the Inclusion of the Soil Erosion Mechanism.....	13T-18
13.4-5.	Recommended Biosphere Dose Conversion Factor Parameters for the Radionuclides Having a Normal Distribution for the Groundwater Release Scenario and the Current Climate	13T-19

TABLES (Continued)

		Page
13.4-6.	Recommended Biosphere Dose Conversion Factor Parameters for the Radionuclides Having a Log-normal Distribution for the Groundwater Release Scenario and the Current Climate	13T-19
13.4-7.	Recommended Biosphere Dose Conversion Factor Parameters for the Radionuclides Having a Shifted Log-normal Distribution for the Groundwater Release Scenario and the Current Climate	13T-19
13.4-8.	Summary of Biosphere Dose Conversion Factors for the Groundwater Release Scenario for the Evolved Climate and their Corresponding Buildup Factors	13T-20
13.4-9.	Dose Factors for the Eruption Phase	13T-21
13.4-10.	Volcanic Eruption Biosphere Dose Conversion Factors (rem/(pCi/m ²)).....	13T-22
14-1.	Summary of Supplemental Models and Analyses.....	14-2
14.1-2.	Repository Features and Hypothetical Operating Modes that Produce a Range of Temperatures	14T-1
14.2-1.	Key Documents Supporting the Analysis of Disruptive Processes and Events	14T-2
14.3.3.2-1.	Summary of the Number of Waste Packages Contained within a Conduit Diameter for the Operating Modes Presented in Table 14.1-2.....	14T-2
14.3.3.4-1.	Waste Particle Sizes Used in Total System Performance Assessment and in the Sensitivity Analysis for Volume 2 Using New Distributions	14T-3
14.3.3.5-1.	Desert Rock Wind Speed Cumulative Probability Distribution.....	14T-4
14.3.3.7-1.	Volcanic Eruption Event Input Parameters for Total System Performance Assessment Supplemental Model.....	14T-5
14.3.3.7-2.	Igneous Intrusion Groundwater Transport Event Input Parameters for Total System Performance Assessment Supplemental Model	14T-6

INTENTIONALLY LEFT BLANK

ACRONYMS

AFC	active fracture concept
AECL	Atomic Energy of Canada Limited
AFM	active fracture model
AML	areal mass loading
AMR	analysis model report
ANC	acid neutralizing capacity
ANL	Argonne National Laboratory
ASTM	American Society for Testing and Materials
ATC	Alluvial Testing Complex
BDCF	biosphere dose conversion factor
BWR	boiling water reactor
CADI	contingent average daily intakes
CCT	critical crevice temperature
CDF	cumulative distribution function
CEDE	committed effective dose equivalent
CFD	computational fluid dynamics
CNWRA	Center for Nuclear Waste Regulatory Analysis
CSNF	commercial spent nuclear fuel
DCF	dose conversion factor
DDT	discrete-heat-source, drift-scale, thermal-conduction
DFM	discrete fracture model
DHLW	DOE high-level radioactive waste
DKM	dual permeability model
DMTH	discrete-source, mountain-scale, thermal-hydrologic
DOE	U.S. Department of Energy
DST	drift-scale test
EBS	engineered barrier system
ECRB	Enhanced Characterization of the Repository Block
EDA	Enhanced Design Alternative
EPRI	Electrical Power Research Institute
ESF	Exploratory Studies Facility
FCC	face-centered cubic
FEPs	features, events, and processes
FHH	Frankel-Halsey-Hill
FU	fractional uncertainty
GCM	generalized corrosion model
HIC	hydrogen induced cracking
HLW	high-level waste
HTOM	higher-temperature operating mode

ACRONYMS (Continued)

IAEA	International Atomic Energy Agency
ICPP	Idaho Chemical Processing Plant
ICRP	International Commission on Radiological Protection
INEEL	Idaho National Engineering and Environmental Laboratory
IHSI	Induction Heating Stress Improvement
LADS	License Application Design Selection
LDTH	line-averaged-heat-source, drift-scale, thermal-hydrologic
LMTH	line-source, mountain-scale thermal-hydrologic
LRO	long-range order
LTCTF	Long-Term Corrosion Test Facility
LTOM	lower-temperature operating mode
MIC	microbiologically influenced corrosion
MINC	multiple interacting continua
MPM	mixed potential model
MSTH	multiscale thermal-hydrologic
MTC	mass transfer coefficient
MTHM	metric tons of heavy metal
MTI	Materials Technology Institute
MTU	metric tons of uranium
NC-EWDP	Nye County Early Warning Drilling Program
NFE	near-field environment
NRC	U.S. Nuclear Regulatory Commission
NTS	Nevada Test Site
OIS	oxygen isotope stage
PDM	point defect model
PSHA	probabilistic seismic hazard analysis
PVHA	probabilistic volcanic hazard analysis
PWR	pressurized water reactor
RH	relative humidity
REE	rare earth element
RMEI	reasonably maximally exposed individual

ACRONYMS (Continued)

S&ER	Yucca Mountain Science and Engineering Report
SCC	stress corrosion cracking
SCE	saturated calomel electrode
SDT	smear-heat-source, drift-scale, thermal-conduction
SHE	standard hydrogen electrode
SMT	smear-heat-source, mountain-scale, thermal-conduction
SNF	spent nuclear fuel
SRP	Snake River Plain
SZ	saturated zone
TC	thermal-chemical
TCP	tetrahedrally close-packed
TEDE	total effective dose equivalent
TH	thermal-hydrologic
THC	thermal-hydrologic-chemical
THM	thermal-hydrologic-mechanical
TM	thermal-mechanical
TSP	total suspended particles
TSPA	total system performance assessment
TSPA-SR	total system performance assessment for the site recommendation
TSPA-VA	total system performance assessment for the viability assessment
TTT	time-temperature-transformation
UMTRA	Uranium Mill Tailings Remedial Action
USGS	U.S. Geological Survey
UTM	Universal Transverse Mercator
UZ	unsaturated zone
VA	viability assessment
YMP	Yucca Mountain Site Characterization Project

INTENTIONALLY LEFT BLANK

1. INTRODUCTION

The U.S. Department of Energy (DOE) is considering the possible recommendation of a site at Yucca Mountain, Nevada, for development as a geologic repository for the disposal of high-level radioactive waste and spent nuclear fuel. To facilitate public review and comment, in May 2001 the DOE released the *Yucca Mountain Science and Engineering Report* (S&ER) (DOE 2001 [DIRS 153849]), which presents technical information supporting the consideration of the possible site recommendation. The report summarizes the results of more than 20 years of scientific and engineering studies. A decision to recommend the site has not been made: the DOE has provided the S&ER and its supporting documents as an aid to the public in formulating comments on the possible recommendation.

When the S&ER (DOE 2001 [DIRS 153849]) was released, the DOE acknowledged that technical and scientific analyses of the site were ongoing. Therefore, the DOE noted in the Federal Register Notice accompanying the report (66 FR 23013 [DIRS 155009], p. 2) that additional technical information would be released before the dates, locations, and times for public hearings on the possible recommendation were announced. This information includes: (1) the results of additional technical studies of a potential repository at Yucca Mountain, contained in this *FY01 Supplemental Science and Performance Analyses: Vol. 1, Scientific Bases and Analyses*; and *FY01 Supplemental Science and Performance Analyses: Vol. 2, Performance Analyses* (McNeish 2001 [DIRS 155023]) (collectively referred to as the SSPA) and (2) a preliminary evaluation of the Yucca Mountain site's preclosure and postclosure performance against the DOE's proposed site suitability guidelines (10 CFR Part 963 [64 FR 67054 [DIRS 124754]]).

By making the large amount of information developed on Yucca Mountain available in stages, the DOE intends to provide the public and interested parties with time to review the available materials and to formulate and submit comments. Before determining whether to recommend the Yucca Mountain site, the Secretary will consider public and stakeholder comments, as well as the available technical information.

1.1 BACKGROUND

The *FY01 Supplemental Science and Performance Analyses* is intended to supplement information contained in analysis and model reports supporting the S&ER (DOE 2001 [DIRS 153849]), which summarizes the extensive scientific and engineering analyses the DOE has conducted to assess how a potential repository might perform in the future. The S&ER describes the data collected during site characterization and the preliminary design of the repository facilities and waste packages that would contribute to the safe disposal of waste. Section 4 of the report explains the processes that could affect the ability of the site to isolate waste. These include both natural processes and processes caused or affected by human activities, such as the construction of the potential repository. Natural processes include the flow of water through the unsaturated zone of rock above the water table, water flow in the saturated zone of rock below the water table, and geochemical processes (such as dissolution or mineral precipitation) that could result in the transport of radionuclides.

Near the waste emplacement drifts, the natural system would be perturbed by the mechanical excavation of the drifts and by the heat generated by radioactive decay in the emplaced waste. The heat and the mechanical stresses could affect the natural processes in complex ways. The coupling of these natural and man-made processes may introduce additional complexity into models of repository performance. Therefore, the S&ER (DOE 2001 [DIRS 153849]) also explains how these coupled thermal-hydrologic-geochemical-mechanical processes would be likely to affect the long-term performance of the repository. These processes affect both the natural and the engineered barriers, including the drip shields, the waste forms, the waste packages, and the invert below the waste packages. In addition to the hydrologic and geochemical processes that would act in and around the potential repository, disruptive events, such as the possibility of volcanic eruptions, could affect the integrity of the repository. The S&ER describes the likelihood and consequences of disruptive events at Yucca Mountain.

The S&ER (DOE 2001 [DIRS 153849], Section 4.4) summarizes the results of a comprehensive quantitative analysis of the possible future behavior of a Yucca Mountain repository. This analysis, known as the *Total System Performance Assessment for the Site Recommendation* (TSPA-SR) (CRWMS M&O 2000 [DIRS 153246]), combines the results of detailed conceptual and numerical models of each of the individual and coupled processes in a single probabilistic model that can be used to assess how a repository might perform over long periods of time.

Despite the extensive scientific studies described in the S&ER (DOE 2001 [DIRS 153849]), the DOE has always recognized that significant uncertainties will remain in any assessment of the performance of a repository over thousands of years, as discussed in the S&ER (DOE 2001 [DIRS 153849], Sections 1.5, 4.1, and 4.4). These uncertainties are attributable to a variety of causes, ranging from uncertainty regarding the fundamental processes that may affect radionuclide migration to uncertainty related to the design and operation of the potential repository. For this reason, one part of the DOE approach to dealing with uncertainty relies on multiple lines of evidence that may contribute to the understanding of the performance of the potential repository. Another part of the DOE approach is a commitment to continued testing, monitoring, and analysis beyond the possible recommendation of the site.

This report has been prepared to address several specific aspects of the existing uncertainties related to the performance of a potential Yucca Mountain repository. It describes new information developed since the completion of the S&ER (DOE 2001 [DIRS 153849]) and its key supporting references, the TSPA-SR (CRWMS M&O 2000 [DIRS 153246]) and the analysis model reports and process model reports cited therein.

1.2 GOALS AND SCOPE

Based on internal reviews of the S&ER (DOE 2001 [DIRS 153849]) and other documents, the DOE has identified and performed several types of analyses to supplement the treatment of uncertainty in support of the consideration of a possible site recommendation. The information in this report is intended to supplement, not supplant, that contained in the analysis and model reports and process model reports supporting the S&ER. In general, the studies and analyses described in this document provide additional information of three types:

Unquantified Uncertainties Analysis—Specific uncertainties that were not treated explicitly in the S&ER and the TSPA-SR (CRWMS M&O 2000 [DIRS 153246]) are quantified. Unquantified uncertainties include parameter bounds, conceptual models, assumptions and, in some cases, input parameters consisting of statistically biased or skewed distributions. The primary goals of this effort were to provide insights into the significance of the unquantified uncertainties and the degree of conservatism in the overall assessment of repository performance in the TSPA-SR.

Updates in Scientific Information—New information has been developed for some of the process models that are important to performance. This work includes new experimental results, new conceptual models, and new analytical approaches, as well as the results of continued research. It also includes the identification and discussion of multiple lines of evidence that have been used directly, to support modeling, or indirectly, to develop confidence in modeling results. The primary goals of this effort were to provide insights into the impacts of the new scientific results and improved models (i.e., those updated since completion of the S&ER) and to develop additional confidence in the models and parameters used for total system performance assessment (TSPA).

Lower-Temperature Operating Mode Analysis—Because some of the processes that can affect performance are a function of the environment in the repository (e.g., temperature and humidity), the uncertainties associated with models of these processes also depend on environmental variables. In particular, operating the repository at temperatures above 96°C would result in water boiling and condensing, which requires models of flow and transport that are more complex—and possibly more uncertain—than models at lower temperatures. Therefore, the effects of a range of thermal operating modes on projected system performance, including lower operating temperatures in the potential repository (e.g., below 96°C at the drift wall or below 85°C at the waste package surface), have been evaluated. The uncertainties associated with various process models have been analyzed over a range of temperatures. The primary goals of evaluating a range of thermal operating modes were to provide insights into the effect of thermal parameters on predicted repository performance, including the uncertainty of those predictions, and to increase confidence in the predicted repository performance over a range of thermal conditions.

1.2.1 Outline of Report

This report describes the supplemental analyses that have been performed and the results of incorporating those analyses into a supplemental TSPA. It consists of two volumes: *FY01 Supplemental Science and Performance Analyses: Vol. 1, Scientific Bases and Analyses* and

FY01 Supplemental Science and Performance Analyses: Vol. 2, Performance Analyses (McNeish 2001 [DIRS 155023]). Volume 1 focuses on the technical work conducted within each process model area, encompassing uncertainty quantification, updated science and models, and lower-temperature operating mode analyses. Volume 2 describes the performance assessment analyses conducted using the updated information documented in Volume 1.

Table 1-1 shows the supplemental analyses that have been produced, the rationale for obtaining that supplemental information (i.e., unquantified uncertainties, updated scientific information, or lower-temperature operating mode analyses), and the section in this report where the work is documented. The last two columns of the table indicate how the supplemental information described in this volume is evaluated in the performance assessment analyses described in Volume 2 (McNeish 2001 [DIRS 155023]).

Section 2 of this volume describes the methodology used to define and conduct the updated analyses described in this report. The remaining sections are organized around the major processes that are expected to occur in Yucca Mountain and the proposed repository system. The structure of this document generally follows that of the S&ER (DOE 2001 [DIRS 153849]). Figure 1-1 illustrates the processes and their relationships.

Each of Sections 3 through 14 begins with a brief description of the conceptual basis for the process model supporting the S&ER (DOE 2001 [DIRS 153849]) and the TSPA-SR (CRWMS M&O 2000 [DIRS 153246]). Each section includes a description of new information and analyses that have been conducted and the results obtained using that new information. The specific content and the level of detail in Sections 3 through 14 vary, depending on the extent of the analyses that have been performed. The discussion may range from a summary level to detailed descriptions and analyses of the supplemental information. Depending on what specific information has been collected, the discussions may include the quantification of uncertainties, updated scientific information and models, and thermal sensitivity analyses. Where relevant, each section includes a discussion of other lines of evidence that provide additional evidence for and/or confidence in the process models. Finally, each section describes how the results of the new information at the process level were carried through to the abstracted models used for the supplemental TSPA analyses, which are documented in Volume 2 (McNeish 2001 [DIRS 155023]).

1.3 RATIONALE

1.3.1 Quantification of Uncertainties

As described in the S&ER (DOE 2001 [DIRS 153849]), many uncertainties associated with long-term repository performance were addressed quantitatively and probabilistically in the process models and performance assessment analyses. However, some uncertainties in processes and parameters were addressed through the use of bounding or conservative assumptions that were intended to simplify the analysis and ensure that the results were technically defensible. In a few cases, assumptions may have led to non-conservatism when implemented in the model. The use of bounding values and conservative assumptions generally yields model simulations that predict poorer performance (i.e., higher projected doses) than analysts expect. However, because the degree of conservatism for each process or parameter has not been quantified, it is

difficult to assess the extent to which the total system results may also be conservative. This report describes the quantification of some of the uncertainties that were unquantified in the TSPA-SR (CRWMS M&O 2000 [DIRS 153246]). Unquantified uncertainties include parameter bounds, conceptual models, assumptions, point estimates, or input parameters that use statistically biased or skewed distributions.

1.3.1.1 Types of Uncertainties

Accounting for, classifying, and understanding the implications of uncertainties is a critical part of modeling any complex system. Managing those uncertainties is a critical part of designing and operating any complex system. Uncertainties may arise from such aspects as incomplete understanding, limited information, or lack of data, in addition to the uncertainties inherent in developing any model of a natural or engineered system. The DOE considers uncertainties of several different types, and incorporates them in several different ways, in evaluations and estimates of repository performance.

Scenario Uncertainty—Scenario uncertainty refers to uncertainty about how future states of the world will evolve. It includes the uncertainty associated with the features, events, and processes that may impact various components of the repository system. Scenarios of plausible future states of the repository system, as well as their likelihood of occurrence, must be inferred from direct and indirect field evidence; those scenarios that meet the criteria for likelihood of occurrence and impact to annual dose should be incorporated into assessments of repository performance.

Model Uncertainty—All models are simplifications of the real system being modeled, and simplifications necessarily introduce uncertainties. Model uncertainty encompasses several types: uncertainty in conceptual models, uncertainty in the mathematical descriptions of conceptual models, and uncertainty in the numerical implementation of models in computer codes.

Parameter Uncertainty and Variability—The parameters of the mathematical models used to predict the performance of the repository system are subject to both uncertainty and variability. Uncertainty in model parameters may arise from imperfect knowledge or limited data. Variability may arise from the randomness or heterogeneity of physical characteristics in the engineered system, natural system, or biosphere. In some cases, variability is modeled by including it as uncertainty in model parameters.

Spatial and Temporal Variability—For large-scale (e.g., igneous activity) and small-scale (e.g., rock porosity) processes and properties, variability over time and over the area of the repository may have an important impact on performance. Because variability is an intrinsic property of a system, it cannot be reduced with additional information. Because it has an important impact on performance, variability is included explicitly in some process and TSPA models.

1.3.1.2 Quantified and Unquantified Uncertainties

In the process models and the TSPA-SR model supporting the S&ER (DOE 2001 [DIRS 153849]), some uncertainties are quantified and others are unquantified. Quantified

uncertainties are those for which a detailed, unbiased, quantitative description of uncertainty (e.g., a probability distribution) has been developed from available data. An unbiased estimate is one that is neither deliberately conservative nor deliberately optimistic, that neither underestimates nor overestimates performance. In some cases, unbiased quantitative estimates of uncertainty were not feasible, for example, because of the limited availability of data or process complexity. Some uncertainties were not quantified because the range of possible scenarios, processes, models, hypotheses, and parameter values made little or no difference to the overall model results, so computational efficiency was gained by choosing a single representation of the uncertainty. Unquantified uncertainties in the TSPA-SR and supporting models include alternative models, alternative hypotheses, particular assumptions, and single point estimates used to represent an uncertain property value. Unquantified uncertainty may also exist when model inputs are treated probabilistically if the range of inputs is chosen to be a conservative bound on the range of all possible values.

1.3.1.3 Rationale for Quantifying Previously Unquantified Uncertainties

The DOE deliberately chose a mix of quantified, best estimate (realistic), and unquantified (typically conservative) models and parameter values to develop a defensible, compliance-based evaluation of the potential performance of the repository system. This evaluation is included in the analysis and model reports supporting the S&ER (DOE 2001 [DIRS 153849]). However, both the DOE and external reviewers of the Yucca Mountain Site Characterization Project (YMP) (e.g., the Nuclear Waste Technical Review Board and Advisory Committee on Nuclear Waste) recognize that additional insights into repository performance can be gained from analyzing the assumptions underlying the process models. Also, further examination of the sensitivity of the total system model to these assumptions and other uncertainties may provide relevant information about the significance of the uncertainties (i.e., the importance of a specific uncertainty to repository performance).

The mix of conservative, potentially nonconservative, and realistic inputs makes it difficult to interpret the uncertainty in annual dose estimates over time produced by the TSPA-SR model. Because some inputs are clearly conservative, the annual dose estimates do not represent a best or most realistic estimate of actual performance. However, since some inputs may not be conservative, it is not clear that the annual dose estimates are entirely conservative.

It is difficult to quantify the degree of conservatism among the different process models that compose the TSPA-SR (CRWMS M&O 2000 [DIRS 153246]). In coupled models, conservatisms and assumptions in one model can mask the importance of another. It is not possible to quantify the relative conservatism in a model or its parameters without evaluating the impact of the model or parameter on the output of the fully coupled model. It is also not possible to say how conservative a specific process model is without looking at how that input affects the annual dose estimates from the TSPA-SR model.

Finally, even if each model and input were conservative, the degree to which those conservative inputs would result in a conservative annual dose estimate is not clear. The mixture of inputs makes it difficult to ascertain the degree of conservatism in the overall TSPA-SR. The quantification of uncertainties discussed in this report represents an effort to develop an understanding of the degree of conservatism in the annual dose estimates from the TSPA-SR.

1.3.2 Updated Scientific Bases and Analyses

In addition to quantifying specific uncertainties previously unquantified, the DOE has continued to improve its scientific understanding of and the technical bases for the process and performance assessment models. This document describes updates to the process models that have occurred since the models supporting the S&ER (DOE 2001 [DIRS 153849]) were developed and documented. These updates appear as discussions of new or more extensive data, revised process models, and updated abstractions for the supplemental TSPA model. The updates are an expected result of the ongoing scientific and engineering analyses supporting the DOE, and they represent the progress that has been made over the period since the documents supporting the S&ER (DOE 2001 [DIRS 153849]) were finalized. The SSPA report provides a vehicle for documenting that additional information and evaluating its significance in performance analyses.

1.3.3 Thermal Sensitivity Analyses

The third element of the new information and technical improvements since the analyses and model reports supporting S&ER (DOE 2001 [DIRS 153849]) were completed is a set of analyses designed to increase understanding of the effects of a range of operating modes and temperatures on potential repository performance.

1.3.3.1 Thermally Driven Uncertainties

Two uncertainties related to thermal effects on potential repository performance are: (1) the way Yucca Mountain will respond to the heat generated by emplaced waste, and (2) the long-term performance of the materials used to package the waste when subjected to the expected repository environment.

Coupled Processes—As the temperature of the host rock rises, the extent, magnitude, duration, and significance of thermally induced coupled processes may also increase. These coupled processes include such effects as:

- Thermal hydrology (heat influencing water movement)
- Changes in rock matrix and fracture flow properties
- Dissolution, movement, and precipitation of salts and minerals.

Materials Corrosion—A key component of the flexible design summarized in the S&ER (DOE 2001 [DIRS 153849]) is the waste package, which is designed to isolate waste from the environment for an extended period of time. The outer shell of the waste package consists of a thick layer of corrosion-resistant Alloy 22, which forms a primary barrier to water contacting the waste. As Summarized in the S&ER, process model results indicate that the outer barrier has an extremely long lifetime, with a median time to first failure of 80,000 years (DOE 2001 [DIRS 153849], Section 4.2.4.4). Because of the key role the waste package plays in performance assessments, it is important to understand the potential failure modes of Alloy 22, particularly its susceptibility to localized corrosion.

Findings about localized corrosion of Alloy 22 in highly aggressive environments suggest a range of conditions under which the material may be more susceptible to localized corrosion. These specifically include aggressive environments where the temperatures are high and the relative humidity is such that an aqueous film containing salts can form on the surface of the material. Analyses summarized in the S&ER (DOE 2001 [DIRS 153849], Section 2.1.5) indicate that the susceptibility of Alloy 22 to corrosion can be significantly reduced by maintaining waste package surface temperatures below about 85°C or relative humidity below about 50 percent.

1.3.3.2 Rationale for Evaluating a Range of Thermal Operating Modes

The overall DOE strategy for handling uncertainties is to recognize and incorporate them to the extent possible, and to take steps to reduce or mitigate those uncertainties that may have a major impact on estimates of potential repository performance. Uncertainties can be *reduced* through additional scientific and technical studies; the effect of uncertainties can be *mitigated* by engineering design choices. Uncertainties that do not appear to have the potential to significantly impact performance assessments, or uncertainties for which reduction and/or mitigation measures are not available or effective, are typically accepted and incorporated into the process models and total system analyses. For example, in the analyses and models supporting the S&ER (DOE 2001 [DIRS 153849]), uncertainties related to the effect on process models caused by different thermal operating modes (e.g., operating the repository at lower temperatures) have been tested through sensitivity studies, but have otherwise not been incorporated in the TSPA-SR model. The process models have been examined to assess the possible impact of the uncertainties, but no additional measures have been taken to reduce or mitigate the effects of those uncertainties. The DOE is currently considering options for reducing or mitigating those uncertainties in the future.

This report presents several analyses performed to gain additional insight into the effect that repository temperatures may have on the uncertainty associated with specific process models. The goal of these analyses is to assess the extent to which the DOE's and the public's confidence in performance assessments might be improved if thermal uncertainties were mitigated by lowering the temperatures in the emplacement drifts and on the surface of the waste package. As stated previously, maintaining the host rock temperature below the boiling point of water may reduce uncertainties associated with coupled processes (Anderson et al. 1998 [DIRS 101656]; Cohon 1999 [DIRS 147531]). Similarly, uncertainties about localized corrosion rates may be mitigated by avoiding operating temperatures and humidity levels that could lead to an increased susceptibility of Alloy 22 to corrosion.

Refining the design and operating mode of the potential repository has been an ongoing, iterative process involving scientists, engineers, and decision-makers. The design and mode of operations of a potential repository have evolved as the DOE has learned more about the site and the performance contribution of various design and operating attributes. Engineering and design analyses demonstrate that there are a number of potential operational practices the DOE could employ to manage the repository environment S&ER (DOE 2001 [DIRS 153849], Section 2.1.4) and achieve lower operating temperatures. Because the physical processes judged to be most sensitive to thermal effects (i.e., coupled processes and materials corrosion) are relatively unaffected by the parameters that could be used to control operating temperatures, the DOE has

chosen in this report to evaluate thermal effects through focused evaluations of specific process models and system-level sensitivity analyses. Supplemental analyses look at a range of thermal operating modes including total system level analyses for a higher-temperature operating mode and lower-temperature operating mode and analyze their impact on specific processes and performance, including uncertainty in performance. If a decision is ultimately made to operate the repository to meet different thermal goals, a fully specified design and operating mode that can be demonstrated to meet those goals will be developed.

1.4 OVERVIEW OF ANALYSIS PROCESS

For this evaluation, the DOE has identified, considered, and evaluated the most recent and relevant information about Yucca Mountain and the potential repository system that is available from all sources, inside and outside the YMP. This information has been used to quantify uncertainties, update conceptual and numerical models, and provide additional lines of evidence about the possible future behavior of a repository. To the extent possible, the information has been incorporated in an updated supplemental TSPA model and evaluated for two thermal operating modes: for a repository operated as described in the S&ER (DOE 2001 [DIRS 153849]) and for a repository operated at temperatures that do not exceed 85°C. The sections below summarize the overall processes by which the new information discussed in this document was generated, evaluated, and analyzed.

1.4.1 Quantifying Uncertainties

The process for evaluating unquantified uncertainties involved: (1) identifying unquantified uncertainties to be evaluated; (2) developing more representative, quantified descriptions of those uncertainties; and (3) evaluating the implications of those newly quantified uncertainties for repository performance.

1.4.1.1 Identifying Unquantified Uncertainties

The first step in the process of quantifying uncertainties was to identify a set of process models and parameter inputs to the TSPA model for which significant uncertainty has not been quantified (i.e., where a conservative or nonconservative representation exists in the present performance assessment). Recent studies have focused on identifying potentially important unquantified uncertainties (CRWMS M&O 2000 [DIRS 153246], Appendix F; Cline 2000 [DIRS 153193]). From this set of models and parameters, a subset was identified that is expected to include those most important to annual dose estimates—either annual dose during the 10,000-year period covered by the proposed regulations or longer-term annual dose, out to hundreds of thousands of years (see Section 2.1.1). The longer time period was considered because annual doses over long time periods may produce insights about uncertainty in annual dose that are relevant to all time periods. In selecting uncertainties to address in these supplemental analyses, the DOE considered both the potential impact on TSPA results and the feasibility of modifications to the model and parameter inputs to the TSPA.

1.4.1.2 Quantifying Previously Unquantified Uncertainties

To quantify the uncertainties associated with the identified models and parameters, technical investigators developed unbiased representations of the specified uncertainties. To assist them, an iterative series of interviews were held with representatives from each of the main process model areas affecting performance. The interviews were followed by supplemental calculations and analyses. The emphasis in the discussions was on the physical realism of the models and parameter estimates. The technical investigators used their knowledge of project-specific data, literature data, analogue systems or processes, and the technical judgment of the broader scientific and engineering community to develop these unbiased representations. Specific implementation of the unbiased representations took a variety of forms, as described in Sections 3 through 14. Those forms range from new or updated parameter distributions to new or updated conceptual and mathematical models.

1.4.1.3 Evaluating Alternative Representations

The impacts of the new representations for previously unquantified uncertainties were evaluated through updated process models, sensitivity analyses, and supplemental TSPA analyses using the updated uncertainty treatment. The representations were implemented and the form and rationale for them documented. The implications of these new representations for process-level model results are discussed in Sections 3 through 14 of this document.

For many of these newly quantified uncertainties, supplemental TSPA sensitivity analyses were also conducted, as described in Volume 2 (McNeish 2001 [DIRS 155023]). These included subsystem performance analyses, TSPAs, and analyses similar to those documented and discussed in the TSPA-SR (CRWMS M&O 2000 [DIRS 153246]). The calculated annual doses from the revised representations have been compared to the estimates from the TSPA-SR.

1.4.2 Updating Scientific Bases and Analyses

In addition to the newly quantified uncertainties, additional scientific data have been collected, models have been revised, and analyses have been conducted since the TSPA-SR (CRWMS M&O 2000 [DIRS 153246]). In many cases, technical investigators have summarized new experimental data, updated process models to reflect an improved understanding, or abstracted models that more completely propagate process knowledge into the performance analyses. The incremental update to the scientific bases supporting the S&ER (DOE 2001 [DIRS 153849]) is documented in Sections 3 through 14.

1.4.3 Evaluating a Range of Thermal Operating Modes

The repository design and operating mode described in the S&ER (DOE 2001 [DIRS 153849]) are flexible enough to meet a range of potential thermal conditions or goals. A series of analyses has been conducted to determine feasible thermal ranges and the engineering and operating changes that would allow the potential repository to achieve specified operating temperature limits. For process models where thermal load potentially has an impact on the modeling and model results, technical investigators evaluated repository performance under different thermal loads. In some cases, this required updates to the technical models, which are indicated in Table 1-1 and discussed in Sections 3 through 14.

1.4.3.1 Selecting a Thermal Range

The first step in defining and conducting a thermal sensitivity analysis is to determine the thermal range that should be considered. A number of different thermal goals and constraints have been proposed, specifically focused on lower temperatures in the drift and on the surface of the waste package. A range of operating temperatures was selected for these thermal sensitivity analyses. The high end of the range corresponds to the flexible design and higher-temperature operating mode described in the S&ER (DOE 2001 [DIRS 153849]). The low end corresponds to an operating mode where the average maximum temperatures on the surface of the waste package do not exceed 85°C following closure of the potential repository (Table 2-1).

1.4.3.2 Identifying Operational Changes to Achieve Thermal Goals

The DOE identified a variety of operational changes that would result in lower temperatures in the potential repository. For a variety of thermal environments, the operating parameters that could affect potential repository temperatures were specified, along with the types of changes to those parameters that would be necessary to achieve various operating temperatures. This step also identified other key performance parameters that could be affected by the changes necessary to achieve lower operating temperatures, and is described more fully in Section 2.3 of this report.

1.4.3.3 Evaluating Performance

To evaluate performance over the thermal range being considered, the DOE conducted full supplemental TSPAs for both ends of the thermal range (Table 2-1). The results of the supplemental TSPA evaluations are documented in Volume 2 (McNeish 2001 [DIRS 155023]). In the process model analyses described in this volume, other parts of the thermal range were also evaluated.

1.5 QUALITY ASSURANCE

An activity evaluation was performed for this work activity in accordance with AP-2.21Q, *Quality Determinations and Planning for Scientific, Engineering, and Regulatory Compliance Activities* [DIRS 154534], and it was determined that activities supporting the development of this work and activities documented in this technical product are quality-affecting activities. This technical product and associated activities have been prepared subject to the requirements of the *Quality Assurance Requirements and Description* (DOE 2000 [DIRS 149540]) and implementing procedures. This document was prepared in accordance with the *Technical Work Plan for FY01 Supplemental Science and Performance Analyses: Volume 1-Scientific Bases and Analyses, Volume 2-Performance Analyses* (BSC 2001 [DIRS 155055]). There are no deviations from the technical work plan in this technical product.

The activity evaluation and a Process Control Evaluation for Supplement V, prepared in accordance with AP-SV.1Q, *Control of the Electronic Management of Information* [DIRS 153202]), are attached to the technical work plan. Section 10 of the technical work plan describes the controls that will be used in the electronic management of information for this work activity. The technical work plan provides important planning details and should be consulted if questions or issues arise related to this document and the work activities it describes.

As described in Section 1.2, the goal of the additional analyses presented in this technical report is to provide insights into the effects of uncertainty and both conservatism and optimism that were not evaluated in the family of analysis model reports that supported the S&ER (DOE 2001 [DIRS 153849]) and the TSPA-SR (CRWMS M&O 2000 [DIRS 153246]). Additional analyses are presented to examine the potential performance-related effects associated with operating the repository over a range of thermal operating modes. To provide these insights, the baselined models and analyses used as the technical basis for the TSPA-SR and the S&ER have been modified or extended beyond the bounds utilized in the TSPA-SR (CRWMS M&O 2000 [DIRS 153246]). These alternative representations are provided to evaluate the sensitivity of model performance to these unquantified uncertainties and to incorporate appropriate thermal dependencies into the conceptual representations used in the performance assessment. These alternative representations do not replace those documented in the supporting references to the TSPA-SR or the S&ER. While it may be necessary to modify a parameter distribution or model to examine the effects of these alternative representations, the models used as a basis for the TSPA-SR are not changed; these examinations are simply exploratory sensitivity analyses to provide the necessary insights into system behavior. In many respects, these analyses are no different than the types of sensitivity analyses, barrier importance analyses, and neutralization analyses presented in the TSPA-SR and the *Repository Safety Strategy: Plan to Prepare the Safety Case to Support Yucca Mountain Site Recommendation and Licensing Considerations* (CRWMS M&O 2001 [DIRS 154951]). If any of the revised models or analyses documented in this technical report are deemed to be more appropriate for the intended use of evaluating repository performance, they will be validated and documented in accordance with the quality assurance requirements for models and analyses in AP-3.10Q, *Analyses and Models* [DIRS 154517]. Until such time, they are considered scoping in nature to provide insights into the significance of uncertainty that was not explicitly evaluated in the TSPA-SR.

As a result of the special quality assurance controls applied as described in the Technical Work Plan (BSC 2001 [DIRS 155055]), not all of the models, analyses, and data used in this study are fully qualified. It has not yet been determined which, if any, of the models, analyses, and data need to be fully qualified. Because of quality assurance requirements, the models, analyses, and data used in this study are not intended to be used, as is, in a license application if the Yucca Mountain site is found to be suitable for the development of a repository.

1.6 COMPUTER SOFTWARE USAGE

A number of software codes were used or discussed in this study (Table 1-2). All qualified codes were appropriate for the intended use, and they were used only within the range of validation. All qualified codes were obtained from Software Configuration Management in accordance with AP-SI.1Q, *Software Management* [DIRS 154886].

The software name and version, software tracking number, qualification status reference information, location used, and computer type used are identified in Table 1-2. Reference to software codes within the text will indicate the software name and version, and the reader can use that information and this table to obtain other pertinent information.

Some references within the text may be to families of codes (e.g., the FEHM codes or the ASHPLUME codes). These references are generic in nature and are not intended to identify specific software or versions.

For each unqualified code, a software activity plan for use of unqualified software and a software user request have been submitted to Software Configuration Management. Several commercial software codes (e.g., THERMO-CALC, DICTRA, and FIDAP) were not submitted to Software Configuration Management due to software licensing issues. As only one copy of each of these codes exists on the Yucca Mountain Project, there is no technical issue regarding whether or not the correct version of the code was used. These codes are documented as part of Deficiency Report BSC-01-D-088 or Corrective Action Report BSC-01-C-002.

Commercial off-the-shelf software Tecplot V7.0, GMT V3.3.6, mView V2.20, EarthVision 5.1, SigmaPlot 4.0, and Microsoft Excel SR-1 were used to plot data documented within this report and the references specified. This report and the references document the technical decisions made by the analyst to arrive at the conclusions in this report. Where these plotting software were used, the analyst used professional judgment to determine the best display of the data. All of the technical decisions made regarding the use of the data displayed on the charts and plots in this report are documented in the body of the report, in the references specified for each figure, or both.

INTENTIONALLY LEFT BLANK

Table 1-1. Summary of Supplemental Models and Analyses

Key Attributes of System	Process Model (Section of S&ER)	Topic of Supplemental Scientific Model or Analysis	Reason For Supplemental Scientific Model or Analysis			Section of Volume 1	Performance Assessment Treatment of Supplemental Scientific Model or Analysis (Discussed In Volume 2)		
			Unquantified Uncertainty Analysis	Update in Scientific Information	Lower-Temperature Operating Mode Analysis		TSPA Sensitivity Analysis	Included in Supplemental TSPA Model	
Limited Water Entering Emplacement Drifts	Climate (4.2.1)	Post-10,000-year Climate Model		X		3.3.1	X	X	
	Net Infiltration (4.2.1)	Infiltration for post-10,000-year Climate Model		X		3.3.2	X	X	
	Unsaturated Zone Flow (4.2.1)	Flow in PTn			X		3.3.3		
		3-D flow fields for cooler design; flow fields for post-10,000 yr climate, lateral flow; variable thickness of PTn; fault property uncertainty			X	X	3.3.4		
		Effects of lithophysal properties on thermal properties			X		3.3.5		X
	Coupled Effects on UZ Flow (4.2.2)	Mountain-scale Thermal-Hydrologic effects			X	X	3.3.5		
		Mountain-scale Thermal-Hydrologic-Chemical effects			X	X	3.3.6		
		Mountain-scale Thermal-Hydrologic-Mechanical effects			X	X	3.3.7		
	Seepage into Emplacement Drifts (4.2.1)	Flow-focussing within heterogeneous permeability field; episodic seepage		X		X	4.3.1, 4.3.2, 4.3.5	X	X
		Effects rock bolts and drift degradation on seepage		X			4.3.3, 4.3.4		
	Coupled Effects on Seepage (4.2.2)	Thermal effects on seepage		X		X	4.3.5	X	X
		Thermal-Hydrologic-Chemical effects on seepage		X		X	4.3.6		
		Thermal-Hydrologic-Mechanical effects on seepage			X	X	4.3.7		

Table 1-1. Summary of Supplemental Models and Analyses (Continued)

Key Attributes of System	Process Model (Section of S&ER)	Topic of Supplemental Scientific Model or Analysis	Reason For Supplemental Scientific Model or Analysis			Section of Volume 1	Performance Assessment Treatment of Supplemental Scientific Model or Analysis (Discussed In Volume 2)	
			Unquantified Uncertainty Analysis	Update in Scientific Information	Lower-Temperature Operating Mode Analysis		TSPA Sensitivity Analysis	Included in Supplemental TSPA Model
Long-Lived Waste Package and Drip Shield	Water Diversion Performance of EBS (4.2.3)	Multiscale thermal-hydrologic model, including effects of rock dryout	X		X	5.3.1		X
		Thermal property sets	X	X		5.3.1		X
		Effect of in-drift convection on temperatures, humidities, invert saturations, and evaporation rates	X		X	5.3.2		
		Composition of liquid and gas entering drift	X		X	6.3.1	X	X
		Evolution of in-drift chemical environment	X		X	6.3.3	X	X
		Thermo-Hydro-Chemical model comparison to plug-flow reactor and fracture plugging experiment		X		6.3.1		
		Rockfall		X		6.3.4		
	In-Drift Moisture Distribution (4.2.5)	Environment on surface of drip shields and waste packages	X			5.3.2, 7.3.1		
		Condensation under drip shields	X			8.3.2	X	
		Evaporation of seepage	X		X	8.3.1 5.3.2	X	X
		Effect of breached drip shields or waste package on seepage	X		X	8.3.3	X	X
		Waste package release flow geometry (flow-through, bathtub)	X			8.3.4	X	
	Drip Shield Degradation and Performance (4.2.4)	Local chemical environment on surface of drip shields (including Mg, Pb) and potential for initiating localized corrosion	X			7.3.1		

Table 1-1. Summary of Supplemental Models and Analyses (Continued)

Key Attributes of System	Process Model (Section of S&ER)	Topic of Supplemental Scientific Model or Analysis	Reason For Supplemental Scientific Model or Analysis			Section of Volume 1	Performance Assessment Treatment of Supplemental Scientific Model or Analysis (Discussed In Volume 2)	
			Unquantified Uncertainty Analysis	Update in Scientific Information	Lower-Temperature Operating Mode Analysis		TSPA Sensitivity Analysis	Included in Supplemental TSPA Model
Long-Lived Waste Package and Drip Shield	Waste Package Degradation and Performance (4.2.4)	Local chemical environment on surface of waste packages (including Mg, Pb) and potential for initiating localized corrosion	X			7.3.1		
		Aging and phase stability effects on A-22	X	X		7.3.2	X	
		Uncertainty in weld stress state following mitigation	X			7.3.3	X	X
		Weld defects	X			7.3.3	X	X
		Early failure due to improper heat treatment	X		X	7.3.6	X	X
		General corrosion rate of A-22: Temperature dependency	X		X	7.3.5	X	X
		General corrosion rate of A-22: Uncertainty/variability partition	X			7.3.5	X	X
		Long-term stability of passive films on A-22	X			7.3.4		
		Stress threshold for initiation of stress corrosion cracking	X	X		7.3.3	X	X
		Probability of non-detection of manufacturing defects		X		7.3.3	X	X
		Number of defects		X		7.3.5	X	X
		Distribution of crack growth exponent (repassivation slope)	X	X		7.3.7	X	X
Limited Release of Radionuclides from the Engineered Barriers	In-Package Environments (4.2.6)	Effect of HLW glass degradation rate and steel degradation rate on in-package chemistry	X		X	9.3.1	X	X
	Cladding Degradation and Performance (4.2.6)	Effect of initial perforations, creep rupture, stress corrosion cracking, localized corrosion, seismic failure, rock overburden failure, and unzipping velocity on cladding degradation	X		X	9.3.3	X	X

Table 1-1. Summary of Supplemental Models and Analyses (Continued)

Key Attributes of System	Process Model (Section of S&ER)	Topic Of Supplemental Scientific Model or Analysis	Reason For Supplemental Scientific Model or Analysis			Section of Volume 1	Performance Assessment Treatment of Supplemental Scientific Model or Analysis (Discussed In Volume 2)		
			Unquantified Uncertainty Analysis	Update in Scientific Information	Lower-Temperature Operating Mode Analysis		TSPA Sensitivity Analysis	Included in Supplemental TSPA Model	
Limited Release of Radionuclides from the Engineered Barriers	DHLW Degradation and Performance (4.2.6)	HLW glass degradation rates	X	X	X	9.3.1			
	Dissolved Radionuclide Concentrations (4.2.6)	Solubility of neptunium, thorium, plutonium, and technetium	X	X	X	9.3.2	X	X	
	Colloid-Associated Radionuclide Concentrations (4.2.6)	Colloid mass concentrations	X			9.3.4	X		
	EBS (Invert) Degradation and Transport (4.2.6, 4.2.7)	Diffusion inside waste package		X	X		10.3.1	X	X
		Transport pathway from inside waste package to invert		X	X		10.3.2		
		Sorption inside waste package		X	X		10.3.4	X	X
		Sorption in invert		X	X		10.3.4	X	X
		Diffusion through invert		X			10.3.3	X	X
		Colloid stability in the invert		X			10.3.5		
		Microbial transport of colloids		X	X		10.3.6		

Table 1-1. Summary of Supplemental Models and Analyses (Continued)

Key Attributes of System	Process Model (Section of S&ER)	Topic of Supplemental Scientific Model or Analysis	Reason For Supplemental Scientific Model or Analysis			Section of Volume 1	Performance Assessment Treatment of Supplemental Scientific Model or Analysis (Discussed In Volume 2)	
			Unquantified Uncertainty Analysis	Update in Scientific Information	Lower-Temperature Operating Mode Analysis		TSPA Sensitivity Analysis	Included in Supplemental TSPA Model
Delay and Dilution of Radionuclide Concentrations by the Natural Barriers	Unsaturated Zone Radionuclide Transport (Advective Pathways; Retardation; Dispersion; Dilution) (4.2.8)	Effect of drift shadow zone - advection/diffusion splitting	X		X	11.3.1	X	X
		Effect of drift shadow zone - concentration boundary condition on EBS release rates	X			11.3.1		
		Effect of matrix diffusion	X			11.3.2, 11.3.3		
		3-D transport			X	11.3.2		
		Effect of coupled Thermo-Hydrologic, Thermo-Hydro-Chemical, and Thermo-Hydro-Mechanical processes on transport		X	X	11.3.5		
	Saturated Zone Radionuclide Flow and Transport (4.2.9)	Groundwater specific discharge	X	X		12.3.1	X	
		Effective diffusion coefficient in volcanic tuffs	X			12.3.2	X	
		Flowing interval spacing				12.3.2	X	
		Flowing interval (fracture) porosity	X			12.3.2	X	
		Effective porosity in the alluvium	X			12.3.2	X	
		Correlation of the effective diffusion coefficient with matrix porosity	X			12.3.2	X	
	Bulk density of the alluvium	X	X		12.3.2	X	X	

Table 1-1. Summary of Supplemental Models and Analyses (Continued)

Key Attributes of System	Process Model (Section of S&ER)	Topic of Supplemental Scientific Model or Analysis	Reason For Supplemental Scientific Model or Analysis			Section of Volume 1	Performance Assessment Treatment of Supplemental Scientific Model or Analysis (Discussed In Volume 2)	
			Unquantified Uncertainty Analysis	Update in Scientific Information	Lower-Temperature Operating Mode Analysis		TSPA Sensitivity Analysis	Included in Supplemental TSPA Model
Delay and Dilution of Radionuclide Concentrations by the Natural Barriers	Saturated Zone Radionuclide Transport (4.2.9)	Retardation for radionuclides irreversibly sorbed on colloids in the alluvium	X	X		12.3.2	X	
		No matrix diffusion in volcanic tuffs case				12.5.2	X	
		Presence or absence of alluvium				12.5.2	X	
		Sorption coefficient in alluvium for I, Tc	X	X		12.3.2	X	X
		Sorption coefficient in alluvium for Np, U	X	X		12.3.2	X	
		Sorption coefficient for Np in volcanic tuffs	X			12.3.2	X	
		Kc model for groundwater colloid concentrations Pu, Am		X		12.5.2	X	
		Enhanced matrix diffusion in volcanic tuffs				12.5.2	X	
		Effective longitudinal dispersivity	X	X		12.3.2	X	
		New dispersion tensor		X		12.3.2		
		Flexible design				X	12.3.2	
	Different conceptual models of the large hydraulic gradient and their effects on the flow path and specific discharge			X		12.3.1		
	Hydraulic head and map of potentiometric surface			X		12.3.1		
	Biosphere (4.2.10)	Receptor of interest	X			13.3.1		
		Comparison of dose assessment methods	X			13.3.2		
		Radionuclide removal from soil by leaching	X			13.3.3		
		Uncertainties not captured by GENII-S	X			13.3.4		
Influence of climate change on groundwater usage and BDCFs		X			13.3.5, 13.3.7			
BDCFs for groundwater and igneous releases				X		13.3.6, 13.3.8, 13.4	X	X

Table 1-1. Summary of Supplemental Models and Analyses (Continued)

Key Attributes of System	Process Model (Section of S&ER)	Topic of Supplemental Scientific Model or Analysis	Reason For Supplemental Scientific Model or Analysis			Section of Volume 1	Performance Assessment Treatment of Supplemental Scientific Model or Analysis (Discussed In Volume 2)	
			Unquantified Uncertainty Analysis	Update in Scientific Information	Lower-Temperature Operating Mode Analysis		TSPA Sensitivity Analysis	Included in Supplemental TSPA Model
Low Mean Annual Dose Considering Potentially Disruptive Events	Volcanism/Igneous Activity (4.3.2)	Probability of dike intersection of repository for the operating mode described in S&ER		X		14.3.3.1		X
		Scaling factors to evaluate impacts of repository design changes			X	14.3.3.2		
		Contribution to release of Zones 1 and 2		X		14.3.3.3	X	
		Sensitivity to waste particle size distribution		X		14.3.3.4	X	
		New wind speed data		X		14.3.3.5	X	X
		Explanation of method for handling ash/waste particle size and density		X		14.3.3.6		
		Volcanism inputs for Supplemental TSPA Model		X		14.3.3.7		X
		New aeromagnetic data		X		14.3.3.8		

NOTE: S&ER = *Yucca Mountain Science and Engineering Report* [DOE 2001 [DIRS 153849)].

^a Performance assessment treatment of supplemental scientific model or analysis discussed in SSPA Volume 2 (McNeish 2001 [DIRS 155023]).

Table 1-2. Computer Software

Software Name	Software Version	Software Tracking Number (STN)	Qualified	DIRS Reference Number	Location Used	Computer Type Used
2kgrid8.for	1.0	10503-1.0-00	No	154787	LBNL	3
3DEC	2.0	10025-3.0-00	Yes	150512	LV, LLNL	3
add_repo_nodes.f	1.0	10548-1.0-00	No	155081	LANL	1
AddBound	1.0	10357-1.0-00	Yes	152823	LBNL	1
ANSYS	5.2SGI	30013-5.2SGI	Yes	152788	LV	4
ANSYS	5.6.2	10145-5.6.2-00	Yes	154671	LV	2
ASHPLUME	1.4LV-dll	10022-1.4LV-dll	Yes	154748	LV	3
AssignRock	1.0	10465-1.0-00	Yes	154321	LBNL	1
bot_sum.f	1.0	10349-1.0-00	Yes	153471	LBNL	2
CalBT.for	1.0	10504-1.0-00	No	154788	LBNL	3
CORPSCON	5.11.08	10547-5.11.08-00	No	155082	LANL	3
CutDrift	1.0	10375-1.0-00	Yes	152816	LBNL	1
CutNiche	1.3	10402-1.3-00	Yes	152828	LBNL	1
CWD	1.00	10363-1.0-00	Yes	152624	LV	3
DCPT	1.0	10078-1.0-00	Yes	132448	LBNL	3
DCPT	2.0	10078-2.0-00	No	154342	LBNL	3
Delb.dat	1.0	10507-1.0-00	No	154791	LBNL	3
DICTRA	2.0	10391-2.0-00	No	155083	LLNL	1
DRKBA	3.3	10071-3.3-00	Yes	149991	LV	3
EARTHVISION	5.1	10174-5.1-00	Yes	152614	LBNL	4
EQ3/6	7.2b	UCRL-MA-110662	Yes	153964	SNL	3
EQ6	7.2bLV	10075-7.2bLV-00	Yes	127275	SNL	3
EXT	1.0	10047-1.0-00	Yes	134141	LBNL	1
FEHM	2.11	10086-2.11-00	No	155084	SNL	1 and 3
FEHM	2.10	10086-2.10-00	Yes	132447	SNL	1 and 3
FEHM	2.00	10031-2.00-00	Yes	146971	SNL	1
FIDAP	8.0	10549-8.0-00	No	155189	LLNL	3
FLAC3D	2.0	10502-2.0-00	No	154783	LBNL	3
FLAC3D	2.0	10502-2.0-00	Yes	154783	LV	3

Table 1-2. Computer Software (Continued)

Software Name	Software Version	Software Tracking Number (STN)	Qualified	DIRS Reference Number	Location Used	Computer Type Used
FLUENT	5.5	10550-5.5-00	No	155190	LLNL	1
GENII-S	1.4.8.5	30034 V1.4.8.5	Yes	117076	LV	3
get_a_layer_v0.f	1.0	10221-1.0-00	Yes	147025	LBNL	1
GoldSim	6.04.007	10344-6.04.007-00	Yes	151202	LV	3
Gpzones.dat	1.0	10509-1.0-00	No	154792	LBNL	3
GSLIB	1.0 Module SISIM V1.203	10001-1.0MSISIMV1.203-00	Yes	134136	LBNL	1
GSLIB	2.0 Module SISIM V2.0	10098-2.0MSISIMV2.0-00	Yes	146609	LBNL	1
GVP	1.02	10341-SRR-1.02-00	Yes	152496	LV	3
hsource_v0.f	1.0	10225-1.0-00	Yes	147031	LBNL	1
Image Pro Plus	4.1	10422-4.1-00	No	155085	LLNL	1
INFIL	2.0	10307-2.0-00	No	139422	USGS	3
infil2grid	1.7	10077-1.7-00	No	154793	LBNL	3
ITOUGH2	3.2	10054-3.2-00	Yes	154337	LBNL	1
ITOUGH2	3.2_drift	10055-3.2_DRIFT-00	Yes	112757	LBNL	1
iTOUGH2	4.0	10003-4.0-00	Yes	139918	LBNL	1 and 2
iTOUGH2	4.4	10003-4.4-00	No	154784	LBNL	1
mddf.f	2.0	10456-2.0-00	Yes	154347	LBNL	1
Meshbd.f	1.0	10467-1.0-00	Yes	152871	LBNL	1
MINCgridv1.f	1.0	10469-1.0-00	Yes	154343	LBNL	2
MING	1.0	30018 V1.0	Yes	145225	SNL	3
mininipresf.f	1.0	10470-1.0-00	Yes	152872	LBNL	1
minrefine3df.f	1.0	10472-1.0-00	Yes	152880	LBNL	1
mk_generGL.f	1.0	10476-1.0-00	Yes	154349	LBNL	1
MkTable	1.00	10505-1.00-00	Yes	154921	LV	3
MoveMesh	1.0	10358-1.0-00	Yes	152824	LBNL	1
MSTHAC	6.4.2	10419-6.4.2-00	No	155324	LLNL	1
MULTIFLUX	1.0	10485-1.0-00	No	155087	SNL	1
MVIEW	2.20	10072-2.20-00	Yes	155201	LV	1, 2, and 4
NUFT	3.0s	10088-3.0s-00	Yes	127906	SNL, LLNL, LV	1
parallelf.java	1.0	10457-1.0-00	Yes	154346	LBNL	3

Table 1-2. Computer Software (Continued)

Software Name	Software Version	Software Tracking Number (STN)	Qualified	DIRS Reference Number	Location Used	Computer Type Used
Perm2Mesh	1.0	10359-1.0-00	Yes	152826	LBNL	1
RADPRO	3.22	10204-322-00	Yes	148637	LLNL	1
Routine Rick1	1.0	10474-1.0-00	Yes	154344	LBNL	1
SCCD	2.01	10343-SRR-2.01-00	Yes	152499	LV, SRR	3
SOLVEQ/CHILLER	1.0	10057-1.0-00	Yes	153217	LBNL	3
T2R3D	1.4	10006-1.4-00	Yes	113942	LBNL	1 and 2
THERMO-CALC	VM	10170-M-00	No	155088	LLNL	1
tin.dat	1.0	10512-1.0-00	No	154794	LBNL	3
TOUGH2	1.11MEOS9nTV1.0	10065-1.11MEOS9NTV1.0-00	Yes	113943	LBNL	1
TOUGH2	1.4	10007-1.4-01	Yes	146496	LBNL	1 and 2
TOUGH2	1.5	10007-1.5-00	No	154322	LBNL	1 and 2
TOUGHREACT	2.3	10396-2.3-00	No	153101	LBNL	1 and 2
TOUGHREACT	2.2	10154-2.2-00	Yes	153219	LBNL	1 and 2
vf_con.for	1.0	10466-1.0-00	Yes	154345	LBNL	3
WAPDEG	4.0	10000-4.0-2.0	Yes	155166	LV	3
Wingridder	2.0	10024-2.0-00	No	154785	LBNL	3
Wingridder	1.1	10024-1.1-00	Yes	154341	LBNL	3
XTOOL	10.1	10208-10.1-00	Yes	148638	SNL, LLNL, LV	1
YMESH	1.53	10172-1.53-00	Yes	147574	LLNL	1

NOTE: Computer type: (1) SUN UltraSparc, (2) DEC-Alpha, (3) PC, (4) SGI INDIGO.

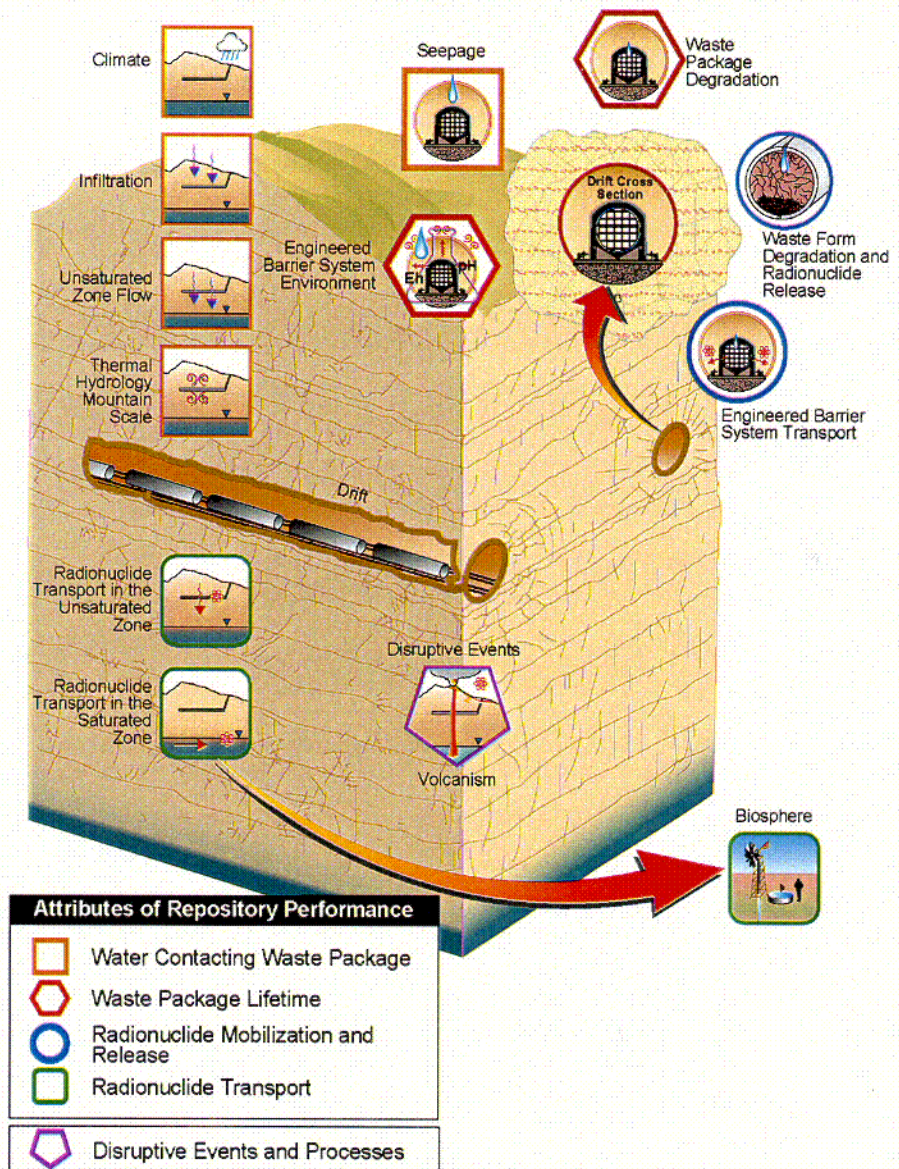


Figure 1-1. Components of the SSPA Analyses, showing the Relationship of Major Processes Expected to Occur in the Mountain and the Potential Repository System

COI

INTENTIONALLY LEFT BLANK

2. METHODS AND APPROACH

2.1 QUANTIFICATION OF UNCERTAINTIES

The U.S. Department of Energy (DOE) identified a variety of uncertainties, arising from different sources, during its assessment of the performance of a potential repository at the Yucca Mountain site. In general, the number and detail of process models developed for the Yucca Mountain site, and the complex coupling among those models, make the direct incorporation of all uncertainties difficult. The DOE has addressed these issues in a number of ways using an uncertainty strategy that is focused on producing a defensible, compliance-based evaluation of the performance of a potential repository. As part of that evaluation, many uncertainties have been treated in a defensible (typically conservative) manner in the analyses and model reports supporting the *Yucca Mountain Science and Engineering Report (S&ER)* (DOE 2001 [DIRS 153849]). Conservative assumptions and parameter bounds have been used to increase defensibility or decrease modeling complexity.

The result is that the DOE has used a mix of probabilistic representations and single-valued estimates to characterize parameters. There are also cases where more than one conceptual model may be consistent with available data and observations. In the absence of definitive data or compelling technical arguments for a specific conceptual, process, or abstracted model, a conservative representation was chosen. This approach has been used in other projects to demonstrate compliance with a regulatory standard (Goodwin et al. 1994 [DIRS 124152]), but it does not permit quantification of the degree of conservatism associated with projected performance relative to the regulatory standard. Mixing various degrees of conservatism in models and parameter representations reduces the transparency of the analysis and makes the development of coherent and consistent probability statements about projected repository performance difficult.

Accompanying the recognition of inherent uncertainties and a need for transparency is the responsibility to identify and communicate the uncertainties as clearly and meaningfully as possible. The DOE initiated the assessment of the treatment of uncertainties described in this volume to improve this identification and communication. Work has been done to quantify some previously unquantified uncertainties and evaluate their implications for overall repository performance. The approach used to evaluate these uncertainties is described below.

2.1.1 Identification of Unquantified Uncertainties

2.1.1.1 Preliminary Identification of Conservatism

The evaluation began with the identification and definition of models and parameter inputs to total system performance assessment (TSPA) for which uncertainty has not been quantified (i.e., a conservative or nonconservative representation exists in the present performance assessment). Several recent studies focused on identifying potentially important unquantified uncertainties (CRWMS M&O 2000 [DIRS 153246], Appendix F; Cline 2000 [DIRS 153193]).

The *Total System Performance Assessment for the Site Recommendation (TSPA-SR)* (CRWMS M&O 2000 [DIRS 153246], Appendix F) identifies approximately 25 process model and TSPA-SR components in which key system attributes were modeled in a conservative manner.

The report also describes the rationale for these conservatisms. In a separate activity, other project technical reviewers conducted a preliminary evaluation of how realistic the process models are based on an assessment of model parameters and assumptions (Cline 2000 [DIRS 153193]). The reviewers selected 87 model components and evaluated them for representativeness, importance to the process model, and importance to repository performance. These evaluations were based on the professional judgment of the reviewers. The results of this preliminary evaluation suggest that levels of conservatism are found throughout the models and that the conservatisms were used as a way to address uncertainty. Many of these model components can be modified, or alternative representations can be developed to more realistically or fully capture uncertainties, and the impacts of those changes evaluated through supplemental analyses.

The TSPA-SR (CRWMS M&O 2000 [DIRS 153246]) and Cline (2000 [DIRS 153193]) provided a starting point for identifying the unquantified uncertainties to be addressed in the analyses documented in this report.

2.1.1.2 Selection of Uncertainties to be Quantified

TSPA analyses and associated sensitivity analyses have been conducted to identify those inputs to which the calculated annual dose estimates are most sensitive (e.g., CRWMS M&O 2000 [DIRS 153246]). However, sensitivity and uncertainty analyses can identify as contributors to uncertainty only those inputs that have been treated as variable (e.g., those quantities represented by a range of values). Uncertainties that were not represented in the models as uncertain inputs (e.g., single-valued estimates) cannot be identified as important contributors in uncertainty analyses. Therefore, the identification of unquantified uncertainties was extended beyond those identified by the activities described in Section 2.1.1.1. The results of those activities provided a starting point for discussions and consultations with Yucca Mountain Site Characterization Project technical investigators to gain insights into which unquantified uncertainties are most important to performance. Insights and suggestions from independent review groups (e.g., the Nuclear Waste Technical Review Board) on important uncertainties were also considered as part of the identification of unquantified uncertainties in the performance assessment modeling. Technical experts directly involved in the TSPA-SR modeling (CRWMS M&O 2000 [DIRS 153246]) have the most comprehensive understanding of which inputs have the greatest potential to affect the dose estimates. The project technical investigators have the most comprehensive understanding of how uncertainties in their area of technical expertise were treated and where conservatisms, nonconservatisms, and single-valued assessments may exist. In selecting unquantified uncertainties to address in the near-term, technical experts considered both the potential impact on TSPA results and the feasibility of modifications to the model and parameter inputs to the TSPA. Based on these objectives, the uncertainties listed in Table 1-1 were selected for these supplemental evaluations.

2.1.2 Quantification of Unquantified Uncertainties

To quantify the uncertainties associated with the various models and parameters identified in Table 1-1, technical investigators were asked to develop unbiased representations of the identified uncertainties. Unbiased estimates are neither deliberately conservative nor deliberately optimistic. To assist in this effort, an iterative series of discussions, followed by

supplemental calculations and analyses, were held with representatives from each of the process model areas shown in Table 1-1. The emphasis in the discussions was on the physical realism of the models and parameter estimates. The technical investigators used their knowledge of project-specific data, literature data, analogue systems or processes, and the technical judgment of the broader scientific and engineering community to develop these unbiased distributions.

In these discussions, a facilitator worked with the technical experts to develop complete expressions of uncertainties. Each discussion included the technical investigators who initially developed the process models abstracted for use in the TSPA and the performance assessment modelers familiar with the TSPA model and the specific input parameters. At the beginning of each discussion, facilitators provided an introduction to the use of expert judgment in quantifying uncertainties. This introduction included a discussion of the motivational and cognitive biases that can affect uncertainty assessments, as well as the responsibility of the technical investigators to consider and evaluate alternative interpretations and represent the uncertainty that would be expressed by the larger technical community.

During each discussion, the current treatment of each component in the TSPA-SR (CRWMS M&O 2000 [DIRS 153246]) was described, including the technical bases for the assessment and the manner in which the model has been abstracted for use in the performance assessment. This was followed by a consideration and discussion of alternative, more representative modeling approaches and parameter distributions. In some cases, the parameter/model uncertainty identified was broken down into several parts for more efficient uncertainty quantification. For example, for the waste form degradation topic, in-package chemistry (principally pH and the partial pressure of carbon dioxide) is primarily related to the rate of degradation of the internal components of the waste package. The components for which uncertainties were not quantified in the TSPA-SR included the high-level waste glass and steel support structures. These components include the high-level waste glass and steel internal support structures, so representative degradation rates and their uncertainties were developed for these components, as described in Section 9.3. The technical investigators were also asked to consider the implications of a lower-temperature operating mode (LTOM) for the uncertainties being evaluated. In this LTOM, waste package surface temperature does not exceed 85°C during the postclosure period (see Section 2.3).

2.1.2.1 Development of New Information

The discussions were followed by a period of time during which the investigators could further develop their models and consider how uncertainties could best be represented. In updating their models and uncertainty treatment, the investigators considered the applicability of more representative (e.g., less conservative) models, the probability distributions for input parameters, and modeling uncertainties. Investigators compiled applicable data, conducted necessary calculations, and developed updated uncertainty distributions. Often the original conservative models and parameter assumptions were made because large uncertainties existed. Thus, the revised estimates were expected to indicate a broad range for the uncertain quantity. The objective was to quantify the uncertainties with probability distributions to the greatest extent possible, based on the judgment of the investigators. In addition to parameter distributions, in some cases alternative conceptual models were identified to provide a more representative assessment of the processes that may affect repository performance. After each period of

evaluation, the investigators met again and reviewed the models and parameters as a group until a consensus was reached that the uncertainties have been properly characterized. The technical bases (e.g., available data, modeling results, analogues, and professional judgment) and results of the assessments are documented in Sections 3 through 14 of this volume.

2.1.2.2 Evaluation of Newly-Quantified Uncertainties

The new information related to the uncertainty quantification was abstracted for the TSPA models, so the updated process model inputs and TSPA parameters capture the full range of newly quantified uncertainties. The method, approach, and analyses of overall system performance are described in Volume 2 (McNeish 2001 [DIRS 155023]).

2.2 UPDATED SCIENTIFIC BASES AND ANALYSES

The scientific analyses and models that provide the bases for the TSPA-SR (CRWMS M&O 2000 [DIRS 153246]) process models are provided in the analysis model reports supporting the S&ER (DOE 2001 [DIRS 153849]). These reports describe the key attributes of the system and the process models at the time of their development. That understanding is represented by observational and experimental data analyses, models of relevant processes, and representations of conceptual model and parameter uncertainties. Abstractions of this technical understanding are made to represent the essential elements of each process in the performance analyses. Sections 3 through 14 describe supplemental analyses based on updates to these scientific bases.

Modifications to the work presented in the S&ER (DOE 2001 [DIRS 153849]) include updates based on the newly-quantified uncertainties, new or updated models and analyses, and analyses to evaluate the effects of thermal operating modes. These assessments are summarized in Table 1-1 and described in detail in subsequent sections of this volume. In many cases, an assessment conducted to evaluate previously unquantified uncertainties is not easily distinguishable from an updated model. For example, neptunium solubility is identified in Table 1-1 as an unquantified uncertainty for which a bounding solubility was used (as a function of pH). To quantify the uncertainty, applicable solubility data were compiled and a new conceptual model was developed that draws on analogies to the dissolution of schoepite. Application of this conceptual model and consideration of available experimental data resulted in a revised solubility relationship that quantifies the associated uncertainties (see Section 9.3.4). Clearly, this assessment would fall in the updated-model category, but it is also in the unquantified uncertainty category.

In other cases, updates have focused on incorporating new data, using better model calibration, or building more physically representative models, without an explicit focus on uncertainty quantification. Finally, for some of the updates shown in Table 1-1, sensitivity analyses have been conducted to determine the potential importance of a parameter or a model without a concerted attempt to quantify the uncertainties in those parameters or models.

2.3 THERMAL SENSITIVITY ANALYSES

During development of the S&ER (DOE 2001 [DIRS 153849]), a systematic evaluation was performed to determine design features and operational practices that could be used to manage

the thermal environment in the repository, and particularly to produce a LTOM. This evaluation was updated in a design analysis (BSC 2001 [DIRS 154554]). Volume 2 (McNeish 2001 [DIRS 155023]) describes the results of a TSPA conducted for one LTOM within the range of potential options. This option, described in Section 2.3.4, was selected in part because it could be analyzed with the same models used to analyze the higher-temperature operating mode. Sensitivity studies at the process model level are used to explore the behavior of the system at other points in the range of thermal operating modes considered. The evaluation of the options identified in the S&ER (DOE 2001 [DIRS 153849]) and *Low Temperature Subsurface Layout and Ventilation Concepts* (BSC 2001 [DIRS 154554]) will be considered during the selection of the design and operating modes for the potential repository.

2.3.1 Design and Operating Mode Evolution

As discussed in Section 1.3.3 of this report, refining the design for the potential repository and the mode in which the design is operated has been an ongoing, iterative process involving scientists, engineers, and decision-makers. The repository design under consideration is flexible in that it can be operated over a range of thermal conditions. The iterative design process has focused on improving the understanding of the contribution of design features to the performance of a potential repository and to uncertainty in that performance. The approach used to evaluate performance over a thermal range examines the relationship of design features and operational practices to the range of operating temperatures and environmental conditions and evaluates the performance and uncertainties associated with the temperature variation. If an operational parameter is shown to have a significant effect on the performance of the repository, it is evaluated further to assess its impact.

Evaluations considering the performance of a design over a range of thermal operating modes provide information to guide the future development of the repository design and operations. The evolution of the design and operating mode will take advantage of insights gained through performance analyses. The flexible design, which will continue to evolve for license application if the Yucca Mountain site is recommended, will include a set of operational parameters that can be managed to accommodate a waste stream with potentially evolving thermal characteristics. Adjustments will continue during the emplacement period based on updated information pertaining to the waste stream and other repository variables.

The evaluation of the performance characteristics of the potential repository design over a range of operating conditions is an important step in the evolution of the design of a repository at Yucca Mountain. While certain details of design have been defined to understand the environmental conditions as input to the performance analyses, the focus of the evaluations presented in this document is on quantification of uncertainty in performance, rather than on verification of the functionality of specific design features or operational concepts. Thus, the evaluations are based on the thermal performance implications of the design and accompanying range of operating modes, rather than on the specific details of how the operating mode might be implemented as an optimized design.

2.3.2 Range of Thermal Operating Modes and Bases

The S&ER (DOE 2001 [DIRS 153849]) describes a flexible design that could be operated over a range of temperatures. These alternative thermal operating modes would each have advantages and disadvantages in analyses of potential repository performance.

Three possible operating strategies are discussed below. Total system performance assessments for the first and third examples are presented in Volume 2 (McNeish 2001 [DIRS 155023]). Other sensitivity studies are described in Sections 3 through 14 of this report to gain insights into the effect that managing the thermal environment in the repository might have on repository performance.

Manage Boiling Fronts within the Rock Pillars and Peak Cladding Temperatures—The higher end of the thermal operating mode under consideration provides a moderate temperature repository environment compared to the design described in the, *Viability Assessment of a Repository at Yucca Mountain* (DOE 1998 [DIRS 101779]). This mode, which is the basis for the evaluations in the S&ER (DOE 2001 [DIRS 153849]), is intended to keep the boiling fronts from coalescing in the rock pillars between the emplacement drifts, preserving the capability of the rock mass to drain percolation flux through the repository horizon at all times. The close spacing of waste packages with thermally blended inventories in this higher-temperature operating mode achieves a relatively uniform distribution of rock temperatures along the drift, limiting potentially complex thermal-mechanical effects resulting from a varying thermal gradient along the drift axis. This operating mode would also meet a design requirement established to maintain the integrity of the cladding by not exceeding a spent nuclear fuel (SNF) cladding temperature of 350°C. The higher-temperature operating mode described in Table 2-1 addresses this strategy.

Keeping Drift Wall Temperatures Below Boiling—In the operating mode described in the S&ER (DOE 2001 [DIRS 153849]), the rock temperatures within the first several meters outside the emplacement drifts exceed the boiling point of water for about a thousand years. One possible lower-temperature objective is to keep all the rock in the repository below the boiling point of water to reduce uncertainties associated with coupled thermal-hydrologic-chemical-mechanical processes driven by the boiling of water. The lower-temperature operating mode in Table 2-1 addresses this operating strategy.

Manage Waste Package Surface Temperatures to Reduce Uncertainty in Corrosion Rates—The lower-temperature end of the range of thermal operating modes was defined by considering the potential for reducing uncertainty in the rate of corrosion for Alloy 22. Evidence described in the S&ER (DOE 2001 [DIRS 153849], Section 2.1.5) indicates that corrosion rates are dependent on both temperature and humidity, and that at temperatures below about 85°C and relative humidity (RH) below 50 percent, the susceptibility of Alloy 22 to crevice corrosion is very low. Operating the repository so that the temperature and relative humidity are below this window of crevice corrosion susceptibility may increase confidence that corrosion will not significantly reduce waste package service life. Measurements to date in repository-relevant water chemistries have shown very low general corrosion rates and no crevice corrosion of Alloy 22 (DOE 2001 [DIRS 153849], Sections 4.2.4.1 and 4.2.4.2). However, extrapolating measurements taken over short times (years) to the periods mandated in regulatory requirements

(e.g., 10,000 years) introduces uncertainties. The lower-temperature operating mode described in Table 2-1 addresses this strategy.

2.3.3 Operating Flexibility to Achieve a Range of Thermal Operating Modes

There are many ways of combining operational parameters to limit repository temperatures. Some of the possible combinations are discussed in the S&ER (DOE 2001 [DIRS 153849], Section 2.1.5) and several preliminary engineering evaluations, most notably *Low Temperature Subsurface Layout and Ventilation Concepts* (BSC 2001 [DIRS 154554]), *Operating a Below-Boiling Repository: Demonstration of Concept* (CRWMS M&O 2000 [DIRS 152146]), and *Natural Ventilation Study: Demonstration of Concept* (CRWMS M&O 2000 [DIRS 152269]). Figure 2.3.4-1 illustrates the variables affecting the thermal performance of the repository, from waste forms to emplacement drifts. Within the constraints imposed by the physical system, the repository can be operated in lower-temperature modes while also meeting other technical operational objectives. Drift wall and waste package temperatures and in-drift relative humidity can be managed by altering three operational features of any specified underground layout (CRWMS M&O 2000 [DIRS 152146], Section 3.2):

- Varying the thermal load to the repository by managing the thermal output of the waste packages
- Managing the period and rate of drift ventilation prior to repository closure
- Varying the distance between waste packages in emplacement drifts.

These factors are described below. Other operational parameters, such as long-term post-emplacement natural ventilation, could also be used to reduce peak repository temperatures (CRWMS M&O 2000 [DIRS 152269]). In addition, altering design features, such as emplacement drift spacing, could be used in conjunction with variations in operational parameters to achieve a lower-temperature repository environment.

Thermal Output of the Waste Packages—The major source of heat in the repository is commercial SNF, which will likely have a wide range of thermal outputs. The thermal load of the repository is directly related to the amount of thermal energy generated by radioactive decay in the fuel emplaced in it. The thermal energy contained in the fuel, in turn, is directly related to its age (time after removal from the reactor) and burnup (time and power level at which the fuel was irradiated in the reactor). The age and burnup of SNF received for emplacement in a repository will vary considerably, so the current operational plan for the repository specifies that the DOE will manage the fuel inventory by one or more of the following approaches:

- Fuel blending (placing low heat output fuel with high heat output fuel within a waste package)
- De-rating (limiting the number of SNF assemblies to less than the waste package design capacity)

- Placing high heat output fuel in smaller waste packages
- Aging (delaying emplacement of high heat output fuel until radioactive decay has reduced its heat level).

Managing the average thermal output of waste packages through any of these means can reduce peak temperatures in the repository (CRWMS M&O 2000 [DIRS 152146], Section 3.2).

Duration and Rate of Forced Ventilation—During active repository operations, some of the heat generated by the emplaced waste and the moisture in the surrounding rock can be removed from the repository by forced ventilation of the loaded emplacement drifts. The peak repository temperatures can be reduced by increasing the duration and rate of emplacement drift ventilation (CRWMS M&O 2000 [DIRS 152146], Section 3.2.3).

Distance Between Waste Packages—The distance between waste packages in emplacement drifts is another operational feature that can be modified to manage repository temperature. As waste packages are spaced farther apart, the average linear thermal density in the drift (measured in kilowatts of heat output per meter of drift length) decreases, delivering less heat per unit volume of the host rock when the drift-to-drift spacing remains fixed (CRWMS M&O 2000 [DIRS 152146], Section 3.2.2).

Natural Ventilation—Post-emplacement natural ventilation removes heat and water vapor without the use of fans, using the natural buoyancy of air heated by the waste. The subsurface ventilation system, described in the S&ER (DOE 2001 [DIRS 153849], Section 2.3), could support both forced and natural ventilation. To facilitate natural ventilation, the ventilation system would be enhanced through a combination of air balancing techniques, which involves managing features such as size of ventilation shaft diameters, location and number of intake/exhaust openings, and flow controls (CRWMS M&O 2000 [DIRS 152269]).

2.3.4 Assessing the Performance of a Range of Operating Modes

For the purpose of the *FY01 Supplemental Science and Performance Analyses*, a configuration was selected that allowed focusing of resources on analyses of uncertainties in parameters and on subsystem and total system performance. Should the Yucca Mountain site be determined suitable and be recommended for development by the DOE and the President, engineering and scientific analyses in support of the development of a license application may use other configurations and operations concepts, considering other criteria in addition to performance and uncertainty criteria.

The nominal case analyses for the evaluation of the high and low ends of the thermal operating modes each use the same repository configuration. The footprint of the repository on three sides was determined from proximity to faults, the water table, and the surface. The southern boundary could be extended somewhat to emplace the waste in a larger area to achieve lower temperatures (Figure 2.3.4-2). The waste packages, with a capacity of up to 21 pressurized water reactor fuel assemblies and a peak output at emplacement not to exceed 11.8 kW, would be placed on long-lived pallets within emplacement drifts with a 5.5-m diameter. The drifts would be spaced 81 m apart, and temperatures would be limited during the preclosure period by forced

ventilation. The higher-temperature operating mode would require about 50 years of ventilation with a heat-removal efficiency of 70 percent. The LTOM is modeled as requiring about 300 years of ventilation with an efficiency of 80 percent. Analyses of each thermal operating mode include uncertainty ranges for a number of important parameters, including infiltration rates of water into the mountain. Table 2-1 compares the two cases evaluated in the SSPA with the case used in the TSPA-SR (CRWMS M&O 2000 [DIRS 153246]).

In addition to the higher-temperature operating mode and lower-temperature operating mode analyses, a number of sensitivity analyses were performed to investigate the sensitivity of component, subsystem, and total system performance to conceptual model uncertainties, intrinsic parameter uncertainties, and design operation concept parameters. Some of these sensitivity analyses were performed at the process model level to explore the performance of the potential repository. Process-level analyses and sensitivity studies provide an alternative line of evidence to regression analyses of the (abstracted) total system performance analysis. Other independent lines of evidence used to increase confidence in projections of repository performance include laboratory and field measurements, natural and engineering analogues, and corroborating information from the technical literature.

All of the base case and sensitivity analyses include some common elements. In addition to the repository footprint, the common elements of these evaluations include the following.

Waste Package—The performance evaluations of thermal operating modes evaluated in this report use a corrosion-resistant Alloy 22 outer shell and a structurally strong stainless steel inner shell. In addition to the enhanced shell design, the waste package has a three lid design. A three lid design is used to accommodate stress mitigation techniques in the closure weld area. The additional length of this modified lid has been included in the supplemental analyses, which accounts for the difference in linear thermal loading difference between the S&ER higher-temperature operating mode and the SSPA higher-temperature operating mode.

Inventory—Ability to emplace at least 70,000 metric tons of heavy metal SNF and high-level radioactive waste.

Emplacement Drift Diameter—Emplacement drifts have a 5.5-m diameter.

Drip Shields—Continuous drip shields of corrosion-resistant titanium are assumed to cover the waste packages to divert seepage and limit advective transport of radionuclides from waste packages that may fail earlier than their intended service lifetime.

INTENTIONALLY LEFT BLANK

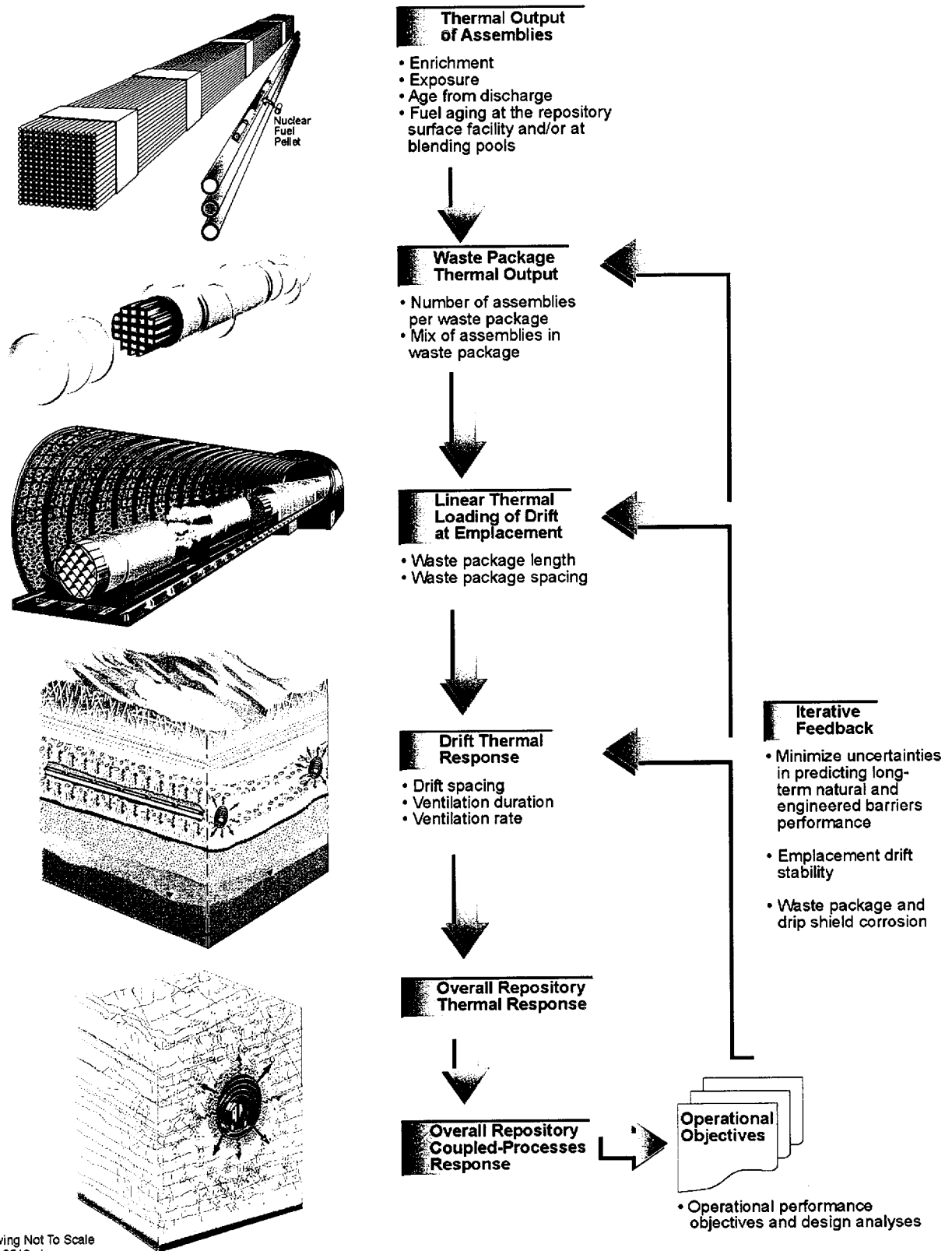
Table 2-1. Comparison of Higher-Temperature and Lower-Temperature Operating Modes Evaluated in the Fiscal Year 2001 Supplemental Science and Performance Analyses with the Design Analyzed in the Yucca Mountain Science and Engineering Report

Parameters	Science and Engineering Report Flexible Design Higher-Temperature Operating Mode ^a	SSPA Higher-Temperature Operating Mode	SSPA Lower-Temperature Operating Mode
Waste package spacing	0.1 m	0.1 m	Variable, with 1.2 m (average)
Maximum waste package thermal loading	11.8 kW	11.8 kW	11.8 kW
Linear thermal loading objective at emplacement	1.45 kW/m	1.35 kW/m	1.13 kW/m
Years of forced ventilation after start of the emplacement	50	50	300
Years of natural ventilation after forced ventilation period	0	0	0
Number of waste packages	~11,000	~11,000	~11,000
Size of pressurized water reactor waste packages	21 PWR	21 PWR	21 PWR
Required emplacement area	~1150 acres	~1,150 acres	~1,464 acres
Average waste package maximum temperature	>96°C	~160°C	<85°C

Source: DOE 2001 [DIRS 153849].

NOTE: ^aCRWMS M&O 2000 [DIRS 153849].

INTENTIONALLY LEFT BLANK

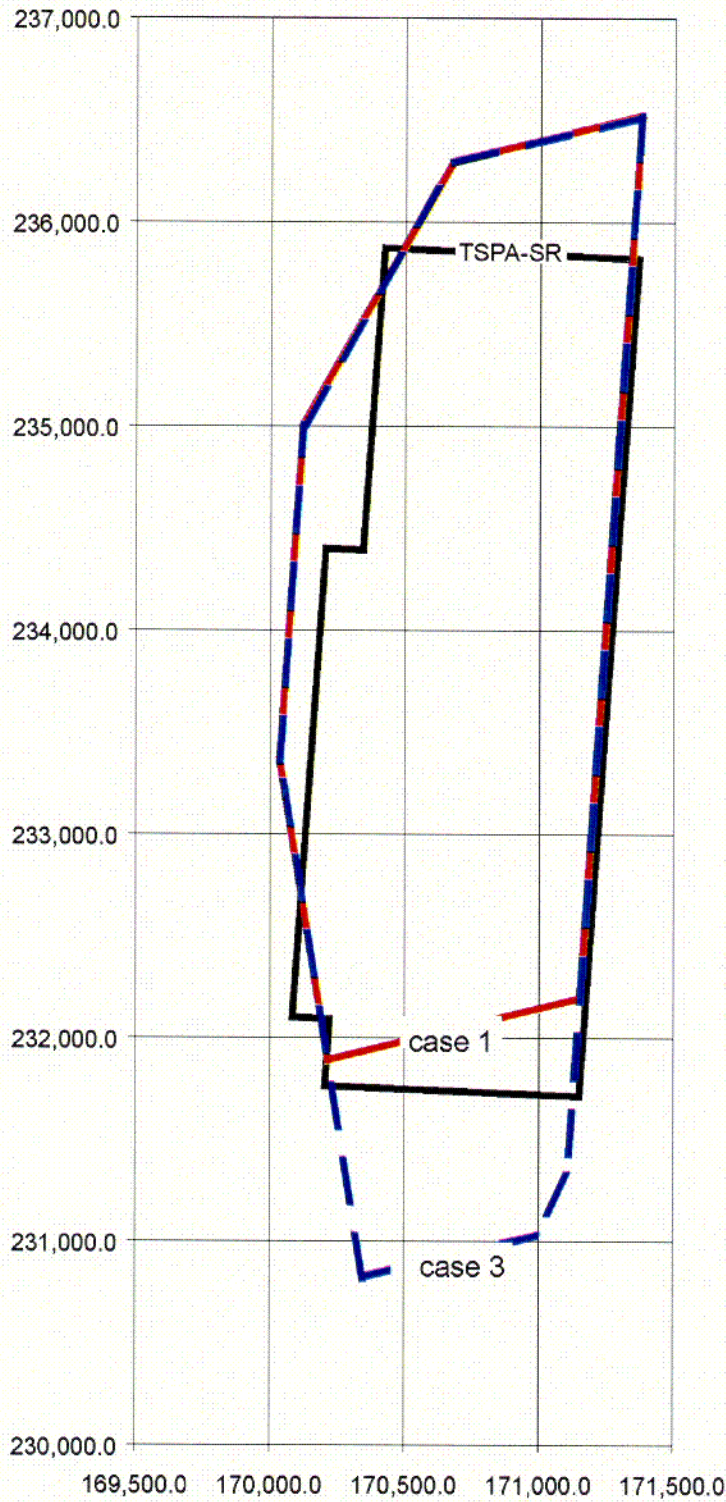


Drawing Not To Scale
154_0513.ai

154_0513.ai

Source: DOE 2001 [DIRS 153849], Figure 2-8.

Figure 2.3.4-1. Variables Affecting the Thermal Performance of the Potential Repository



154_0052.ai

154_0052.ai

NOTE: Higher-temperature (case 1) and lower-temperature (case 3) operating modes. For comparison, the footprint used in the TSPA-SR (CRWMS M&O 2000 [DIRS 153246]) is shown.

Figure 2.3.4-2. Footprints Used in the Thermal Hydrology Analyses

CO2

3. UNSATURATED ZONE FLOW

3.1 INTRODUCTION AND CONCEPTUAL BASIS

This section summarizes process modeling and uncertainty studies performed to refine our current understanding of water movement through the unsaturated zone (UZ) under ambient and thermal conditions, including the base-case thermal-loading scenario and the lower-temperature design. The understanding of the unsaturated flow is evolved from decades of site characterization and model calibration, with the bases described at length in the *Unsaturated Zone Flow and Transport Model Process Model Report* (CRWMS M&O 2000 [DIRS 151940]), which is supported by 24 detailed analysis and model reports. Figure 3.1-1 shows the relationships between the main UZ processes, with those that have undergone substantial revisions highlighted. The revisions extend previous evaluations to longer time frames, larger areal extents, and more coupled processes, in the direction of more realistic representations of the Yucca Mountain site to accommodate alternative thermal operating modes for a potential repository.

The ambient and predicted three-dimensional UZ flow fields are based on different climate states and infiltration scenarios, over large areas and alternative thermal-loading schemes needed to satisfy the performance criteria for the potential repository. The UZ mountain-scale models supply direct inputs to the drift-scale seepage models described in Section 4 and the UZ transport models described in Section 11. All other models for engineered barriers and for saturated zone and biosphere are also closely related to the unsaturated flow field. Modeling a realistic flow field and quantification of its uncertainties improves our understanding of the performance of the potential repository system.

The UZ models are representations of water movement affected by climate above the UZ, rock hydrologic properties of tuff matrix, fractures, and faults above the water table, and thermal impacts controllable by design of the potential repository. A dry climate and a deep water table characterize the ambient condition at Yucca Mountain. The current dry climate is likely to be replaced in the future by a wetter climate. Porous and fractured, welded and nonwelded, fault-bounded tuff layers may be modified by prolonged thermal influences. However, the conceptual basis developed over decades of investigations remains the same. The site representation of alternating tuff layers bounded by faults is consistent with the known geology of the site. Rock properties based on measurements in surface-based boreholes and cores are confirmed and modified by additional testing and observations along underground drifts. Long-term thermal tests continue to refine understanding of coupled processes.

3.2 TREATMENT OF UNSATURATED FLOW-RELATED ISSUES IN ANALYSIS AND MODEL REPORTS

The schematic in Figure 3.1-1 illustrates some of the UZ flow-relevant models. The following is a discussion of the key factors affecting unsaturated flow, how they were addressed in the Analysis Model Reports, and more recent analyses and model developments. These sections represent new work and extensions of existing work. Table 3-1 identifies the primary reason for the development of each section and indicates which of these analyses have been included in Total System Performance Assessment (TSPA) calculations.

Table 3-1. Summary of Supplemental Models and Analyses

Key Attributes of System	Process Model (Section of S&ER)	Topic of Supplemental Scientific Model or Analysis	Reason For Supplemental Scientific Model or Analysis			Section of Volume 1	Performance Assessment Treatment of Supplemental Scientific Model or Analysis ^a		
			Unquantified Uncertainty Analysis	Update in Scientific Information	Lower-Temperature Operating Mode Analysis		TSPA Sensitivity Analysis	Included in Supplemental TSPA Model	
Limited Water Entering Emplacement Drifts	Climate (4.2.1)	Post-10,000-year Climate Model		X		3.3.1	X	X	
	Net Infiltration (4.2.1)	Infiltration for post-10,000-year Climate Model		X		3.3.2	X	X	
	Unsaturated Zone Flow (4.2.1)	Flow in PTn			X		3.3.3		
		3-D flow fields for cooler design; flow fields for post-10,000 yr climate, lateral flow; variable thickness of PTn; fault property uncertainty			X	X	3.3.4		
		Effects of lithophysal properties on thermal properties			X		3.3.5		
	Coupled Effects on UZ Flow (4.2.2)	Mountain-scale Thermal-Hydrologic effects			X	X	3.3.5		
		Mountain-scale Thermal-Hydrologic-Chemical effects			X	X	3.3.6		
		Mountain-scale Thermal-Hydrologic-Mechanical effects			X	X	3.3.7		

NOTE: S&ER = *Yucca Mountain Science and Engineering Report* (DOE 2001 [DIRS 153849]).

^a Performance assessment treatment of supplemental scientific model or analysis discussed in SSPA Volume 2 (McNeish 2001 [DIRS 155023]).

3.2.1 Climate

Process Description—Potential future climate conditions at Yucca Mountain were analyzed in two analysis model reports (AMRs): *Future Climate Analysis* (USGS 2000 [DIRS 136368]) and *Documentation of Million-Year TSPA* (CRWMS M&O 2000 [DIRS 153038]). The future climate at Yucca Mountain for the next 10,000 years is treated as a sequence of three climate states: modern (interglacial) climate for 400 to 600 years, monsoon climate for 900 to 1,400 years, and glacial-transition (intermediate) climate for the balance of the 10,000-year period. The glacial-transition climate occurs either preceding or following the colder or wetter full glacial climate states. Three additional full-glacial climate states are specified within the longer period of 1,000,000 years, with different climate stages timed with the earth orbital clock. Full-glacial stages encompass about 21 percent over the next 1,000,000 years. The intermediate climate is the dominant climate for the next 1,000,000 years, as described in Section 3.3.1.5.

Current Modeling Approach and Uncertainties—The interpretation of past climates is the basis for potential future climate predictions. Both future climate reports used paleoenvironmental and paleoclimate reconstructions based on microfossil evaluations in Owens Lake cores and calcite isotope records from Devils Hole. The sequence and duration of past climate periods are identified from the records and applied to the Yucca Mountain site with similar climate setting. The precipitation and temperature records of present-day meteorological stations at colder and wetter sites are selected to represent future climate states. Each of the future climate states is identified with analogue sites that represent upper-bound, mean, and lower-bounded precipitation scenarios.

The use of paleoecological and paleoclimatic records and analogue site data is the basis of future climate predictions and for evaluation of associated data uncertainties. The climate is assumed to be cyclical with 400,000-year periods and the climate changes are assumed to relate to earth orbital precession and eccentricity parameters. Uncertainties are associated with these and other issues for the timing, duration, and nature of climate changes over the next 1,000,000 years. Tectonic changes and other climate forcing functions have remained relatively constant during the past 1 million years and are expected to remain relatively constant for the next 500,000 years, but may impact future climate at the 1-million-year time scale. Unanticipated, unknown, and unmeasurable future events and human-induced (anthropogenic) changes can be considered, but cannot be predicted. The modeling approach and uncertainties for climate in both AMR revisions and recent evaluations are discussed in detail in Section 3.3.1.

3.2.2 Net Infiltration

Process Description—Net infiltration is the fraction of precipitation (including snowmelt and surface water run-on) that moves through the ground surface and to a depth where the liquid water can no longer be removed by evaporation or transpiration by plants. The approach to simulate net infiltration is documented in *Simulation of Net Infiltration for Modern and Potential Future Climates* (USGS 2001 [DIRS 154674]), for three climate states in the next 10,000 years with associated upper-bound, mean, and lower-bound rates. The estimates of net infiltration are based on the precipitation rates and temperatures predicted for the future climates, for different locations and for each climate state. The net infiltration distributions are used as direct inputs at the upper boundary of the UZ Flow and Transport Model. Relatively high net infiltration rates

occur generally in the northern portion of the site at high elevations and along the ridge where fractured bedrock is exposed. Additional predictions for 10,000 years to 1,000,000 years after present are documented in *Documentation of Million-Year TSPA* (CRWMS M&O 2000 [DIRS 153038]).

Current Modeling Approach and Uncertainties—The infiltration model uses a distributed parameter, water-balance approach for simulating net infiltration processes through the root zone and run-off processes along the washes. The net infiltration model was calibrated with moisture profiles along a network of neutron-logged boreholes, soil and bedrock hydrologic properties, meteorological data, and flow measurements along washes. Vertical one-dimensional flow of infiltrating water through the root zone is assumed and is supported by field data indicating the absence of ponding of water, which would hydraulically facilitate lateral flow. The root-zone parameters were adjusted to extrapolate from present day conditions at Yucca Mountain to those anticipated to occur under future climate conditions.

Uncertainties from the future climate analysis contribute to the uncertainties in the net infiltration model. The uncertainty in net infiltration from imperfect knowledge of input parameters has been quantified for the intermediate (glacial-transition) climate, the dominant climate in the next 1,000,000 years. Extensive time series data of borehole water-contents, water-potential at soil/bedrock contacts, and stream flow measurements caused by transient precipitation events were collected to calibrate the modern (present day) models. Other uncertainties include the use of a water balance approach, the parameter adjustments for future climate states, and the onset of lateral flows at interfaces under episodic infiltration events and during wetter climates. The modeling approach and uncertainties for infiltration in both the AMR revision and recent evaluations are discussed in detail in Section 3.3.2.

3.2.3 Lateral Flow in Paintbrush Nonwelded Hydrogeologic Unit

Process Description—Net infiltration through the fractured bedrocks in the Tiva Canyon welded tuff unit is dominated by significant fracture flow before entering the Paintbrush nonwelded hydrogeological unit (PTn), as discussed in *Conceptual and Numerical Models for UZ Flow and Transport* (CRWMS M&O 2000 [DIRS 141187], p. 21), *Calibrated Properties Model* (CRWMS M&O 2000 [DIRS 144426], p. 28), and *UZ Flow Models and Submodels* (CRWMS M&O 2000 [DIRS 122797], p. 159 and Attachment II). With its characteristics of high matrix porosity and low fracture frequency and the existence of tilted layers of nonwelded vitric and bedded tuff units, PTn can effectively damp out episodic infiltration pulses and divert percolating water to the intercepting faults and fault zones. The difference between infiltration distribution above the PTn and percolation distribution below the PTn is substantiated by geochemical data collected in the field. More significant lateral flow in PTn is shown in more recent development, based on geochemical data.

Current Modeling Approach and Uncertainties—Current modeling approach uses: pneumatic data from sampling points above, within, and below the PTn to calibrate the effective vertical permeability through the PTn and faults; saturation and water potential data to calibrate the unsaturated characteristic parameters; and geochemical data to differentiate alternative conceptual models. The PTn can be represented by fine grids determined by geological data or by coarse grids with anisotropic permeability for the effects induced by multiple tuff layers. It is

also feasible to match the observed chloride spatial distribution in the potential repository horizon by adjusting the infiltration distribution.

The development of alternative conceptual models is used to address uncertainties associated with: lateral flows at PTn interfaces and within the PTn, the role of PTn in damping spatial and temporal variabilities, and the sustainability of fast flow paths (fractures and faults) through heterogeneous PTn units. The PTn tuffs have strong capillary and imbibition potentials. Systematic collections of hydrologic and geochemical data, together with conduction of controlled flow tests, are the bases to iteratively calibrate and validate the models and determine the effective parameters. The chloride data, together with other geochemical and age data, will continue to play an important role in determining the percolation distributions below the PTn to the potential repository horizon in the fractured Topopah Spring welded tuff unit (TSw). Significant lateral flow in the PTn leads to relatively uniform percolation distribution below PTn, in comparison with infiltration distribution above the PTn near the ground surface. Relatively uniform percolation could reduce the variability and associated uncertainties in assessment of UZ waste-isolation capacities. The modeling approach and uncertainties for lateral flow in the PTn in AMR revisions and recent evaluations are discussed in detail in Section 3.3.3.

3.2.4 Three-Dimensional Unsaturated Zone Flow Field

Process Description—The development of the three-dimensional flow field throughout the UZ, from the ground surface to the water table, has evolved over a decade, as documented in *UZ Flow Models and Submodels* (CRWMS M&O 2000 [DIRS 122797]) and in *Unsaturated Zone Flow and Transport Model Process Model Report* (CRWMS M&O 2000 [DIRS 151940]). The comprehensive UZ Flow and Transport Model and its submodels continue to evolve by calibration and validation against all relevant hydrologic, geothermal, and geochemical data. Net infiltration from the ground surface is redistributed by layers of welded and nonwelded tuff units, by interactions between fracture and matrix flow, and by lateral flows along layer interfaces to faults. Below the potential repository, significant lateral diversions are associated with perched water bodies, especially in the northern part of the potential repository block, as a result of zeolites immediately above and within the Calico Hills nonwelded tuff unit (CHn).

Current Modeling Approach and Uncertainties—The current basic model uses a steady-state moisture flow assumption, a volume-averaged modeling approach with dual-permeability model representation of fractures and tuff matrix, and a multilayer three-dimensional gridblock approximation, with each hydrogeologic unit characterized by averaged and calibrated rock properties. The calibrated property sets are developed for upper-bound, mean, and lower-bound infiltration rates of the modern (present-day) climate, to match observed ambient conditions of matrix liquid saturation, water potential and temperature data, perched water data, pneumatic data, and geochemical data. Multiple three-dimensional flow fields were generated to evaluate sensitivities to climate scenarios (including new simulations for the full-glacial stages), variable infiltration maps, and different perched water conceptual models (flow-through and by-passing the zeolitic CHn). The three-dimensional flow fields are direct inputs to TSPA calculations and to other process models. Thermal effects from potential repository heating were evaluated with the UZ Flow and Transport Model, taking the coupled processes into account.

Uncertainties in boundary conditions (especially the infiltration rates and distributions) and in rock properties contribute to uncertainties in the three-dimensional flow fields. Sensitivity and bounding studies were used to identify and quantify uncertainties. Confidence in the current understanding of the UZ system is built by comparing model and submodel results with sufficient data and evaluations to qualify/quantify sensitivity to processes, parameters, conceptual models, and numerical approaches. In the complex UZ system at Yucca Mountain, many aspects of flow and transport processes are not completely understood. These include infiltration boundary conditions, spatial variability of rock properties (especially in CHn and in faults), and the appropriateness of conceptual model assumptions (e.g., steady-state, fracture flow characteristics, fracture-matrix interaction, gridblock averaging, and scaling). Uncertainties are addressed by bounding and sensitivity studies as discussed in DOE 2001 ([DIRS 153849], Sections 4.1.1.2 and 4.1.1.3).

The focus of the site characterization and the UZ flow model study in the past several years has been on the primary potential repository block for the baseline (Enhanced Design Alternative [EDA] II, higher-temperature) design (DTN: SN9907T0872799.001 [DIRS 111485]). The primary block is accessible by surface-based boreholes and by two drifts of the Exploratory Studies Facility (ESF). The most recent UZ flow analyses address the impact of a new siting area for the potential repository, developed with the intent of creating cooler temperatures in the drift environment, by emplacing nuclear wastes at a lower density over a larger area than the primary area. Issues and uncertainties associated with the expanded potential repository include high infiltration and high water table in the north, absence of PTn along some washes and faults, and insufficiency of subsurface data, especially in the new southern block. The modeling approach and uncertainties for three-dimensional UZ flow field in both the AMR and process model report revisions and recent evaluations are discussed in detail in Section 3.3.4.

3.2.5 Thermal-Hydrologic Effects on Unsaturated Mountain-Scale Flow

Process Description—The mountain-scale thermal-hydrologic (TH) models provide analyses of temporal and spatial variability in the UZ conditions under thermal loads. The basic approach to modeling the mountain-scale effects of heat released by the nuclear wastes in emplacement drifts is documented in *Mountain-Scale Coupled Processes (TH) Models* (CRWMS M&O 2000 [DIRS 144454]). The original study used the EDA II design with an initial thermal load of 72.7 kW/acre (1.45 kW/m of drift) and a forced ventilation period of 50 years, during which 70 percent of the decay heat was assumed to be removed. To lower the drift wall temperature below the boiling point, lower areal thermal load (67.7 kW/acre or 1.35 kW/m of drift), longer forced-ventilation period (300 years), and higher heat-removal efficiency (80 percent) are evaluated. Thermal conductivity and heat capacity of the rock mass are modified to account for the lithophysal porosity in the tuff matrix properties. This lower-temperature operating mode results in a maximum temperature of 85°C at the drift wall, and therefore no boiling within the rock mass or fractures. For other sections of this report, the lower-temperature operating mode may be defined differently.

Current Modeling Approach and Uncertainties—Three- and two-dimensional simulations were conducted to address large-scale TH issues relating to climate and infiltration, interface of the potential repository unit (TSw) with the upper PTn and lower CHn units, perched water bodies, faults, and water table. The two-dimensional models contained local refinements to

explicitly represent the 5-m diameter emplacement drifts and in the pillars between drifts spaced 81 m apart. Induced temperature changes have effects at drift walls, within the pillars, at perched water bodies, at the water table, and throughout the UZ system. The coupled TH processes can change the extent of two-phase and dryout zones around the drifts, induce large liquid and gas flux in the near- and far-field environments, redistribute the moisture, and affect the drainage potential through the pillars.

Uncertainties in the UZ flow system model contribute to uncertainties in the mountain-scale TH processes. Additional uncertainties are associated with in-drift processes, including ventilation effects and heat-transfer mechanisms, removal of moisture and heat, and uneven distributions of heat loading. In the TH models, rock properties and boundary conditions are fixed. Some of the coupled effects are further evaluated in mechanical and chemical coupled process models (Sections 3.3.6 and 3.3.7). The uncertainties associated with spatial heterogeneity and scales are also evaluated in the Sections 4 and 11 on TH effects on seepage and on transport. Small-scale heater tests provide data near the drifts and enhance understanding of the coupled processes. For the mountain scale, confidence in the TH models can be built by application of the same modeling techniques for geothermal analogues, with extensive data on exploration and production data history over wide ranges of multi-phase conditions, geologic settings, and calibration experiences. The modeling approach and uncertainties for TH effects on mountain-scale flow in the AMR revision and recent evaluations are discussed in detail in Section 3.3.5.

3.2.6 Thermal-Hydrologic-Chemical Effects on Mountain-Scale Flow and Geochemistry

Process Description—The mountain-scale thermal-hydrologic-chemical (THC) model provides analyses of thermal loading effects on flow and geochemistry in the UZ. This is a new model developed from the models and data documented in two AMRs: the *Mountain-Scale Coupled Processes (TH) Models* (CRWMS M&O 2000 [DIRS 144454]), and the *Drift-Scale Coupled Processes (DST and THC Seepage) Models* (CRWMS M&O 2001 [DIRS 154426]). The mountain-scale models focus on coupled THC processes related to variations in infiltration rate, structure, lithology, rock properties, mineral dissolution and deposition, and flow processes at the mountain or potential repository scale. Small scale effects such as mineral precipitation in the boiling zone are captured in other sections of the drift-scale THC model.

Current Modeling Approach and Uncertainties—A two-dimensional grid was derived from the mountain-scale TH model with the same geologic layering, hydrologic and thermal properties, and thermal loading scenarios. The grid includes an extension of several hundred meters below the water table to provide a far-field constant-temperature boundary. Thermodynamic and kinetic parameters, calibrated against drift-scale heater tests, are used in the mountain-scale evaluations. The initial and infiltrating water chemistry was taken from matrix pore water collected near the ongoing drift-scale test (DST). Condensation and dryout/boiling can affect concentration through dilution and evaporation. Elevated temperature can enhance reaction rates and shift thermodynamic stabilities of coexisting minerals. Release of carbon dioxide out of water and transport in the gas phase via advection and diffusion can have a large effect on pH, mineral-water reactions, and reaction rates.

Uncertainties in mountain-scale flow (including gas convection, liquid flow focusing, and diversion) contribute to uncertainties in mountain-scale THC processes. Other uncertainties include thermodynamic and kinetic data of vitric and zeolitic tuffs, precipitating mineral assemblages, effective mineral-water reactive areas in heterogeneous unsaturated fracture rocks, fracture and lithophysal hydrologic properties, and distributions of water and gas chemistry in the UZ and in the infiltrating water. Sensitivity studies were conducted to understand the impact of THC processes on the mineral changes during thermal periods in the zeolitic CHn, on matrix porosity reduction in the TSw, on enhanced precipitation at the edges of the potential repository block with gas convection, and on many other THC effects. The modeling approach and uncertainties for THC effects on mountain-scale flow and geochemistry in both AMR revisions and recent evaluations are discussed in detail in Section 3.3.6.

3.2.7 Thermal-Hydrologic-Mechanical Effects on Mountain-Scale Flow

Process Description—A new coupled thermal-hydrologic-mechanical (THM) model is developed to calculate the impact of THM processes on flow at the mountain scale. Two well-established codes, TOUGH2 V1.5 for TH processes and FLAC 3D V2.0 for mechanical processes, are coupled together through carefully designed linkage routines. Four types of conservation equations are solved, including two mass-balance equations for the two fluid (liquid and gas) components, one energy (heat) balance equation, and one momentum conservation equation for the rock deformation forces. The mechanical behavior of porous and fractured media responds to changes in temperature, in effective stress, and in strain, resulting in permeability, porosity, and flow-field changes.

Current Modeling Approach and Uncertainties—A two-dimensional model is constructed with vertical layering extended from the ground surface to the water table. Laterally, the model extends from the centerline of the potential repository to a far-field outer boundary located at distance of 5,000 m to the east, over twice the radius of waste emplacement area (2,160 m). The thermal loading, ventilation period, and heat removal efficiency are the same as the values used by the mountain-scale TH model.

Uncertainties in the TH model contribute to uncertainties in THM model. Similar to any newly developed model, uncertainties are relatively large and require substantial input data to conduct the calibration, validation, and thereby build confidence in the models. Calculated changes of permeability depend on such factors as rock stiffness parameters and residual permeability values, heterogeneity of hydrologic and mechanical properties, boundary conditions, dimensionality of the model, and realistic geometries. Geotechnical engineering field and laboratory studies are needed to quantify the uncertainties of THM impact. The modeling approach and uncertainties for THM effects on mountain-scale flow in recent evaluations are discussed in detail in Section 3.3.7.

3.3 UNCERTAINTY ANALYSIS

3.3.1 Climate Model

3.3.1.1 Introduction

This section summarizes climate model developments since the *Total System Performance Assessment for the Site Recommendation* (TSPA-SR) (CRWMS M&O 2000 [DIRS 153246]). The initial release of the climate model, described in *Future Climate Analysis* (USGS 2000 [DIRS 136368]) and summarized in Section 3.3.1.3, addressed climate change for the next 10,000 years. The revision to the climate model focused on predicted precipitation rate and temperature values for glacial climate states that may occur in the next 1 million years, as discussed in *Documentation of Million-Year TSPA* (CRWMS M&O 2000 [DIRS 153038]) and summarized in Section 3.3.1.4. These preliminary climate predictions beyond 10,000 years were included in the TSPA-SR (CRWMS M&O 2000 [DIRS 153246], Section 3.2.5) to support transport sensitivity analyses. Associated uncertainties related to estimating the timing, duration, and nature of climate change are discussed in Section 3.3.1.8. The climate analyses for the next 1 million years are used as input to the updated infiltration model (Section 3.3.2). The new net infiltration results from the infiltration model, in turn, are used in the recent simulations of the flow and transport model (Section 3.3.4) for predicting the flow and transport subject to future climate states over the next 10,000 or 1 million years.

Uncertainties associated with the conceptual model, reliance on interpretation of past climatic conditions as input, and bounding assumptions are inherent to any estimates derived from predictions of future climates. Although the Environmental Protection Agency and U.S. Nuclear Regulatory Commission regulations 40 CFR Part 197 (64 FR 46976 [DIRS 105065]) set a period of 10,000 years for which the U.S. Department of Energy must demonstrate compliance with the radiological protection standard, the U.S. Environmental Protection Agency regulations contemplate post-10,000 year analysis of peak dose in the Environmental Impact Statement, and the National Academy of Sciences has discussed estimating climate beyond 10,000 years as a possible indicator of future repository performance (64 FR 46976 [DIRS 105065], pp. 46993 to 46995). The intent of examining disposal system performance beyond 10,000 years is to estimate its long-term performance to see if dramatic changes can be anticipated. To address uncertainties in system performance, it is necessary to derive estimates of mean annual temperature and precipitation rate. The two analyses of potential future climate conditions for Yucca Mountain, *Future Climate Analysis* (USGS 2000 [DIRS 136368]) and *Documentation of Million-Year TSPA* (CRWMS M&O 2000 [DIRS 153038]), used paleoenvironmental and paleoclimate reconstructions based on evaluations of geological evidence from the Owens Lake Basin, located on the eastern side of the Sierra Nevada mountain range approximately 160 km west of Yucca Mountain, and Devils Hole, located approximately 50 km south of Yucca Mountain. These evaluations are used to estimate future climate conditions. The approach used in both analyses:

- Identifies the sequence, duration, and impact of past climate states (glacial, interglacial, monsoon, and intermediate) suggested by the Owens Lake and Devils Hole paleoenvironmental records

- Selects present-day meteorological stations (analogue stations) to represent these past climate states and uses the record of daily temperature and precipitation from these stations to represent future climate and precipitation
- Compares the relations of delta oxygen-18 Devils Hole reconstructed climate interval (approximately 400,000 to 60,000 years before present) to orbital parameters from celestial mechanics theory to identify a pattern of past climates
- Projects this pattern into the future to establish the nature and timing of future climate change.

Microfossil records of diatoms and ostracodes from cores drilled at Owens Lake have been used to interpret regional climate history from their implied paleoenvironments, provide insight into glacial and interglacial climate change, and provide a means of comparing past climates with each other. Devils Hole is an active extensional fracture in the Paleozoic limestone that composes the regional Paleozoic aquifer. Calcite has precipitated on the walls of the fracture during the last 500,000 or more years, leaving a delta oxygen-18 record of precipitation-derived infiltrating water flowing through the fracture (CRWMS M&O 2000 [DIRS 153038], Section 6.4.1).

3.3.1.2 Goal of Climate Model

The goal of the climate model is to provide precipitation and temperature input data, as well as uncertainty in these data, for the infiltration model (USGS 2001 [DIRS 154674]) under future climate states predicted to occur within the next 1 million years, as discussed in Section 3.3.2. Therefore, predictions of climate and its influence on net infiltration are independent of uncertainties in the thermal load within the repository.

3.3.1.3 Summary of Revision 00 Future Climate Analysis

The climate at Yucca Mountain over the next 10,000 years is treated as a sequence of three climate states (interglacial, monsoon, and intermediate), the timing and characteristics of which are described in *Future Climate Analysis* (USGS 2000 [DIRS 136368]). The present climate state is interglacial. In *Future Climate Analysis* (USGS 2000 [DIRS 136368]), the interglacial and intermediate are referred to as modern and glacial transition, respectively; however to maintain consistency throughout this section, those names are not used. The intermediate climate is a climate state either preceding or following a glacial climate state and is, therefore, neither as cool nor as wet as a glacial climate state. Each climate state is defined by identifying an analogue station, that is, a site whose modern climate approximates the predicted future climate state for Yucca Mountain. The monsoon and intermediate climates are bounded by a range of climate values that have wetter-than-modern upper-bound values and modern or wetter-than-modern lower-bound values relative to the current climate at Yucca Mountain. Tables 3.3.1-1 and 3.3.1-2 list the mean annual precipitation and temperature inferred from the lower- and upper-bound analogue data, which are used as input to the infiltration model to calculate infiltration over the area of the UZ flow and transport model domain. Note that lower and upper bounds refer to precipitation in mm/yr, not temperature.

The precipitation values for the monsoon and intermediate climates exceed those of the present-day climate, indicating that the future climate will be wetter than the modern climate. Temperature, however, also defines an important difference between the modern climate and other climate states. The intermediate climate is cooler than the modern climate, so evaporation is substantially lower than during modern times. A lower level of evaporation means that precipitation can be more readily stored, and hence available for infiltration, than in the current climate. These results are summarized in the *Unsaturated Zone Flow and Transport Model Process Model Report* (CRWMS M&O 2000 [DIRS 151940], Section 3.5).

Uncertainty in climate impact for use in the TSPA is addressed by simulating flow and transport for upper- and lower-bound precipitation and temperature values. The other uncertainty of interest is in the timing of the climate change; durations of 400 to 600 years are expected for the present interglacial climate and 900 to 1,400 years for the monsoon climate, with the intermediate climate extending for the balance of the 10,000-year period in each case (CRWMS M&O 2000 [DIRS 151940], Section 3.5.1.5).

3.3.1.4 Model Development Since Revision 00

Documentation of Million-Year TSPA (CRWMS M&O 2000 [DIRS 153038]) uses the methodology established by and the assumptions set forth in *Future Climate Analysis* (USGS 2000 [DIRS 136368], Sections 6 and 5, respectively) to provide quantified estimates of temperature and precipitation and to estimate the timing of climate states in the Yucca Mountain, Nevada, area for the period from 10,000 to 1 million years beyond the present. This report identifies six potential future climates that alternate during the next 1 million years and proposes minor changes in climate durations predicted for the first 10,000 years from those described in *Future Climate Analysis* (USGS 2000 [DIRS 136368]). In addition to the three climate states mentioned previously, three full glacial climate states are predicted to occur during the next 1 million years.

Based on the paleoclimate record of the full glacial periods recorded in the last 800,000 years, these three full glacial scenarios were selected as representative of the range of severity of full glacial climate stages that may be expected in the next 1 million years. Eight modern meteorological stations were chosen as representative of the upper and lower temperature and precipitation bounds of these three glacial scenarios, as shown in *Documentation of Million-Year TSPA* (CRWMS M&O 2000 [DIRS 153038], Table 6-3). The temperature and precipitation values for the intermediate, monsoon, and interglacial climate states predicted to occur during the next 1 million years are identical to those shown in Tables 3.3.1-1 and 3.3.1-2.

3.3.1.5 Results of Analysis

Past and present climate states were identified based upon geological data (delta oxygen-18 and ostracode fossil data), and the timing of these states was determined by comparison with climate changes calculated from earth orbital parameters using the precession methodology. This methodology assumes that a relationship exists between the timing of long-term past climates and the timing of earth orbital parameters. Orbital parameters can be calculated from basic celestial mechanics, which can be used to estimate the timing of future climates once established (USGS 2000 [DIRS 136368], Section 6.4). Oxygen isotope stages (OISs), established from

studies of marine carbonate delta oxygen-18 records, reflect changes in delta oxygen-18 value of ocean water as continental ice sheets expanded and contracted. The timing and duration of these stages were correlated to the Devils Hole delta oxygen-18 chronology from OIS 11 (the oldest in the available Devils Hole record) through OIS 4 and into OIS 3 (the youngest in the available Devils Hole record). This represents a time interval extending from approximately 400,000 to 60,000 years before the present. Data reported by Petit et al. (1999 [DIRS 109450], Figure 1, p. 430) for Vostok Ice Core delta-deuterium samples were correlated to OIS 3 to 1, representing a time interval of the last 60,000 years. The precession methodology used to time future climate states was based on the past/present point of 399,000 years ago established in *Future Climate Analysis* (USGS 2000 [DIRS 136368], pp. 62 to 63) using the Owens Lake ostracode taxa record, which covers the last 800,000 years (CRWMS M&O 2000 [DIRS 151945], Section 6.3.4.1.2). The past/present point is the point in the past climate series representing the equivalent to the present-day climate. Chronological correlation between the Owens Lake sedimentary record and the Devils Hole delta oxygen-18 record is based on a sediment mass-accumulation curve that is a function of climate and is discussed in *Future Climate Analysis* (USGS 2000 [DIRS 136368], Section 6.5.1).

Ostracode occurrences from the Owens Lake record were used to determine the sequence and nature of past glacial climates in the last 400,000-year climate cycle because the hydrology of Owens Lake is closely linked to climate. Based on the ostracode occurrences, three full glacial climate states of different magnitudes were correlated to specific OISs: OIS 4, OIS 6, and OIS 8/10 (OIS 8 and 10 are grouped together in this analysis because they are similar). The OIS 6 glacial stage had the greatest effective moisture and coldest temperatures contained within the Owens Lake record. However, OIS 16 (centered about 600,000 years before present and outside the Owens Lake record) appears to have had greater effective moisture than OIS 6, based on paleolake records (Reheis 1999 [DIRS 109454], pp. 196 to 205). Therefore, Stage 6/16 is suggested to provide the most conservative effective-moisture estimates, yielding the greatest net infiltration over the Yucca Mountain site. Glacial Stage 8/10 was warmer and wetter relative to OIS 6/16, while glacial Stage 4 was drier and colder than OIS 8/10, but not as cold as OIS 6/16 (CRWMS M&O 2000 [DIRS 153038], Section 6.2).

The durations of each of the different climate states were estimated based on the timing of orbital parameters. The earth-orbital precession methodology was used to time future climate states from 10,000 to 1 million years based on the past/present match point of 399,000 years ago. Future climate is predicted to occur in repeating subcycles of intermediate, interglacial, alternating intermediate and monsoon, and one of three glacial stages. Eleven such four-stage subcycles, ranging from 71,000 to 115,000 years, are predicted to occur during the period between 10,000 and 1 million years, with intermediate, interglacial, monsoon, and glacial accounting for 64, 12, 3, and 21 percent, respectively, of the time as shown on Table 3.3.1-3.

As described in Section 3.3.1.3, the nature of future climate is forecast in terms of upper-, mean, and lower-bound precipitation rates and temperatures based upon meteorological stations at locations that currently have climate conditions similar to past climates observed in the Owens Lake chronological record. Meteorological stations for the interglacial, intermediate (referred to as glacial transition in Section 3.3.1.3), and monsoon climate states are identical to those used in *Future Climate Analysis* (USGS 2000 [DIRS 136368]). Additional meteorological stations were chosen to represent the upper and lower bounds of the glacial climate scenario under Stages 8/10,

6/16, and 4. These glacial stages (OISs) are discussed below: each is briefly described and the analog stations representing their upper and lower bounds are identified (CRWMS M&O 2000 [DIRS 153038], Table 6-3).

Glacial Stage 8/10—Glacial Stage (OIS) 8/10 represents the warmest and wettest of the glacial stages identified in the Owens Lake record, as indicated by the presence of *Candona caudata* and *Limnocythere ceriotuberosa* and the absence of *Cytherissa lacustris*. This combination of ostracodes indicates that the climate was dominated by the mean seasonal or annual latitude of the polar front, with winter-dominated precipitation but without periods of extended dominance by high-pressure, anti-cyclonic circulation.

The area east of the Cascade mountain range in Washington was chosen as a lower bound of the Stage 8/10 analogue (as well as the intermediate climate stage upper-bound analogue) because the region (1) is east of a high mountain range in a rain shadow similar to the Yucca Mountain region; (2) is winter-precipitation dominated; (3) is under the influence of the polar front during the winter; (4) is situated near the average position of the polar front throughout the year; and (5) does not experience extended dominance by cold Arctic high-pressure air. Additionally, ostracodes recovered from glacial stages 8 and 10 in the Owens Lake core occur presently in eastern Washington, supporting the link between distribution and climate. Because the Stage 8/10 upper bound needed to be wetter and slightly cooler than the lower bound, Chewelah, Washington, was selected based on geographic criteria and the fact that it has a mean annual precipitation of approximately 538 mm and a mean annual temperature of approximately 8°C.

Glacial Stage 6/16—Glacial Stage (OIS) 6 appears to have had the greatest effective moisture and the coolest glacial temperatures in the last 400,000-year cycle contained within the Owens Lake fossil record. The presence of the ostracode *Cytherissa lacustris*, which was recovered during much of the OIS 6 time, implies that the climate was dominated by polar and Arctic air masses; the modern distribution of this species is in the Canadian boreal forest and above the Arctic Circle.

Meteorological stations chosen to represent the upper and lower bounds were constrained by the limited distribution of *Cytherissa lacustris* within the United States. It has been collected at Lake Yellowstone, Wyoming, which is a fresh and cold lake. Because this region is dominated by polar air masses, Lake Yellowstone was chosen as the upper bound for the full glacial 6/16 climate state. The annual temperature at this station is cold (0.8°C) because of its high elevation and latitude. Therefore, it may be a conservative analogue. The lower-bound stations (Browning and Simpson, Montana) are in closer agreement with estimated OIS 6 temperatures (5.5°C), even though *Cytherissa lacustris* has not been reported in this locality (CRWMS M&O 2000 [DIRS 153038], Section 6.3.2).

Glacial Stage 4—Glacial Stage (OIS) 4 was drier and colder than Stage 8/10, but not as cold as Stage 6/16; this is inferred from the combined presence of *Cytherissa lacustris*, *Candona caudata*, and *Limnocythere ceriotuberosa* in the Owens Lake record (CRWMS M&O 2000 [DIRS 153038], Section 6.2). Furthermore, analysis of flora in packrat middens suggests a mean annual precipitation between 266 mm and 321 mm and a mean annual temperature between 7.9°C and 8.5°C (Thompson et al. 1999 [DIRS 109464], Table 4, p. 24).

Meteorological stations chosen to represent the upper bound for the Stage 4 climate were identical to those used to represent the lower bound of the Stage 6/16 climate (CRWMS M&O 2000 [DIRS 153038], Table 6-3). The lower bound for Stage 4 is represented by Elko, Nevada, because it experiences cold, wet, snowy winters influenced by either polar lows or Arctic highs and cold, dry summers resulting from both the presence of cool, westerly flows and the absence of subtropical highs in the region. In addition, *Candona caudata* inhabit locations in the Ruby Mountains in northwest Nevada, representative of similar climate conditions measured at the Elko station.

3.3.1.6 Abstraction for Total System Performance Assessment

The 10,000-year proposed regulatory period has been divided into three climate regimes for TSPA calculations: interglacial (present-day), monsoon, and intermediate. In the TSPA-SR (CRWMS M&O 2000 [DIRS 153246], Section 3.2.1) the interglacial and intermediate are referred to as modern and glacial transition, respectively. The ranges of time periods for each climate are 0 to 600 years for the modern climate, 600 to 2,000 years for the monsoon climate, and 2,000 to 10,000 years for the glacial-transition climate. The climate change times are the only climate information used directly by the TSPA model. The other information is used indirectly, through its effects on infiltration. Additional climate effects are imposed by climate-induced changes in the water table and in saturated-zone recharge (Section 12).

For time periods greater than 10,000 years, it is appropriate to use a climate model that includes full-glacial and future interglacial climates in addition to the present-day interglacial, monsoon, and intermediate climates. For this reason, the previous climate model was extended for times up to 1 million years (Section 3.3.1.4). It is based on paleoclimate data in the same way as the 10,000-year climate model. Details of the climate sequence and analogues for the million-year climate are presented in the TSPA-SR (CRWMS M&O 2000 [DIRS 153246], Section 3.2.5) and *Documentation of Million-Year TSPA* (CRWMS M&O 2000 [DIRS 153038], Tables 6-3 and 6-6). A summary of this discussion is provided below.

Six climate states are specified for the post-10,000-year climate sequence: interglacial, monsoon, intermediate, and three different full-glacial climates. The present-day climate is an interglacial climate, used as an analogue for future interglacials as well. The intermediate climate is the same as the glacial-transition climate. Preceding each glacial state in the climate sequence is a period called intermediate/monsoon, when the climate is alternating between those two states. For TSPA simulations, the climate sequence was simplified by combining the alternating intermediate and monsoon climates into a single intermediate climate state. This approximation is acceptable for TSPA because monsoon climate is estimated to occur for less than 7 percent of the intermediate/monsoon climate state.

Temperature and precipitation data from the analogue stations were used in the infiltration model described in Section 3.3.2 to predict infiltration maps. These infiltration maps were then used as input for flow and transport simulations. Mountain-scale UZ flow fields were generated for four new cases for this extended climate analysis: Glacial Stage 6/16 low-infiltration case; Glacial Stage 6/16 medium-infiltration case; Glacial Stage 6/16 high-infiltration case; and Glacial Stage 4 low-infiltration case. All other cases are represented either by these or by a glacial-transition case that was already available. For calculation of UZ transport within the

TSPA simulation, UZ flow is approximated as a sequence of steady-state flow fields controlled by net infiltration rates calculated for each climate state. The UZ flow fields are used sequentially according to the predicted timing (starting time, ending time, duration) of each climate state.

3.3.1.7 Multiple Lines of Evidence

This analysis is based on meteorological data collected at natural analogue sites (the meteorological stations listed in CRWMS M&O 2000 [DIRS 153038], Table 6.3) for the climates expected to occur at Yucca Mountain over the next 10,000 and 1 million years. The prediction of future climates involves multiple lines of evidence: delta oxygen-18 data, fossil ostracode data, and earth-orbital data. The earth-orbital data are determined by celestial mechanics and have a high degree of certainty; they control the timing of climate states. However, the response of climate to the orbital parameters is not known with a high degree of certainty. The other data sets provide corroborative evidence of temperature and salinity changes, from which precipitation is estimated. Analogue stations that presently experience climate similar to that predicted for the future at Yucca Mountain are chosen to have either the indicator ostracode species or conditions favorable for their survival. Precipitation and temperature records for these analogue stations can be used to estimate future year-to-year variability.

3.3.1.8 Summary of Uncertainties and Their Treatment

Uncertainties in estimated future climate states consist of conceptual, data, and parameter uncertainties, which are tabulated below. These uncertainties affect the goal of the report, which is to provide temperature and precipitation values for different climate states. There is no simple or objective way of assessing the nature of uncertainty as it may apply to future climate change over the next 1 million years. If these uncertainties are not accepted, then the future climate bounding estimates would depend on a conservative estimate of climate based on the extreme temperature (cold) and precipitation (wet) values from the previous 400,000-year cycle instead of values estimated herein within the extremes. In general, these uncertainties were considered acceptable, given the intended purpose of the report and the use of its results in the downstream model.

Table 3.3.1-4 summarizes the key conceptual and parametric uncertainties regarding the development of the future climate analysis. Uncertainties are grouped according to category (i.e., conceptual, data, or parameter). Next, the primary uncertainty issue associated with each category is described, followed by possible methods for treating or addressing the uncertainty. Finally, the affected modeling goals are presented.

3.3.1.9 Summary and Conclusions

The future climate over the next 1 million years at Yucca Mountain is treated as a sequence of stages whose timing and characteristics are described in detail in *Documentation of Million-Year TSPA* (CRWMS M&O 2000 [DIRS 153038]). The alternating climate stages include intermediate, monsoon, interglacial, and three glacial stages (OIS 6/16, OIS 8/10, and OIS 4). Each stage is defined by mean annual precipitation rates and temperatures. Tables 3.3.1-5

and 3.3.1-6 list mean annual precipitation and temperature values used as input to the infiltration model discussed in Section 3.3.2 to calculate net infiltration for possible future glacial climate states over the next 1 million years. Precipitation and temperature data for the analog stations (CRWMS M&O 2000 [DIRS 153038], Table 6-3), are presented in DTN: GS000100001221.001 [DIRS 146816]. However, the values in Tables 3.3.1-5 and 3.3.1-6 do not necessarily represent the same analog stations, because the net infiltration model makes adjustments to account for the topography of the UZ flow and transport model area, as described in USGS (2001 [DIRS 154674], Section 6.4.2).

Because of the uncertainties identified in Table 3.3.1-4, only the Glacial Stage 6/16 climate (which would result in the most net infiltration) was used to estimate mean annual precipitation and mean annual temperature for the purposes of calculating net infiltration (BSC 2001 [DIRS 154873]). Selection of this stage is therefore the most conservative approach. To reduce the number of infiltration model simulations required in Section 3.3.2, specific combinations of mean annual temperature and mean annual precipitation from Stage 6/16 meteorological stations were used to infer upper-, mean, and lower-bound values for Stages 8/10 and 4, with the exception that the lower-bound Stage 8/10 is given by the upper-bound intermediate climate shown in Tables 3.3.1-1 and 3.3.1-2. An alternate Stage 6/16 meteorological station is used in Section 3.3.4.4 to represent the lower-bound Stage 8/10 and is provided in parentheses in Tables 3.3.1-5 and 3.3.1-6. Note that lower- and upper-bound refer to precipitation or net infiltration (see lower-bound glacial stage 8/10 in Table 3.3.2-3) in mm/yr, not temperature.

The upper-bound precipitation values for the full glacial climate exceed the upper bound of the present-day interglacial (modern) climate for the region by at least 160 mm/yr, while the lower bound of the Glacial Stage 4 climate is almost identical in value to the interglacial (modern) upper bound. Therefore, all glacial climate stages are wetter than the modern interglacial climate. Temperatures during the glacial climates are cooler than the modern interglacial climate, leading to substantially lower evaporation than presently occurs at Yucca Mountain. A lower level of evaporation means that precipitation will be more readily stored in the root zone (shallow subsurface soil and rocks), and hence available for infiltration, than in the current climate.

3.3.2 Net Infiltration Model

3.3.2.1 Introduction

New predictions of precipitation and temperature for future climates extending to the next 1 million years, described in Section 3.3.1, have resulted in extension of the initial release of the net infiltration model documented in *Simulation of Net Infiltration for Modern and Potential Future Climate* (USGS 2001 [DIRS 154674]) and summarized in Section 3.3.2.3. Preliminary infiltration scenarios for the extended climate regime were conducted for the TSPA-SR (CRWMS M&O 2000 [DIRS 153246]) to conduct transport sensitivity analyses. The new modeling discussed in Sections 3.3.2.4 and 3.3.2.5 encompasses a larger area, reflecting the UZ flow and transport model documented in *UZ Flow Models and Submodels* (CRWMS M&O 2000 [DIRS 122797]). The uncertainty of the infiltration scenario for the glacial-transition climate was assessed using the Monte Carlo method, as reported in the TSPA-SR (CRWMS M&O 2000 [DIRS 153246], Section 3.2.2.3) and summarized in Section 3.3.2.6.

Net infiltration is the fraction of precipitation, snowmelt, or surface water run-on that infiltrates and percolates below the zone of evapotranspiration. Predicted net infiltration varying with location constitutes the upper-boundary condition for flow-field simulations. Estimates of net infiltration presented here are based on the precipitation rates and temperatures for the interglacial/modern, monsoon, intermediate/glacial-transition, and full glacial climates predicted to occur over the next 1 million years, as presented in *Future Climate Analysis* (USGS 2000 [DIRS 136368]) and in *Documentation of Million-Year TSPA* (CRWMS M&O 2000 [DIRS 153038]). Each of these climate states has been identified with three analogue sites that represent upper-bound, mean, and lower-bound precipitation scenarios. These future climate scenarios, in turn, are based on past climates inferred from microfossil and oxygen-isotope data and on earth-orbital parameters, as described in Section 3.3.1 (USGS 2000 [DIRS 136368]; CRWMS M&O 2000 [DIRS 153038]). The approach used to simulate net infiltration using the net infiltration model is documented in *Simulation of Net Infiltration for Modern and Potential Future Climates* (USGS 2001 [DIRS 154674]). The net infiltration model is a quasi three-dimensional numerical model used to simulate surface flow and subsequent percolation of water through the root zone due to the effects of precipitation and temperature at the Yucca Mountain site. The resulting net infiltration estimates are spatially distributed and time-averaged. Uncertainty in net infiltration has been quantified for the intermediate climate, which is the dominant climate for the next 1 million years (as described in Section 3.3.1.5). Unquantified uncertainties in the net infiltration model broadly consist of conceptualization of the processes significant to the hydrologic cycle, numerical representation of the processes, and calibration and validation of the model, as described in detail in Section 3.3.2.8.

3.3.2.2 Goal of the Net Infiltration Model

The goal of the net infiltration model is to use precipitation and temperature data from analogue sites that represent future climate states (USGS 2000 [DIRS 136368]; CRWMS M&O 2000 [DIRS 153038]) to predict net infiltration rates for use as direct input to the UZ flow and transport model. Net infiltration, as calculated by the net infiltration model, is assumed to depend only upon surface processes. Therefore, it is assumed to be independent of the repository thermal regime even though surface temperatures (in the root zone) may become slightly elevated, as shown in Figure 3.3.5-2 or Figure 3.3.5-3. Therefore, the scope of the net infiltration model is limited to surficial hydrologic processes occurring only to the depth of the root zone. In the context of the UZ flow model, the surface (bottom of the root zone) is considered to be a perfectly insulated thermal boundary preventing heat loss to the atmosphere with a constant net infiltration rate as prescribed by the net infiltration model.

3.3.2.3 Discussion of Analysis Model Report Revision 00 Results

The predictions of future climate and precipitation, and the resulting infiltration rates, are documented in *Future Climate Analysis* (USGS 2000 [DIRS 136368]) and *Simulation of Net Infiltration for Modern and Potential Future Climates* (USGS 2001 [DIRS 154674]), respectively. These predictions show that as the climate changes from interglacial to monsoon to intermediate, the mean precipitation and site-average infiltration rates also increase, as shown in Tables 3.3.1-1 and 3.3.2-1, respectively. The highest net infiltration rates occur on the steep north-northeast facing slope of the Prow, the upper channel locations of Solitario Canyon, Drill Hole Wash, Pagany Wash, and Abandoned Wash, and generally in the northern portion of the

site. These results are summarized in *Unsaturated Zone Flow and Transport Model Process Model Report* (CRWMS M&O 2000 [DIRS 151940], Section 3.5.2).

3.3.2.4 Model Development Since Revision 00 of Analysis Model Reports

Additional climate prediction for 10,000 years to 1 million years after present have been documented in *Documentation of Million-Year TSPA* (CRWMS M&O 2000 [DIRS 153038]) and were used to calculate net infiltration rates for full glacial climates expected to occur within the next 1 million years (BSC 2001 [DIRS 154873]). Although the net infiltration model was not initially developed in Revision 00 for a full glacial state, no change has been made to the net infiltration model for its application to the full glacial state in the work described here. In summary, the net infiltration model was used to predict net infiltration at Yucca Mountain for six potential future climates: intermediate, monsoon, interglacial, and three different full-glacial states.

3.3.2.5 Results of Analysis

The net infiltration estimates presented in this section are for the 38.7 km² area used as the modeling domain for the UZ flow and transport model (CRWMS M&O 2000 [DIRS 122797]). Net infiltration rates estimated by the net infiltration model for the UZ flow and transport model domain differ slightly from those actually implemented in the model. This difference results from plan-view discretization effects in the model and the need to spatially average net infiltration rates over each node in the model domain (Bodvarsson 2001 [DIRS 154669], Attachment 12, pp. 203 to 211). Model results from the net infiltration model for the three different full-glacial climates are discussed below and summarized in Table 3.3.2-3.

Glacial Stage 6/16—Figure 3.3.2-1 illustrates net infiltration for the lower, mean, and upper bound for the glacial-climate scenario. Analogue-site data for the mean Glacial Stage 6/16 climate include an average precipitation rate of 429 mm/yr, which for the area of the UZ flow and transport model domain results in an average net infiltration of 87.9 mm/yr. For the lower- and upper-bound Stage 6/16 scenarios, the average net infiltration rate is estimated to be 24.4 mm/yr and 151.0 mm/yr, respectively.

The lower-bound net infiltration rate for this Stage 6/16 climate is therefore 9 mm/yr less than the upper-bound intermediate infiltration rate, while the upper-bound Stage 6/16-infiltration rate is 118.0 mm/yr greater. Therefore, net infiltration rates are significantly higher for the Stage 6/16 climate than for the intermediate, monsoon, or interglacial climates because of the combined influence of high mean annual precipitation rates and lower mean annual temperatures.

Glacial Stage 8/10—To simplify the net infiltration analysis, mean annual precipitation rates and temperatures used to represent the upper, mean, and lower bounds of the Stage 8/10 climate were chosen from meteorological stations, as described in Section 3.3.1.5. These stations are listed in Tables 3.3.1-5 and 3.3.1-6. Given this approximation, the mean and upper-bound net infiltration rates for the Stage 8/10 climate are identical to those for the Stage 6/16 climate. The lower-bound mean annual net infiltration rate for Stage 8/10 is identical to the upper-bound intermediate climate described in Section 3.3.1.3 (Table 3.3.2-1): 33.0 mm/yr, which is

8.6 mm/yr higher than the lower-bound Stage 6/16 rate. Therefore, the Stage 8/10 climate generates the most conservative estimate of net infiltration over the area of the UZ flow and transport model, as indicated by the choice of upper-, mean, and lower-bound mean annual precipitation rates and temperatures from analogue meteorological stations.

Glacial Stage 4—The mean and upper-bound net infiltration rates for Stage 4 are identical to the lower-bound and mean values of the Stage 6/16 climate, respectively. The lower-bound mean annual net infiltration rate for Stage 4 is estimated to be 12.9 mm/yr, which is slightly higher than the upper-bound interglacial (modern, Table 3.3.2-1), mean monsoon, and average of the lower-bound and mean intermediate (glacial transition, Table 3.3.2-1). Therefore, despite the fact that Stage 4 caused the least net infiltration of the three glacial climate stages and hence is least conservative, the Stage 4 climate does on average result in greater net infiltration than the intermediate, interglacial, and monsoon climate scenarios.

3.3.2.6 Abstraction for Total System Performance Assessment

A detailed analysis of infiltration uncertainty was conducted for the intermediate climate (glacial-transition climate in Section 3.3.2.3) using the Monte Carlo method, as documented in the TSPA-SR (CRWMS M&O 2000 [DIRS 153246], Section 3.2.2). The uncertainty in net infiltration (as considered in the TSPA analysis) is considered to result from imperfect knowledge of input parameters used by the net infiltration model. The uncertainty analysis with the intermediate climate focused on twelve key input parameters (Table 3.3.2-2, last entry) for which uncertainty distributions were developed. These distributions were then sampled stochastically for 100 Monte Carlo realizations, yielding 100 estimates of net infiltration rates. The result of the Monte Carlo analysis was an approximately lognormal histogram of net infiltration rates (CRWMS M&O 2000 [DIRS 143244], p. 23 to 27). Specifically, for the intermediate (glacial-transition) climate state, the mean ± 1 standard deviation of the logarithm of net infiltration, in \log_{10} (mm/yr), is 1.25 ± 0.42 . Converted, this means that annual net infiltration will be less than 7 mm in 16 percent of years, less than 17 mm in 50 percent of years, and less than 47 mm in 84 percent of years (numbers approximate). This analysis shows that the lower-bound and upper-bound infiltration rates derived using only analogue meteorological station temperature and precipitation data as shown in Table 3.3.2-1 are not truly bounds when all uncertainties in net infiltration model input parameters for the future climate states are taken into account (see last entry in Table 3.3.2-2). Also, the mean infiltration rate given in Table 3.3.2-1 (derived using only analogue meteorological station temperature and precipitation data) is not the statistical mean when the appropriate probabilistic weighting factors are applied to the net infiltration distribution generated by the Monte Carlo analysis.

The Monte Carlo analysis was constructed to quantify uncertainty in net infiltration rates for the intermediate (glacial transition) climate because that climate is dominant within the 10,000-year regulatory period. The intermediate climate is also the dominant climate state over the next 1 million years in the extended climate model (CRWMS M&O 2000 [DIRS 153038], Section 6.5.3). The uncertainty for the other climate states, and in particular for the full-glacial climates, has not yet been analyzed. Therefore, uncertainty in net infiltration over the next 1 million years is taken to be identical to that of the intermediate (glacial-transition) climate.

3.3.2.7 Multiple Lines of Evidence

Analogue studies that estimated groundwater recharge rates from hydrologic modeling studies provide an indication of infiltration under future glacial climate conditions. The analogue studies were conducted for two small basins in central Nevada (Lichty and McKinley 1995 [DIRS 100589], p. 3). Their purpose was to aid in estimating recharge to the paleohydrologic regime associated with Yucca Mountain under wetter climate conditions. Thus, the two selected sites, 3-Springs and East Stewart basins, are located north of and at a higher elevation than Yucca Mountain, where prevailing climatic conditions are thought to be representative of the range of paleoclimatic conditions near Yucca Mountain during the Quaternary. Both study sites are characterized by high relief and rough terrain, with elevations ranging from about 2,150 to 2,900 m above sea level for 3-Springs Basin and 2,950 to 3,320 m for East Stewart Basin (Lichty and McKinley 1995 [DIRS 100589], p. 3). The climate at 3-Springs Basin is semiarid, with annual precipitation generally in the range of 250 to 350 mm, most of which occurs as snow during winter months. The East Stewart Creek site is a subalpine drainage basin where annual precipitation ranges from 500 to 700 mm, again occurring predominantly as snow.

Two independent modeling approaches were conducted for each site, using observed hydrologic data for a six-year study period (October 1986 through September 1992). One approach used a traditional watershed hydrology method through a precipitation-runoff system that accounts for spatial variability of data. The other approach was based on the conservative nature of the chloride ion in certain geologic environments, using it as a natural tracer to compute a coupled water and chloride-ion mass-balance system of equations to estimate available water for net infiltration.

Results of the modeling approaches support the conclusion that reasonable estimates of average annual recharge to groundwater range from about 10 to 30 mm per year for 3-Springs Basin and from about 300 to 320 mm per year for East Stewart Basin (Lichty and McKinley 1995 [DIRS 100589], p. 26). The semiarid 3-Springs Basin provides net infiltration rates that are in the range between the upper-bound modern and upper-bound glacial-transition climates. The subalpine East Stewart Creek site provides net infiltration rates that are twice as large as the upper-bound Glacial Stage 6/16 climate. Therefore, the 3-Springs site provides a conservative estimate of net infiltration that is expected to occur over the next 10,000 years, while the East Stewart Creek site provides a conservative estimate of net infiltration that is expected to occur over the next 1 million years, as predicted by the net infiltration model.

Multiple lines of evidence for net infiltration under modern climate conditions are reviewed in the *Unsaturated Zone Flow and Transport Model Process Model Report* (CRWMS M&O 2000 [DIRS 151940], Section 3.5.2.8).

3.3.2.8 Summary of Remaining Uncertainties

Uncertainties in the net infiltration model broadly consist of conceptualization of the processes significant to the hydrologic cycle, numerical representation of the processes, and calibration of the model. Table 3.3.2-2 summarizes the key conceptual and parametric uncertainties regarding the development of the net infiltration model. Uncertainties are grouped according to category (i.e., conceptual, data, or parameter). Next, the primary uncertainty issue associated with each

category is described, followed by methods used for treating or addressing the uncertainty. Finally, the affected modeling goals are presented.

3.3.2.9 Summary and Conclusions

The predictions of future climate, precipitation, and resulting infiltration rates show that as climate changes from interglacial (modern) to monsoon to intermediate (glacial-transition) to glacial, the mean precipitation and infiltration rates also increase, as shown in Tables 3.3.1-1, 3.3.1-5, 3.3.2-1, and 3.3.2-3. The glacial climate scenario was subdivided into three stages (6/16, 8/10, and 4) with upper-, mean, and lower-bound mean annual precipitation and temperature data derived primarily from Stage 6/16 meteorological stations. This simplification was made to reduce the number of net infiltration model simulations required to calculate the impact of the glacial climate scenarios and because Stage 6/16 was anticipated to result in the greatest effective moisture and coolest glacial temperatures, and therefore the most conservative net infiltration scenario. Using the meteorological data presented in Tables 3.3.1-5 and 3.3.1-6, the Stage 8/10 glacial climate generated the most conservative estimate for net infiltration over the UZ flow and transport model area (Table 3.3.2-3). These values represent infiltration rates averaged over the model area, and are up to 37 percent higher than those in the TSPA-SR (CRWMS M&O 2000 [DIRS 153246], Table 3.2-6), which are rates averaged over the footprint of the potential repository.

3.3.3 Percolation Redistribution and Flow in the Paintbrush Nonwelded Hydrogeologic Units

3.3.3.1 Introduction

This section summarizes the modeling and uncertainty studies performed to evaluate percolation flux distribution and flow in the Paintbrush nonwelded (PTn) hydrogeologic units. Since the TSPA-SR (CRWMS M&O 2000 [DIRS 153246]), new field geochemical data have been used to calibrate the spatial distribution of net infiltration (see Section 3.3.3.4.1) and the anisotropy of permeability of the PTn (see Section 3.3.3.4.3) in UZ flow model simulations. Detailed PTn flow models have been constructed to evaluate lateral flow within the PTn caused by capillary barrier effects (see Section 3.3.3.4.2).

Flow in the PTn is important because the new flow simulation results from this study suggest that water flow within and through the PTn likely will be matrix dominated except, possibly, in the vicinity of major through-going fault zones that may create fracture-dominated preferential flow pathways through the unit. The PTn acted as a buffer, damping out variations in the transient net infiltration, so that flow beneath the PTn was essentially steady-state. The PTn redistributed percolation flux in space as well as in time. Lateral flow diverted net infiltration above the potential repository area eastward to the Ghost Dance and Drill Hole Wash faults. Flow thus diverted bypassed the potential repository block.

3.3.3.2 Modeling Goals

The goals of the models used to study percolation distribution and flow in the PTn are:

- Evaluate the effects of the spatial distribution of net infiltration on percolation distribution and flow in the PTn
- Assess bounds on net infiltration rates, spatial distribution patterns, net infiltration rate variability, and associated uncertainties
- Evaluate the effects of lateral flow within the PTn on percolation and chloride redistribution
- Provide a methodological and conceptual basis for modeling percolation flux and lateral flow within the PTn
- Develop calibration procedures using natural and anthropogenic environmental tracers
- Identify conceptual uncertainties and estimate the uncertainty and variability of model-relevant parameters.

3.3.3.3 Discussion of Analysis Model Report Revision 00 Results

The PTn consists of nonwelded and vitric horizons and bedded tuffs intersected by faults and fault zones. The percolation distribution in the potential repository level below the PTn determines the degree of seepage into drifts, which in turn affects the performance of waste packages and engineered barrier systems. Uncertainties in the conceptual model, the data used for calibration, and flow and transport parameters in the current model were discussed in detail in *Calibrated Properties Model* (CRWMS M&O 2000 [DIRS 144426]) and *UZ Flow Models and Submodels* (CRWMS M&O 2000 [DIRS 122797]).

In addition to geologic and hydrologic information, geochemical data provide information on flow patterns within the UZ, including the PTn. Distribution of chemical constituents depends on the hydrologic and geochemical processes associated with surface precipitation, evapotranspiration, fracture-matrix interactions of flow and transport, large-scale mixing via lateral transport, and the history of climate changes and recharge. Natural and anthropogenic environmental tracers provide useful data for evaluating the processes over various time and space scales. By synthesizing geochemical, geologic, and hydrologic data, the model results enhance the understanding of flow and transport processes and the development of hydrologic parameter sets and conceptual models.

The initial issue of *UZ Flow Models and Submodels* (CRWMS M&O 2000 [DIRS 122797]) focused on the formulation of methodologies and the conceptual bases of using matrix pore-water geochemical data for flow model calibration. Analysis and modeling of pore-water geochemical data are documented in that AMR. Pore-water chemical concentration data were analyzed and modeled using three-dimensional chemical transport simulations and analytical methods. Water net infiltration-rate calibrations were performed using the pore-water chloride concentrations. Model results of chloride distributions match the observed data better using the

calibrated present-day-mean net infiltration rates than using the present day mean net infiltration rates without calibration (CRWMS M&O 2000 [DIRS 122797], Section 6.4). In addition, an analytical method was developed to analyze the transient transport of chemicals. This method was compared against the results of three-dimensional simulations under the same flow conditions and was able to capture major chloride and chlorine-36 transient behavior and trends predicted by the simulations (CRWMS M&O 2000 [DIRS 122797], Section 6.4.3.2).

3.3.3.4 Model Development Since Total System Performance Assessment for Site Recommendation

The following sections describe three developments in the evaluation of three-dimensional flow within the PTn since the TSPA-SR (CRWMS M&O 2000 [DIRS 153246]). These studies were done to test simulation models by comparing their results to all available qualified data, and revising where appropriate. Such revision, termed model calibration, increases confidence in the model and reduces associated uncertainties. Section 3.3.3.4.1 describes the use of chloride data to evaluate distribution of net infiltration with isotropic permeability within the PTn. Section 3.3.3.4.2 describes the use of a detailed two-dimensional model of the PTn to evaluate the importance of lateral flow due to capillary barrier diversion within the unit. Finally, in Section 3.3.3.4.3, the present-day mean net infiltration map developed by the infiltration model (Figure 3.3.3-1) was left unchanged, but the chloride data were matched by adjusting the anisotropy of the PTn. Thus, both of these conceptual models match the chloride data better than the initial models. A three-dimensional dual-permeability model and the T2R3D V1.4 and TOUGH2 V1.4 codes were employed for the simulations.

3.3.3.4.1 Chloride-Based Net Infiltration Rate

Net infiltration is defined as the penetration of surface water below the root zone to a depth from which it can no longer be removed by evapotranspiration. The infiltration model (USGS 2001 [DIRS 154674]) described in Section 3.3.2 provides net infiltration flux values (mm/yr), which are applied (as a boundary condition) to top-layer gridblock cells (Figure 3.3.3-1). By water balance, net infiltration flux is the sum of precipitation and run-on minus the sum of runoff and evapotranspiration, all of which vary spatially. As precipitation falls, it acquires chloride by uptake of aerosols from the atmosphere. As a result, precipitation, run-on, and runoff contain a known concentration of chloride. Infiltrating water has a higher chloride concentration than precipitation because some water, but no chloride, is lost to evapotranspiration. The net infiltration maps that are output by the infiltration model can therefore be used to calculate the chloride concentration of infiltrating water. The net infiltration flux and associated chloride concentration vary spatially over the site (Figure 3.3.3-1). When these are used as boundary conditions, the flow and transport model simulates chloride concentration everywhere in the UZ. Essentially no chloride is contributed by dissolution of UZ minerals. These simulated chloride concentrations can be compared with measurements on pore water samples to calibrate the model.

A systematic study incorporating new data from borehole SD-6 (DTN: GS981008312272.004 [DIRS 153677]) and calibration procedures has been conducted since the initial release of the infiltration model (USGS 2000 [DIRS 123650]). This study is documented in Bodvarsson (2001 [DIRS 154669], Attachment 11, pp. 72 to 83). As in that report, the available chloride data were

used to calibrate the net infiltration distribution without changing the hydrologic properties of the PTn. Measurements of pore water chloride concentrations offer a spatially distributed data set for assessing UZ flow and transport processes and for testing conceptual models. Calibration was done by dividing the surface infiltration area into nine regions (Figure 3.3.3-2) according to the availability and range of chloride data, the range of present-day mean net infiltration data (shown in Figure 3.3.3-1), and hydrogeologic and hydrostructural features. The chloride field data were assigned to corresponding simulation cells based on pore water sample locations. The revised water net infiltration flux for each simulation cell was computed using the chloride net infiltration flux and the assigned chloride concentration data from the cell. For cells where chloride data were not available, the net infiltration flux was interpolated based on the calculated net infiltration flux in nearby cells within the same region and the surface area of the cell. The map of chloride-based calibrated net infiltration is shown in Figure 3.3.3-2. Averaged present-day mean net infiltration was applied to regions where regional chloride data is unavailable (Regions I, II, and VIII). The overall and regional net infiltration volume and rates for the net infiltration schemes before and after the calibration are given in Table 3.3.3-1. In this table, before-calibration flow rates and fluxes (Figure 3.3.3-1) are the output from the infiltration model (DTN: GS000399991221.002 [DIRS 147022]), and after-calibration flow rates and fluxes (shown also in Figure 3.3.3-2) are the values after calibrating against chloride data. The result of calibrating the net infiltration map against chloride data was to increase the overall net infiltration by 9 percent but to decrease it in Region III, so net infiltration over the potential repository footprint is decreased. Three-dimensional flow and chloride transport simulations were conducted using both the present-day mean net infiltration from the infiltration model (Figure 3.3.3-1) and the chloride-based calibrated present-day mean net infiltration (Figure 3.3.3-2) to assess the two net infiltration schemes.

3.3.3.4.2 Lateral Flows Induced by Capillary Barriers within the Paintbrush Nonwelded Hydrogeologic Units

In unsaturated flow, water movement is generally, but not always, downward. One cause of lateral flow is the capillary barrier effect. This is caused by differences in moisture tension across an interface between adjacent hydrologic units. If moisture tension is greater in the upper unit (negative capillary pressure gradient), water will tend to flow laterally along the interface rather than downward. The PTn unit primarily consists of non- to partially welded tuffs and extends from the base of the densely to moderately welded, crystal-poor vitric subzones of the Tiva Canyon Tuff to the top of the densely welded, crystal-rich vitric subzone of the Topopah Spring welded tuff (TSw) (Buesch et al. 1995 [DIRS 145631], Table 4). Thus, the PTn encompasses the nonwelded, crystal-poor vitric subzone of the lower Tiva Canyon Tuff (Tpcpv), the pre-Tiva Canyon Tuff bedded tuff (Tpbt4), the Yucca Mountain Tuff (Tpy), the pre-Yucca Mountain Tuff bedded tuff (Tpbt3), the Pah Canyon Tuff (Tpp), the pre-Pah Canyon Tuff bedded tuff (Tpbt2), and the non- to partially and moderately welded, crystal-rich vitric subzones of the upper Topopah Spring Tuff (Tptrv). The dip of these layers is generally to the east at about ten degrees or lower. Within the PTn, several layers (Tpcpv1, Tpbt4, Tpbt2, Tptrv3, and Tptrv2) are less than 10 m thick within the potential repository footprint while other layers (Tpy, Tpbt3, and Tpp) show considerable variation in thickness across the potential repository area, with each showing a thinning trend to the south.

In the site-scale UZ flow model, the PTn unit is represented by six model layers (PTn21 through PTn26) (CRWMS M&O 2000 [DIRS 122797]). In the PTn lateral-flow modeling study, refined grids of these layers are used within the PTn to capture detailed flow behavior associated with capillary barriers. Six x-z grids in three vertical cross sections, with discretization as fine as $\Delta x = \Delta z = 1$ m, are used to evaluate the sensitivities to boundary conditions, net infiltration distributions, fracture/matrix properties, and fault properties.

Typical of the model results is the plot of vertical capillary gradients at Easting 171200, Northing 235119 (Figure 3.3.3-3). This figure shows that the simulated capillary-barrier effect is especially strong in layers PTn21 and PTn23 (Wu et al. 2001 [DIRS 154918], pp. 23 to 27). In the figure, negative capillary pressure gradients are defined for upward flow and positive for downward flow. The upward matrix capillary gradients within layers PTn21 and PTn23 are about 0.1 (bar/m), equal to the gravity gradient ($\rho_w \times g \approx 0.1$ bar/m), thus allowing lateral flow of water to occur. Negative matrix capillary pressure gradients also occur below 1,260 m above sea level, but these are too weak to offset gravity except at an elevation of 1,240 m, where they are opposed by an opposite gradient in the fracture network. Another negative matrix capillary pressure gradient occurs at an elevation of about 1,400 m, in the Tiva Canyon welded hydrogeologic unit where TCw11 overlies TCw12, but this interface is interrupted by topography and is not present everywhere. Matrix flow can therefore occur only in the horizontal direction within these layers. Fracture capillary barriers develop within layer PTn23, but not within layer PTn21. Figure 3.3.3-3 shows that near the bottom of layer PTn21, fracture capillary gradients are downward. The strong spikes shown in the figure signify the permeability and capillary contrast between layers.

The significant lateral (i.e., near-horizontal) flow implied by the model results within the PTn diverts a large amount of the percolation flux to a very narrow zone near the down-slope fault boundaries. Lateral flow modeled within the PTn is so strong that net infiltration patterns on the ground surface have little effect on flow within the PTn. In two-dimensional flow simulations of a 100-m long east-west cross section at Northing 235119 m, the percolation flux at the PTn-TSw interface was found to be very similar for three top-boundary conditions: net infiltration uniformly distributed, net infiltration concentrated at the west end (up-dip) of the model, and net infiltration concentrated at the east end (down-dip) of the model (Wu et al. 2001 [DIRS 154918], Section 4.1).

The simulation results with refined grids indicate that net infiltration values have more overall impact on capillary barriers or lateral flow than detailed spatial distributions of net infiltration along the model's top boundary. Figure 3.3.3-4 compares the impact of net infiltration rates on percentage of flow through faults and fault zones. In the figure, faults include the Solitario Canyon, Drill Hole Wash, Pagany Wash, and Toe (eastern boundary) faults. Fault properties are defined in *Calibrated Properties Model* (CRWMS M&O 2000 [DIRS 144426], p. 60 to 63). The figure shows that at the present-day mean net infiltration rate of 5 mm/yr (USGS 2001 [DIRS 154674]), about 25 percent of the percolation flux is laterally diverted into faults within the PTn. The fault zone is defined as the fault column with an additional 20-m wide zone west (up-slope) of each fault; as shown in Figure 3.3.3-4, the fault zone carries about 40 percent of the total flow at this net infiltration rate. As net infiltration increases, the percentage of fault flow decreases. This happens because, under the simulated conditions, both fractures and rock matrix in areas between faults become wetter with increased net infiltration, leading to generally weaker

capillary barriers between rock layers and, consequently, less lateral diversion of water to fault zones.

3.3.3.4.3 Percolation Redistribution by Anisotropic Paintbrush Nonwelded Hydrogeologic Unit Representations

This third set of model studies was performed to resolve the difference between the net infiltration distribution above the PTn and the calibrated net infiltration distribution (developed to match the chloride data below the PTn, as described in Section 3.3.3.4.1) below the PTn. With net infiltration distribution, the present-day mean net infiltration (DTN: GS000399991221.002 [DIRS 147022]), and the TSPA-SR (CRWMS M&O 2000 [DIRS 153246]) site-scale flow model parameters (DTN: LB991121233129.002 [DIRS 147334]), the simulated chloride concentrations are higher at the ESF north ramp, ESF south ramp, northeast Enhanced Characterization of the Repository Block (ECRB), and borehole UZ#16, and lower at the southwest ECRB, than the corresponding sample data (DTN: LA0002JF12213U.001 [DIRS 154760]; DTN: GS961108312261.006 [DIRS 107293]; DTN: LA9909JF831222.004 [DIRS 145598]; DTN: LA9909JF831222.010 [DIRS 122733]; DTN: LA9909JF831222.012 [DIRS 122736]). Low net infiltration rates lead to the higher simulated chloride concentrations at the northeast ECRB, while extreme higher net infiltration rates lead to the lower simulated chloride concentrations at the southwest ECRB. The chloride concentrations in infiltrated water (calculated from water net infiltration flux and chloride infiltration flux at the surface) along the ECRB vary significantly compared to the rather smooth measured concentration data at depth. This difference between surface and deep water chemistry is not expected for a system dominated by vertical flow.

The chloride data (which were matched in Section 3.3.3.4.1 by adjusting the net infiltration map) can also be matched by adjusting the horizontal permeability values, while not changing either present-day net infiltration map input or the vertical permeability values (which were determined by calibration against pneumatic damping and responses over the PTn (CRWMS M&O 2000 [DIRS 144426])). That is, either of these two conceptual models, calibrating the net infiltration map or introducing anisotropy, can be used.

In Section 3.3.3.4.1, chloride data were reconciled with the net infiltration map by adjusting the net infiltration map, while leaving rock properties unchanged. This resulted in less net infiltration over the potential repository footprint. In this Section, the chloride data are reconciled with the net infiltration map by adjusting the rock properties, leaving the net infiltration map unchanged. This has the effect of increasing lateral diversion. Both the new alternatives result in less transport than the original uncalibrated model.

To study the effect of PTn lateral flow on the degree of damping and the chloride distribution, three-dimensional simulations were conducted with increased PTn horizontal permeability (i.e., ratios of horizontal permeability to vertical permeability 10 and 100, respectively).

Figures 3.3.3-5 through 3.3.3-7 compare field data with the model results of chloride concentrations in the ESF and the ECRB, and in borehole UZ#16. The “kh/kv=1” case shown in the figures is the one without changing the PTn permeability field as in the original model. The damping effects vary in different locations and are visible in the figures. As horizontal

permeability is increased, the simulated chloride concentrations in borehole UZ#16 below the PTn hydrogeologic units are decreased and closer to the measured chloride data from pore-water samples. Decreased simulated chloride concentrations were also observed at boreholes NRG-6, NRG-7A, SD-7, SD-12, and UZ#4 as the PTn permeability was increased. Few changes were found, however, at boreholes SD-9 and UZ-14. The increased PTn lateral flow does have effects on the percolation and chemical distributions but the degree of the effects varies. In general the cases with increased PTn lateral flow match the chloride data better than the case with the original PTn permeability field. In order to achieve a more realistic and physically meaningful model, however, further studies are needed to conduct detailed calibrations to the PTn permeability field based on the available chemical distribution data.

3.3.3.5 Abstraction for Total System Performance Assessment

The work reported in this section is devoted to evaluating process model sensitivities and uncertainties. Consequently, simulation results from this study are not used to support any abstraction model that directly supports TSPA. The results found here indicate that the process modeling and associated model abstractions used to represent this component in the total system performance assessment baseline are conservative in that no credit is taken for the effects of this lateral flow component on total system performance. Therefore, any future changes in model abstractions for this component will not diminish the performance as represented in the total system performance baseline.

3.3.3.6 Multiple Lines of Evidence

The average percolation flux rate within the Topopah Spring Tuff of 4.5 mm/yr used in the UZ flow and transport model is based on surface infiltration data and hydrologic properties of the tuff. This rate can be checked against alternative lines of evidence to verify its reasonableness. Furthermore, Montazer and Wilson (1984 [DIRS 100161], pp. 47, 50, and 51) hypothesized that the PTn could cause significant lateral flow such that the flux within the TSw would be smaller than that in the PTn; this hypothesis also can be checked.

The carbon-14 content of UZ gas (after equilibration with pore water), together with water content data, can be used to calculate long-term average percolation fluxes in the TSw. This method is based on residence time of pore waters (Yang et al. 1996 [DIRS 100194], pp. 49 to 55; Yang et al. 1998 [DIRS 101441], p. 16) and water content measured for drill core in the laboratory (Rautman and Engstrom 1996 [DIRS 100642], pp. 26 to 32, and Appendix G; Rautman and Engstrom 1996 [DIRS 101008], pp. 27 to 32, and Appendix G; Engstrom and Rautman 1996 [DIRS 100670], pp. 23 to 28, and Appendix G). The flux is calculated from the total amount of water in the UZ between two elevations and the difference in apparent carbon-14 ages at the top and bottom of the zone in question.

The percolation flux calculated using carbon-14 data from borehole USW UZ-1 and water content data from USW UZ-14 (3 meters away) is 2.5 mm/yr (Yang 2001 [DIRS 154613], Table 2), based on carbon-14 values at the top and bottom of the TSw and total water content for the full thickness. This implies a transport velocity of 2.9 cm/yr. Carbon-14 data are not available from other boreholes, but the carbon-14 data from borehole USW UZ-1 can be regressed against depth to obtain values for percent modern carbon as a function of depth. This

relationship can then be used with water content data for borehole USW UZ-14, UE-25 UZ#16, USW SD-7, USW SD-9, and USW SD-12 to calculate average percolation fluxes of 2.4, 2.7, 1.8, 2.0, and 1.9 mm/yr, respectively, in the TSw (Yang 2001 [DIRS 154613], Table 3). All of these values are smaller than that used in the UZ flow and transport model, and thus, relative to this data set, the model provides a conservative estimate for repository performance.

The carbon-14 method described above was also used by Yang (2001 [DIRS 154613]) to calculate fluxes in the PTn in six boreholes for comparison with fluxes in the TSw. For boreholes USW UZ-14, UE-25 UZ#16, USW NRG-7a, USW SD-7, USW SD-9, and USW SD-12, the calculated average fluxes are 2.8, 2.1, 1.4, 1.1, 1.9, and 1.7 mm/yr (Yang 2001 [DIRS 154613], Table 3). The values for the PTn and TSw are subject to large uncertainties because of error in the analysis for carbon-14 and error propagation in the calculations. For example, the average percolation flux for six boreholes in the PTn by this method is $1.8 + 2.2/-0.9$ mm/yr (Yang 2001 [DIRS 154613], p. 12). As a result, the carbon-14 method is not sensitive enough to detect a lateral diversion of approximately 30 percent of the percolation flux as predicted in simulations discussed in Section 3.3.3.4.2.

3.3.3.7 Summary of Uncertainties and Their Treatment

Table 3.3.3-2 summarizes the key conceptual and parametric uncertainties in the modeling of percolation distribution and flow in PTn.

3.3.3.8 Summary and Conclusions

In previous simulations (CRWMS M&O 2000 [DIRS 122797]), the mean net infiltration value had a large impact on the percolation flux and chloride distributions in the potential repository horizon. The results of the refined models suggest that lateral flow within the PTn hydrogeologic unit may cause significant difference between the net infiltration distribution above the PTn and to the predicted percolation distribution below the PTn. The resulting detailed percolation distribution is fairly uniform, with the damping and lateral flow mechanisms in PTn greatly reducing the spatial heterogeneity of percolation flux compared to the net infiltration predicted by the infiltration model (USGS 2001 [DIRS 154674]). The percolation distribution is more important than the net infiltration distribution to assess the impact of the ambient flow field on the overall system behavior.

Percolation flux affects both waste-canister performance and solute travel times to the accessible environment. The present-day mean net infiltration was calibrated and the percolation distribution was analyzed using pore-water chloride concentration data. Modeled chloride results from three-dimensional simulation using the chloride-based net infiltration map are more uniform and match the chloride data better than the original net infiltration map developed for use in the Revision 00 study. PTn lateral-flow effects on percolation and chloride distribution were also studied by three-dimensional simulation with increased horizontal permeability. The degree of the effect varies by location. As expected, a more uniform chloride distribution under the PTn was observed in most places when lateral-flow effects increased. The combined results provide the means to test the appropriateness of the conceptual model, reduce uncertainties, and quantify parametric uncertainties. Unquantified conceptual uncertainties were assessed in analogue studies and other corroborating observations.

The spatial distribution of chloride concentration suggests a relatively uniform percolation flux beneath the PTn. A uniform percolation flux at the repository horizon could potentially reduce seepage into waste emplacement drifts. In previous interpretations, chloride data was matched by invoking a more uniform distribution of net infiltration at the surface (CRWMS M&O 2000 [DIRS 122797], Figure 6-24). In those simulations lateral flow within the PTn was less significant than vertical flow, resulting in a predominately one-dimensional downward flow pattern. The present interpretation for the uniform percolation flux is that the PTn is more anisotropic than has been described and acts to damp extreme episodic infiltration pulses. Another possible interpretation is the smaller degree of spatial variability for net infiltration at the surface and the smaller lateral movement of percolation between the surface and the potential repository horizon, with a nearly one-dimensional flow pattern.

3.3.4 Three Dimensional Flow Fields

This section summarizes the three-dimensional, steady-state, UZ flow fields generated using TOUGH2 V1.4 and the flow model of Yucca Mountain. These flow fields are used in various analyses, including TSPA calculations. Results must be considered in light of the uncertainty associated with input parameters, conceptual models, and the numerical modeling approach; consequently, the information in this section is presented in the context of uncertainties associated with UZ flow.

Following a brief introduction (see Section 3.3.4.1) and a list of model goals (see Section 3.3.4.2), this section presents the flow field results in three parts: the flow fields for TSPA-SR calculations (see Section 3.3.4.3), the new three-dimensional flow fields for performance assessment calculations to assess post-10,000 year climates using the four new infiltration maps corresponding to the full glacial climate (see Section 3.3.4.4), and the new flow fields related to an extended UZ model domain that would result from a new design for a cooler repository (see Section 3.3.4.5). Modeling abstractions performed for the TSPA were evaluated using the newly developed flow fields (see Section 3.3.4.6), and multiple lines of evidence, such as natural analogues, were examined in support of UZ flow studies at Yucca Mountain (see Section 3.3.4.7). The section on flow fields concludes with a tabulation and discussion of remaining uncertainties (see Section 3.3.4.8), followed by a brief synopsis (see Section 3.3.4.9).

3.3.4.1 Introduction

The UZ flow model, as described in *UZ Flow Models and Submodels* (CRWMS M&O 2000 [DIRS 122797]), simulated ambient conditions and performed predictive studies of changes in the mountain. These changes were caused by climate-related, thermal, and geochemical perturbations. More specifically, the flow model generated three-dimensional flow fields for TSPA calculations and provided input for other process models.

Data collected at Yucca Mountain over the last decade have been used to develop conceptual and numerical models of the hydrologic, geothermal, and geochemical behavior of the site. These data are used to calibrate and validate the flow model and its submodels, building confidence in the flow model description of ambient and future conditions in the UZ system. The comprehensive model calibration and validation studies have been carried out using borehole or tunnel measured saturation, water potential and temperature data, perched water data, pneumatic

data, and geochemical data (CRWMS M&O 2000 [DIRS 122797], Section 6.2; CRWMS M&O 2000 [DIRS 144426], Section 4). In addition, the flow model has been further calibrated and validated using the results of the water infiltration test at Alcove 1 in the ESF (CRWMS M&O 2000 [DIRS 122797], Section 6.8.1). All the three-dimensional flow fields documented in this section have been calibrated against observed field data, including matrix liquid saturations, water potentials, and perched water data.

The flow model and its submodels are relied on for characterizing flow and transport processes at Yucca Mountain. Such a comprehensive goal, which includes all relevant data, makes the models complex. Limitations and uncertainties associated with these models should be recognized to ensure successful application. The accuracy and reliability of the flow model predictions are critically dependent on the accuracy of hydrogeological conceptual models, estimated model properties, other types of input data (e.g., output from the infiltration model), and applied numerical modeling techniques. These models are limited mainly by the current characterization of the mountain system, including the geological and conceptual models (e.g., steady-state moisture flow assumption), the volume-average modeling approach, and available field and laboratory data.

Site investigations have shown that large variability exists in flow and transport properties over the spatial and temporal scales of the mountain. Despite the considerable progress made toward quantifying variability over spatial and temporal scales, the major remaining uncertainties of model parameters are: accuracy of estimated past, present, and future net infiltration rates over the mountain; quantitative descriptions of welded and nonwelded tuff heterogeneity, flow properties, and detailed spatial distributions of the properties within the mountain, especially below the potential repository; sufficiency of field studies, especially for fracture properties of zeolitic units and faults; alternative conceptual models of major fault water-flow transmission; and evidence of lateral diversion as a result of layer heterogeneity within the PTn unit and, as a result of zeolites, immediately above and within the CHn unit. These uncertainties affect the distribution of percolation flux and groundwater travel times in the UZ, as discussed in detail in Section 3.3.4.8.

3.3.4.2 Goals of the Flow Model

The fundamental goal of the flow model is to conceptually represent the UZ system of Yucca Mountain using a numerical model. Yucca Mountain is a complex, heterogeneous hydrogeologic system that is subject to many physical and geochemical processes. The flow model and its submodels are designed to capture these processes. The development of the flow model and its submodels has the following primary objectives:

- To integrate the available data from the UZ system into a single, comprehensive, calibrated three-dimensional model that simulates the ambient hydrologic, thermal, and geochemical conditions and predicts system response to future climate conditions
- To develop a number of submodels with representative boundary and initial conditions specifically for detailed studies of perched water, percolation through the PTn, flow through zeolitic CHn layers, and thermal effects from potential repository heating after waste emplacement

- To quantify the flow of moisture, heat, and gas through the UZ under the present-day and estimated future climate scenarios
- To predict groundwater flow patterns from the potential repository to the water table
- To contribute model parameters and model conditions for other specific studies, such as seepage into drifts
- To provide a defensible and credible model that accounts for relevant UZ flow processes for performance assessment and repository design.

More specifically, the flow model and its submodels provide estimates of important processes relevant to UZ flow regarding the performance of the potential repository, including:

- Spatially variable and temporally averaged values for percolation flux at the potential repository horizon
- The components of fracture and matrix flow and their interaction within and below the potential repository horizon
- The effects of observed perched water zones, associated flow barriers, and lateral flow diversion
- Probable flow paths from the potential repository to the water table
- The effects of faults on flow and transport processes
- The role played by the PTn unit in percolation redistribution, lateral flow diversion, and damping infiltration pulses
- Groundwater flow paths from the land surface to the repository horizon, groundwater and potential radionuclide migration paths from the potential repository to the water table, and breakthrough curves and collection areas at the water table.

3.3.4.3 Discussion of Three Dimensional Flow Fields Used in Initial Reports

As documented in *UZ Flow Models and Submodels* (CRWMS M&O 2000 [DIRS 122797]), 28 three-dimensional steady-state UZ flow fields were generated using the flow model. The purpose of developing multiple flow fields is to help constrain uncertainties, such as those surrounding the distribution and magnitude of net infiltration and the conceptualization of fracture flow in zeolitic rocks (i.e., perched water conceptual models) below the potential repository horizon. Eighteen of the flow fields have been submitted to the TSPA-SR for performance analyses. These 18 simulations were performed using the TSPA numerical grid; 2 perched water conceptual models (flow-through and by-passing); 9 infiltration maps representing 3 climate scenarios; and 3 calibrated fluid and rock parameter sets (CRWMS M&O 2000 [DIRS 122797], Section 7.5).

In the flow model (CRWMS M&O 2000 [DIRS 122797]), the UZ system is represented by a multilayer sequence of hydrogeologic units, approximated by layers of three-dimensional gridblocks. For each hydrogeologic layer within the model, a set of averaged (calibrated) rock properties is developed, as documented in the *Calibrated Properties Model* (CRWMS M&O 2000 [DIRS 144426]). The UZ model domain and the present-day, mean infiltration map with the TSPA grid are shown in Figure 3.3.4-1; the model domain covers a total area of approximately 40 km². Net surface infiltration of water from precipitation that penetrates the evapotranspiration zone is considered one of the most important factors affecting overall hydrologic behavior (as well as radionuclide transport) within the UZ system. The nine infiltration scenarios used for the flow simulations consist of present-day, monsoonal, and glacial-transition climates, each of which has lower-, mean, and upper-bound maps. The statistics of the nine infiltration rates are summarized in Table 3.3.2-1 for average values over the model domain.

Figure 3.3.4-2 illustrates percolation flux at the potential repository horizon, simulated using the present-day mean infiltration scenario with the flow-through perched water conceptual model (CRWMS M&O 2000 [DIRS 122797], Section 6.2.2). The figure shows that the simulated total (matrix plus fracture) percolation flux at the repository level has a nonuniform distribution, which was expected given the nonuniform distribution of net infiltration.

Figure 3.3.4-3 shows the simulated percolation flux at the water table with the same infiltration and perched water model scenarios. Compared to the distributed percolation flux at the potential repository horizon (Figure 3.3.4-2), the water table plot (Figure 3.3.4-3) indicates that significant lateral diversion occurs in the northern part of the model domain where thick zeolitic layers are located, leading to flow focusing along faults. In the southern part of the model domain, where the upper part of the CHn is vitric, flow appears to remain predominantly vertical between the potential repository horizon and the water table. In addition, the statistics of the three-dimensional, steady-state flow fields show that fracture flow makes up more than 80 percent of the total flow at the potential repository horizon and 70 to 90 percent of the total flow at the water table.

3.3.4.4 Three-Dimensional Flow Field Development with Post-10,000 Year Climate Scenarios

To assess post-10,000 year climates and their effects on repository performance, four new three-dimensional steady-state flow fields have been generated since the initial issue of *UZ Flow Models and Submodels* (CRWMS M&O 2000 [DIRS 122797]). These new flow fields have been used in the TSPA-SR. Table 3.3.4-1 lists the information for estimating average percolation fluxes simulated within the potential repository footprint for 13 infiltration scenarios, including four new infiltration maps, which correspond to the full glacial climate, used for simulation of the four new flow fields (see Section 3.3.2.5 and Table 3.3.2-3). These new infiltration scenarios are: (1) "full-glacial, lower bound #1," corresponding to the lower-bound average of Glacial Stage 4, the driest of the three glacial states described in Section 3.3.1; (2) "full-glacial, lower bound #2," corresponding to the "alternate" lower-bound average of net infiltration for Glacial Stage 8/10 (see Section 3.3.1.9); (3) "full-glacial, upper bound #1," corresponding to the upper-bound average of net infiltration for Glacial Stages 8/10 and 6/16, the wettest glacial stages; and (4) "full-glacial, mean #2," corresponding to the mean net infiltration

for Glacial Stages 8/10 and 6/16, as well as the upper bound for Glacial Stage 4. Precipitation, temperature, and net-infiltration for these new infiltration scenarios are summarized in Tables 3.3.1-5, 3.3.1-6, and 3.3.2-3. These new infiltration maps have, on average, much higher net infiltration rates within the UZ model domain than the nine rates listed in Table 3.3.2-1 for the modern, monsoonal, and glacial-transition climate states. Figure 3.3.4-4 shows the “full-glacial, mean #2” infiltration scenario.

The simulations using the four new infiltration maps and TOUGH2 Version 1.4 were conducted using the TSPA grid, the flow-through perched water conceptual model, and three sets of calibrated parameters corresponding to the lower-, mean, and upper-bound present-day infiltration maps. The simulated three-dimensional steady-state flow fields with the higher infiltration rates show larger percolation fluxes through the entire model, with dominant vertical flow in the southern part of the model domain and more focusing of flow into faults in the northern part.

Figures 3.3.4-5 and 3.3.4-6 show examples of the simulated percolation flux at the potential repository horizon and at the water table, respectively, for the “full-glacial, mean #2” infiltration scenario. The percolation pattern at the potential repository horizon (Figure 3.3.4-5) is similar to the surface infiltration map (Figure 3.3.4-4), which indicates little lateral flow within the PTn for this high-infiltration case. However, Figure 3.3.4-6 suggests that large-scale lateral flow to vertical faults occurs within the CHn unit, particularly in the northern part of the model domain, where the unit is extensively altered due to zeolites.

3.3.4.5 Conceptual and Numerical Evaluation of a Lower-Temperature Operating Mode

The most recent UZ flow analyses addressed the impact of an extended repository footprint (BSC 2001 [DIRS 154548]). This potential repository, developed with the intent of creating cooler temperatures in the drift environment, encompasses a larger area than earlier designs (Figure 3.3.4-7). The domain of the flow model as described above does not capture the southern extension of this potential repository; therefore, a new flow model has been developed to evaluate the ambient hydrologic conditions within this larger siting volume. This section describes the general hydrogeologic implications for repository design and presents the modeling setup and the preliminary results calculated using the extended model grid.

3.3.4.5.1 Hydrogeologic Implications for Repository Design

Characterization of the volume of rock at Yucca Mountain within which a potential repository could be constructed has been the focus of numerous geologic, hydrogeologic, and thermal studies. Lithologic layers comprising the potential repository horizon include the following Topopah Spring Tuff subunits: the lower part of the upper lithophysal zone (Ttptul), the middle nonlithophysal zone (Ttptmn), the lower lithophysal zone (Ttptll), and the lower nonlithophysal zone (Ttptln). This geologic volume, considered for hosting a repository, is identified in the *Subsurface Facility System Description Document* (CRWMS M&O 2000 [DIRS 151467], Section 1.2.2.1.8, p. 16).

A number of potential repository design strategies have been proposed over the past several years. Investigative studies to determine the hydrologic, transport, and thermal processes occurring within the repository horizon have often been closely tied to the prevailing draft repository design at the time of the study. The goal of this section is to decouple the details of design from a general understanding of the hydrogeologic implications of waste emplacement within the host rock. However, one principal factor that cannot be completely decoupled from design is seepage of water into waste emplacement drifts. Estimates of seepage depend upon predicted percolation. Additionally, the hydrologic characteristics within a lithologic layer will determine the flux rate at which seepage will occur in an emplacement drift. Since hydrologic characteristics are different within each of the host rock subunits, percentage estimates of seepage for each layer are also expected to differ. Modeling studies described in *Seepage Model for PA Including Drift Collapse* (CRWMS M&O 2000 [DIRS 153314], Section 6.6 and Attachment III, Figures AIII-1 and AIII-2) have shown that the percent of predicted seepage for the Tptpl is much lower than that for the Tptpmn (i.e., much higher percolation rates are needed in the Tptpl to cause seepage). Consequently, information about repository design (e.g., the number of drifts located in each lithologic unit) is essential for estimating the overall potential for seepage.

Data Characterizing the Potential Repository Host Horizon—An understanding of the relationship between repository design and hydrogeologic implications requires an assessment of available data. Types of data collected pertaining to the repository host rock include geologic, rock properties, mineralogic, and geochemical data. Figure 3.3.4-8 shows the location of data collection points used to characterize the potential repository horizon. Characterization data are relatively dense in the vicinity of the ESF (which includes the ECRB Cross Drift); however, north of N 235,100 m, south of N 229,000 m, and west of Solitario Canyon fault lie fewer well-characterized areas. In particular, boreholes from which qualified rock hydrogeologic properties have been obtained (indicated by triangular symbols) are not present in the northern, southern, and western areas of the potential repository horizon, with the exception of borehole USW WT-24. This paucity of data contributes to uncertainty to the understanding of geologic conditions and hydrogeologic flow and transport characteristics in areas surrounding central Yucca Mountain. Furthermore, even at borehole and ESF locations, data are biased vertically, or stratigraphically, to the near-surface rocks. Of the more than 70 surface-based vertical boreholes used in the development of the *Geologic Framework Model (GFM3.1)* (CRWMS M&O 2000 [DIRS 138860]), fewer than half penetrate the rocks below the TSw. Only ten boreholes provide data below the TSw (CRWMS M&O 2000 [DIRS 145771], Section 6.2), necessary for assessment of rock hydrologic properties of the potential repository host horizon.

Data available to characterize the spatial extent and volume of the potential repository horizon include a bedrock geologic map, borehole lithologic contacts, measured stratigraphic sections, and geologic data from the ESF. These data sources are identified in the *Geologic Framework Model (GFM3.1)* (CRWMS M&O 2000 [DIRS 138860], Section 4, p. 19). Each of the lithologic layers of the horizon is continuous beneath Yucca Mountain, except where displaced by large offset faults (e.g., the Solitario Canyon, Bow Ridge, and Dune Wash faults). The total thickness of the repository horizon ranges from about 50 to 230 m. Figure 3.3.4-9 shows a three-dimensional representation and cross-sectional view of the spatial distribution and thickness of the site lithology. The upper surface of the horizon has been clipped to maintain an overburden thickness of 200 m, while the lower surface has been clipped to maintain a water

table standoff distance of 160 m. The overburden and standoff requirements are prescribed in the *Subsurface Facility System Description Document* (CRWMS M&O 2000 [DIRS 151467], Sections 1.2.2.1.9 and 1.2.2.1.4, respectively). Note that in the north-south cross section, the elevation of the host rock units is higher in the south than in the north. This establishes a greater distance between the repository horizon and the water table, which may result in longer groundwater travel times in the UZ beneath southern Yucca Mountain. Figure 3.3.4-10 shows a plan view of the repository siting area for the lower-temperature operating mode (BSC 2001 [DIRS 154548]).

Significance of the PTn and CHn Units—Additional geologic information relevant to the assessment of potential repository performance includes the thickness and continuity of units lying above and below the repository horizon. The PTn and CHn major hydrogeologic units are believed to play an important role in UZ flow and transport (Section 3.3.3). The high matrix porosity and large storage capacity of the PTn may enable this unit to damp and distribute infiltration pulses above the horizon (CRWMS M&O 2000 [DIRS 151940], Section 3.3.3.2), while the occurrence of alteration minerals within the CHn below the potential repository may significantly retard radionuclide migration (CRWMS M&O 2000 [DIRS 138960], Section 6.3.2). Geologic data (BSC 2001 [DIRS 154622], Figure 19) indicate that the PTn ranges in thickness from greater than 165 m beneath northern Yucca Mountain to about 15 m in the south, with breaks in areal coverage along the Solitario Canyon, Iron Ridge, and Dune Wash fault systems (Figure 3.3.4-11). Where the PTn is thin or absent as the result of fault displacement, episodic infiltration/percolation events may perpetuate into the TSw rather than be attenuated and more evenly redistributed within the matrix of the PTn. The assumption that the PTn buffers episodic percolation flux may not always be true, because the role of faults and fractures and the potential for lateral diversion in these thin or absent areas of the PTn are uncertain.

The CHn, defined here as the combination of the Topopah Spring Tuff crystal-poor vitric nonwelded subzone (Ttpv1), the pre-Topopah Spring bedded tuff (Tpbt1), the Calico Hills Formation (Tac), and the pre-Calico Hills Formation bedded tuff (Tactb), ranges in thickness from greater than 300 m in the northeast to less than 50 m in the southwest (Figure 3.3.4-12). Rock properties and mineralogy data suggest that much of the CHn is altered (primarily to sorptive zeolites) beneath Yucca Mountain, except for an area below the southern part of the mountain that remains predominantly vitric (CRWMS M&O 2000 [DIRS 154863], Section 6.5.3; CRWMS M&O 2000 [DIRS 138960], Section 6.3.2). The presence of low-permeability zeolites within the CHn will reduce percolation flux through the rock matrix and divert water to a more permeable pathway (e.g., fracture, fault, unaltered rock), thus limiting sorption and decreasing radionuclide travel times to the water table. The unaltered (vitric), nonwelded portion of the CHn accounts for only a small volume of the entire CHn, and its areal extent diminishes with depth (CRWMS M&O 2000 [DIRS 154863], Section 6.5.3). Although matrix permeabilities are much higher for the vitric CHn than for the zeolitic CHn, the presence of nonwelded vitric material may damp and distribute percolation flux, much like the matrix of the PTn. In light of these characteristics, the existence of the vitric CHn beneath the potential repository horizon is favorable to repository performance.

The presence of fractures within the CHn and their potential to serve as pathways for flow and transport is not well understood, and thus adds significant uncertainty to the modeling studies. Fracture networks occurring within the zeolitic CHn may enable groundwater carrying

radionuclides to bypass the sorptive zeolitic matrix, resulting in decreased travel times to the water table (CRWMS M&O 2000 [DIRS 144331], Section 6.1.1). Currently, this uncertainty is unconstrained, given that the only fracture hydrogeologic data available for the zeolitic CHn are from a single tested interval of borehole UE-25 UZ#16 (CRWMS M&O 2000 [DIRS 145771], Section 6.1.1). Liquid-release testing at Busted Butte, as described in *Unsaturated Zone and Saturated Zone Transport Properties (U0100)* (CRWMS M&O 2000 [DIRS 154024], Section 7), suggests that fractures within the vitric CHn may not play a significant role in flow and transport.

Faults—Faults are another aspect of the site that may have important hydrogeological implications. At the land surface, the infiltration focus may occur along fault zones lying beneath drainages. At depth, permeable faults may serve as conduits for flow where they intersect layers that laterally divert significant amounts of percolation. Faults with low permeability, those that juxtapose permeable rocks against low-permeability rocks, or those with high permeability and low capillary suction may form barriers to lateral flow. Though many different conceptualizations exist, several of which are summarized in *Unsaturated Zone Flow and Transport Model Process Model Report* (CRWMS M&O 2000 [DIRS 151940], Section 3.3.5), sparse data have been collected to surmise the hydrogeologic significance of faults, thus creating uncertainty in modeling studies. Nonetheless, it is reasonable to expect that fault properties vary both with depth and horizontally along an individual fault, as well as from fault to fault. A pattern of predominantly north-trending normal faults has been observed at Yucca Mountain (Figure 3.3.4-8) (BSC 2001 [DIRS 154622], Section 6.4.2). Major faults crosscutting the volume of repository host rock include the Solitario Canyon, Bow Ridge, Iron Ridge, and Dune Wash fault systems. As portrayed in the *Geologic Framework Model (GFM3.1)* (CRWMS M&O 2000 [DIRS 138860]), these faults show large (greater than 100 m) down-to-the-west displacement. The largest of these faults is the Solitario Canyon fault, which exhibits more than 400 m of displacement. Several northwest-trending faults have been observed in the northern part of the site. These faults have small vertical displacements, but coincide with prominent drainages (e.g., Drill Hole Wash, Pagany Wash, Sever Wash). According to the *Geologic Framework Model (GFM3.1)* (CRWMS M&O 2000 [DIRS 138860]), smaller mapped normal faults within the host rock volume include the Ghost Dance, Sundance, “Imbricate,” “SolWest,” Boomerang, and “SolJFat” faults. These faults typically show much less than 100 m of vertical displacement. Although repository design criteria may impose a standoff distance between faults and emplacement drifts, faults may still remain significant features of the flow domain as a result of lateral flow, particularly within the CHn, where zeolites are known to create water perching conditions. If faults are permeable features below the potential repository and transect rock layers with low permeability, then the fully saturated conditions associated with water perched above a low permeability layer may focus water into fault zones in that layer, resulting in reduced travel times to the water table.

Infiltration and Water Table Configuration—Additional uncertainties pertaining to the hydrogeologic implications of repository design are associated with infiltration and water table configuration. The spatial and temporal distribution of net infiltration provides an important upper boundary condition in the UZ flow and transport models. Regardless of design layout, the potential repository would most likely be located below areas of high infiltration as well as areas of low infiltration. The expected consequence of siting a repository below a high-infiltration source is greater percolation flux, compared with siting a repository below low-infiltration areas. Based on current infiltration maps (CRWMS M&O 2000 [DIRS 151940], Section 3.5.2), higher

infiltration rates correlate with higher elevations, such as in the northern part of Yucca Mountain and along the crest of the mountain. Higher infiltration rates are also modeled in Solitario Canyon and in the upper reaches of drainages east of Yucca Crest as a result of surface run-on. Infiltration rates are typically lower in the southern part of Yucca Mountain and beneath thick alluvium to the east. Percolation flux at the repository horizon may therefore be lower, in general, beneath the southern part of Yucca Mountain. This may promote longer groundwater travel times between the potential repository and the water table, and thus enhance repository performance. Uncertainties in percolation flux at the repository horizon arise, in part, out of uncertainties in the distribution of net infiltration.

Because groundwater travel times in the UZ are largely dependent on the distance between the potential repository and the saturated zone, it is important to establish the position of the water table. In general, water table elevations measured in the vicinity of the ESF and below southern Yucca Mountain, east of the Solitario Canyon fault, are consistent with a flat potentiometric surface at an elevation of about 730 m above mean sea level (Tucci et al. 1996 [DIRS 101303], p. 3). West of the Solitario Canyon fault, water levels show consistency at approximately 776 m above mean sea level. It is uncertain whether the 46-m water level transition across the Solitario Canyon fault is abrupt or gradual. Nevertheless, the effect of a gradual versus an abrupt transition, by itself, is not likely to be significant to modeling studies of flow and transport. It is more important to understand the water table configuration beneath northern Yucca Mountain. There has been much debate whether the high water levels observed in boreholes USW WT-24 and USW G-2 represent the regional potentiometric surface or indicate the presence of perched water. If the former hypothesis is true, it would suggest the presence of a large hydraulic gradient beneath northern Yucca Mountain, with water elevations in the north being approximately 300 m higher than those below central and southern Yucca Mountain. The existence of a large hydraulic gradient means a shorter distance exists between the repository horizon and the water table beneath northern Yucca Mountain. This limits the available siting volume for the potential repository, since a standoff distance of 160 m must be maintained between emplacement drifts and the current water table (CRWMS M&O 2000 [DIRS 151467], Section 1.2.2.1.4, p. 15).

Another important aspect of the elevation of the potentiometric surface is the potential for climate induced rises in the water table in the future. The *Yucca Mountain Science and Engineering Report* (DOE 2001 [DIRS 153849], Section 4.3.3.1) describes evidence of past fluctuations in the elevation of the water table near Yucca Mountain. Multiple lines of evidence suggest that a 120-m rise in water table elevation is the maximum potential increase due to a wetter future climate (CRWMS M&O 2000 [DIRS 151940], Section 3.7.5.2). Based on evidence obtained from recent boreholes in the Nye County Early Warning Drilling Program, Paces and Whelan (2001 [DIRS 154724]) concluded that water table fluctuations during the Pleistocene (the past 2 million years) at the sites examined may be limited to 17 to 30 m, rather than the 80 to 120 m range previously suggested. This new data is not consistent with large Pleistocene water table fluctuations at the sites examined, or by inference, beneath Yucca Mountain. Zeolitization of the tuffs, attributed to prolonged contact with water, is interpreted as an indicator of past elevations of the water table (DOE 2001 [DIRS 153849], p. 4-405). At Yucca Mountain, evidence of zeolitization indicates that the water table must have remained about 100 m higher than at present over the thousands of years required for zeolitization of the glassy tuffs. However, the upper boundary of the zeolitic zone is not parallel to the water table,

suggesting that it formed (at least in part) before the tectonic tilting of the tuffs, which occurred more than 12 million years ago, rather than during Pleistocene glacial stages.

In the event of a future climate-induced rise in the water table of 120 m, the northernmost emplacement drifts of the repository layout presented in the *Yucca Mountain Science and Engineering Report* would remain more than about 90 m above the higher water table level (DOE 2001 [DIRS 153849], Figure 1-13; see also Figure 3.3.4-13a). A smaller climate induced water table rise, consistent with recent data (Paces and Whelan 2001 [DIRS 154724]), would result in a minimum distance of about 180 m between the northernmost (closest) emplacement drifts and the water table.

In the TSPA-SR, the effects of a water table rise were incorporated conservatively by including a uniform maximum rise of approximately 120 m of the nearly level potentiometric surface below most of the potential repository (from 730 to 850 m). In the model, the rise in the water table is included for all climate states that are wetter than the modern climate; therefore, the water table rise occurs after 600 yrs (at the transition from modern to monsoonal climate) and persists beyond 10,000 yrs. The effects of the water table rise on the hydraulic gradient beneath the northernmost emplacement drifts were not explicitly included. Therefore, the performance implications of a water table rise on the gradient have not been examined directly. However, conclusions about the performance implications can be drawn from other information related to the Yucca Mountain site. For example, the values of total percolation flux at the water table are generally among the lowest in the area of the northernmost emplacement drifts because extensive zeolitization of the Calico Hills Formation in this area serves to laterally divert flow above the water table (CRWMS M&O 2000 [DIRS 153246], Figure 3.2-8). Similarly, the fraction of the total number of radionuclide particles released from the repository that reached the water table under the medium infiltration case and the glacial transition climate case is generally lowest in the area of the northernmost emplacement drifts (CRWMS M&O 2000 [DIRS 153246], Figure 3.7-11). This information suggests that any errors introduced by the simplified model of a uniform climate induced water table rise in the performance assessments are likely to be small. Furthermore, incorporating the higher water table elevations in the TSPA analyses conducted over longer time frames allows DOE to evaluate the robustness of repository performance beyond the regulatory time period.

The flexible design approach adopted by the DOE includes the ability to continue to enhance the design to best achieve performance-related benefits identified through ongoing analyses (DOE 2001 [DIRS 153849], Executive Summary, p. xxxv). The evolution of the design will be based on a process that includes enhancing components of the design to best achieve the performance-related benefits (DOE 2001 [DIRS 153849], Executive Summary, p. 1). As the design evolves to that to be used to support a license application, should the site designation become effective, the performance related implications of water table rise on the northernmost drifts of the layout will be considered as appropriate. Specifically, the eventual layout will reflect performance considerations.

3.3.4.5.2 Three-Dimensional Flow Field Development with an Extended Model Domain

Model Domain and Numerical Grid—To consider a potential lower-temperature operating mode, a new model domain has been established and a new three-dimensional numerical grid

developed. Figure 3.3.4-7 shows the expanded model domain with the extended repository design, and Figure 3.3.4-13 shows a plan view of the numerical grid created for this model domain. This three-dimensional grid adds refinement in the footprint of the potential repository; as before, gridblocks are aligned along potential emplacement drifts. Note that drift alignment has changed; compare Figures 3.3.4-1 and 3.3.4-13 for the change. The new grid has 1,708 columns of gridblocks and, on average, 47 layers per column. Both the fracture and matrix continua are represented in a dual-permeability grid, which has 164,100 gridblocks and 671,958 connections. As presented below, modeling studies performed with the expanded numerical grid investigate the effects of the present-day mean infiltration scenario on moisture flow at and below the potential repository horizon.

Infiltration Map and Model Parameters—The present-day mean infiltration map used for flow simulations has an average value of 4.4 mm/yr, which is slightly less than the average value in Table 3.3.2-1. The reason for this difference is the consideration of a larger model domain with the extended grid, which captures a southern area with relatively low infiltration. The spatial distribution of the present-day mean infiltration is shown in Figure 3.3.4-14. Higher surface recharge rates occur principally in the northern part of the model domain and along Yucca Crest, east of the Solitario Canyon fault.

Additional modeling input used in the following flow simulations includes the calibrated base case rock hydrologic parameters described in *UZ Flow Models and Submodels* (CRWMS M&O 2000 [DIRS 122797], Table II-1).

Percolation Flux—The total (matrix plus fracture) percolation flux distribution at the repository horizon and at the water table, simulated using the present-day mean infiltration scenario, is shown in Figures 3.3.4-15 and 3.3.4-16, respectively. Compared with the surface infiltration pattern used for the top boundary condition (Figure 3.3.4-14), Figure 3.3.4-15 shows that lateral diversion of flow occurs between the land surface and the repository level. This effect is particularly pronounced in the northern part of the model domain, but is evidenced elsewhere by the increase in flux along fault zones. The lateral flow observed in the simulation results is attributed to the PTn, whose thickness beneath Yucca Mountain increases to the north. Vertical variations in the modeled hydrologic properties of the nonwelded PTn layers, better captured with the refined vertical grid resolution applied within the PTn, create sufficient contrast under the present-day mean infiltration rates to divert flow laterally down-dip. Faults are treated as structural pathways for flow, intercepting the lateral flow and focusing it downward. Previous modeling studies using the same infiltration conditions and base case hydrologic parameters with the TSPA grid, which has coarser vertical resolution within the PTn (Figure 3.3.4-2), show considerably less lateral flow associated with the PTn unit in the northern part of the model domain. Thus, the increased lateral flow seen in the extended model is a reflection of the numerical resolution applied. Greater resolution of intra-layer capillary gradients allows for better resolution of the potential for capillary barrier-driven lateral flow.

Figure 3.3.4-16 presents the simulated percolation flux at the water table. Compared with the surface infiltration map and the distributed percolation flux at the repository horizon (Figures 3.3.4-14 and 3.3.4-15, respectively), Figure 3.3.4-16 shows a much different flow pattern. As a result of extensive zeolitization in the upper CHn, large lateral flow occurs in the northern half of the northern repository block (north of N 234,000 m). This lateral flow is

mainly intercepted by the Drill Hole Wash, Pagany Wash, and Sever Wash faults. Lateral flow also occurs in the southern half of the potential repository domain, where it becomes intercepted by the Sundance and Ghost Dance faults. A relatively high simulated percolation flux not associated with fault zones in the central part of the potential repository footprint reflects the presence of vitric CHn, which does not divert flow laterally to the faults, but funnels it to the bottom of the vitric zone. The distribution of percolation flux simulated with the extended model grid is similar to the distribution of percolation flux simulated with the TSPA grid (Figure 3.3.4-3) for the same infiltration scenario and hydrologic parameter set.

3.3.4.6 Abstraction for Total System Performance Assessment

The work reported in this section is devoted to evaluating process-model sensitivities and uncertainties beyond those associated with the flow fields originally abstracted for the TSPA, which are documented in *Abstraction of Flow Fields for TSPA* (CRWMS M&O 2000 [DIRS 153104], Section 6). Simulation results from the study with the extended repository footprint model are not used to support any abstraction model that directly supports the TSPA. The results found here indicate that the process modeling and associated model abstractions used to represent this component (i.e., three-dimensional flow fields) in the TSPA baseline are representative (or conservative) with respect to the effects of this component on total system performance. Therefore, any future changes in model abstractions for this component will not diminish the potential repository's performance as represented in the total system performance baseline.

3.3.4.7 Multiple Lines of Evidence

Natural analogue studies of fluid flow processes for similar geologic and hydrologic settings provide multiple lines of evidence that support the three-dimensional flow models constructed for Yucca Mountain. These studies help constrain estimates of groundwater flow paths and percolation fluxes, and provide insights into processes controlling fracture and matrix flow under unsaturated conditions. Studies at Yucca Mountain and nearby Rainier Mesa provide the best insights into past and present flow conditions, and they can be used to help constrain models to predict future flow behavior.

Groundwater Travel Times and Fast Flow Regimes—Rainier Mesa, approximately 20 miles northeast of Yucca Mountain, has been the site of extensive underground observations of fluid flow (Wang 1991 [DIRS 109736]). About eight percent of the measured mean precipitation was observed to be infiltrating into one of the tunnels constructed in zeolitic tuffs at Rainier Mesa. This seepage was associated with a small number of faults and fractures (Wang 1991 [DIRS 109736], p. 79). These structural features are thought to be a pathway for flow from perched water above the zeolitic horizon (Wang 1991 [DIRS 109736], p. 82). The seepage is geochemically similar to meteoric water (Wang et al. 1993 [DIRS 108839], p. 677). Tracer tests and tritium samples indicate that the likely rate of fast pathway flow is from one to six years to travel from the surface to the water table, at a depth of 1,000 m. This travel time is orders of magnitude less than the matrix travel time calculated using measured matrix conductivities, but is supported by measurements of bomb-pulse chlorine-36 in several samples from one of the tunnels (Wang et al. 1993 [DIRS 108839], p. 677).

Bomb-pulse chlorine-36 isotope ratios have been found in several locations in the vicinity of some fault zones in the ESF, and indicate fast flow from the ground surface to the depth of the ESF that results in fluid travel times of less than 50 years. Elevated chlorine-36 signatures are confined to the immediate vicinity of faults and other features, suggesting that fast flow zones are localized, and large areas of the potential repository appear to be unaffected by fast path flow (CRWMS M&O 2000 [DIRS 141187]).

Percolation Flux Studies—Several dating methods have been used to constrain percolation fluxes at Yucca Mountain. The ages of calcites in the UZ have been used as a tool for estimating percolation fluxes (Marshall and Whelan 2000 [DIRS 154415]). Chloride content of pore waters and carbon-14 content of UZ gas, together with water content data, can be used to calculate long-term average percolation fluxes in the TSw. The carbon-14 method is based on residence time of pore waters (Yang et al. 1996 [DIRS 100194]; Yang et al. 1998 [DIRS 101441], p. 16) and water content measured for drill core in the laboratory (Engstrom and Rautman 1996 [DIRS 100670], pp. 23 to 28, and Appendix G; Rautman and Engstrom 1996 [DIRS 100642], pp. 26 to 32, and Appendix G; Rautman and Engstrom 1996 [DIRS 101008], pp. 27 to 32, and Appendix G). The flux is calculated from the total amount of water in the UZ between two points and the difference in apparent carbon-14 ages at the top and bottom of the zone in question. The use of relative ages eliminates the effect of any inherited carbon-14 ages that the groundwater may have acquired from surficial materials or soil gases.

The percolation flux calculated using the carbon-14 data from borehole USW UZ-1 and the water content data from borehole USW UZ-14 (3 m away) is 2.5 mm/yr (Yang 2001 [DIRS 154613], Table 2, and pp. 7 and 11), based on carbon-14 values at the top and bottom of the TSw and total water content for the full thickness of the unit. This equates to a transport velocity of only 2.9 cm/yr. Similar data sets are not available from other boreholes, but the carbon-14 data from borehole USW UZ-1 can be regressed against depth to obtain values for percent modern carbon as a function of depth. This relationship can then be used with water content data for boreholes USW UZ-14, UE-25 UZ#16, USW SD-7, USW SD-9, and USW SD-12 to calculate average percolation fluxes of 2.4, 2.7, 1.8, 2.0, and 1.9 mm/yr, respectively (Yang 2001 [DIRS 154613], Table 3). All of these values are significantly smaller than those used in the UZ flow and transport model (4.5 mm/yr) (CRWMS M&O 2000 [DIRS 151940], Table 3.7-4); thus, relative to this data set, the model provides a conservative estimate of repository performance.

3.3.4.8 Summary of Uncertainties Related to Three-Dimensional Unsaturated Zone Flow Fields

Establishing confidence in model simulations of the three-dimensional flow processes occurring at Yucca Mountain requires sufficient input data regarding model boundary conditions and spatial variability of the hydrologic characteristics of the system, in addition to appropriately defined conceptual models and numerical modeling techniques. Given the complexity of the UZ system at Yucca Mountain, none of these aspects can be completely understood. However, through sensitivity and bounding studies, a model can be used to identify and quantify uncertainty. Major uncertainties in the calculated UZ flow fields are discussed in this section and summarized in Table 3.3.4-2.

3.3.4.8.1 Conceptual Uncertainties

Steady-State Ambient Moisture Flow Assumption—Use of steady-state conditions for flow field development is a simplifying assumption supported by pneumatic and isotopic data that suggest the PTn unit, where present, effectively damps episodic infiltration pulses such that water flow below the PTn is approximately steady. If, alternatively, significant transient flow persists below the PTn, it may affect the simulation of percolation flux and estimated groundwater travel times in the UZ.

Applicability of van Genuchten Model to Unsaturated Fracture Flow—Because better alternatives are lacking, it is assumed that the van Genuchten relationships (van Genuchten 1980 [DIRS 100610], pp. 892 to 893), originally developed for porous media, can be used for liquid flow in the active fracture continuum. However, the physics of water flow in fracture networks is not exactly the same as in porous media. Uncertainties arising from the use of the van Genuchten approach include the predicted moisture conditions within fractures and the rock matrix. This affects capillary strength or, more specifically, capillary-barrier effects, which in turn affect predictions of seepage. Modeling studies using alternative methods, such as discrete fracture networks, or alternative moisture functions, such as Brooks-Corey relations (Brooks and Corey 1966 [DIRS 119392]), may prove useful in treating this uncertainty. However, these alternatives may have greater uncertainty than the methods currently used. More laboratory testing and field data collection could reduce uncertainty.

Model Used to Calculate Fracture/Matrix Flow Components—As discussed in *Conceptual and Numerical Models for UZ Flow and Transport* (CRWMS M&O 2000 [DIRS 141187], Section 6.4), a dual-permeability model (DKM) has been used in the UZ flow and transport model as the baseline approach for calculating flow and transport between fractures and the matrix. Capillary pressure and concentration gradients between fractures and the matrix are presented using a single-matrix-node approximation that cannot accurately describe the steep fronts near fracture-matrix interfaces because the matrix is treated as a single continuum in the DKM. This issue is especially important for modeling matrix diffusion and radionuclide transport in the UZ. Therefore, using the DKM may introduce some uncertainties into simulations of UZ flow and transport, which can be reduced by using more accurate matrix discretization schemes. A more detailed discussion of these schemes is provided in Section 11.3.2.

Effect of Large Gridblock Averaging and Vertical Resolution on Flow Fields—The distribution of simulated percolation flux and flow focusing is affected by the averaging of relatively detailed net infiltration data (available at 30 m spacing) onto large gridblocks of the flow model. Within the flow model, local peaks in the net infiltration map are typically averaged with nearby values that are much lower in magnitude. Though the total mass flux is conserved, loss of detail with regard to spatial variability can limit the ability of the flow model to capture areas of focused or fast path flow. Adding detailed numerical resolution to the repository footprint and along fault zones helps to reduce these averaging effects in critical areas. In addition to lateral resolution, model results are influenced by vertical grid resolution. Studies from the flow model have shown that enhanced vertical grid resolution within the PTn unit leads to more lateral flow. The representativeness of these results is uncertain given the assumed lateral continuity of rock properties. Comparing the modeling results against the observed data

helps determine optimal gridblock size. Moreover, this indicates the importance of maintaining consistent discretization throughout model development (i.e., calibration and flow field prediction).

Layer-Averaged Rock Properties—Because lateral variability in rock characteristics exists at Yucca Mountain, the use of spatially uniform parameters assigned within each model layer is a simplifying assumption that creates uncertainty in the model results. Sensitivity analyses with laterally heterogeneous rock properties could identify and quantify uncertainty associated with the layered approach. A model incorporating lateral heterogeneity is expected to show less lateral flow and more flow focusing.

Conceptual Model of Flow Within and Below Perched Water Zones—Zeolitically altered layers at the base of the TSw and within the CHn are believed to reduce percolation flux, lead to the development of perched water, and create lateral diversion. The extent to which these flow phenomena are affected by fractures and faults within zeolitic rocks is largely unknown, creating uncertainty in model results. Different perched water conceptual models have been developed in an attempt to bound uncertainty associated with the role of fractures in zeolitic rocks below the potential repository horizon. One conceptual model for perched water (the flow-through model) assumes that there are no large-scale, vertically connected fractures within the zeolitic rocks. However, fractures within zeolites are theorized to have greater permeability than the altered matrix; therefore, in this model some of the percolation flux passes vertically through the zeolitic CHn, while the rest is laterally diverted within perched water zones toward faults. Another conceptual model for perched water (the by-passing or unfractured zeolite model) assumes that fractures contribute no secondary permeability to the zeolitic rocks, which means the water perching mechanism is controlled only by the low-permeability matrix. This conceptual model creates more lateral flow diversion. As with fractures, alternative fault parameters have been used in simulations to evaluate model sensitivity.

3.3.4.8.2 Data and Parameter Uncertainties

Upstream Models—Net surface infiltration of water from precipitation that penetrates the evapotranspiration zone of the mountain is considered the most important factor affecting overall hydrologic behavior, in addition to radionuclide transport, within the UZ system. Uncertainties surrounding the distribution and magnitude of net infiltration are constrained by the development of upper-, mean, and lower-bound models for the present-day, monsoonal, glacial-transition, and full glacial climates. Flow fields are simulated for each of these scenarios. In addition, the location and nature of the vitric-zeolitic transition within the CHn is uncertain as modeled in the rock properties model of Yucca Mountain, which has implications for simulated percolation flux distributions, preferential flow paths, and radionuclide transport.

Rock Hydrologic Parameters Used for Model Calibration and Validation—The lack of data with which to characterize the hydrologic properties of fractures and major faults within and below the CHn makes estimation of fracture and fault flow components highly uncertain. A reevaluation of fracture parameters of the CHn using the Busted Butte test data and additional sensitivity analyses are needed to reduce this uncertainty.

3.3.4.9 Summary and Conclusions

A number of three-dimensional steady-state flow fields have been developed, as documented in *UZ Flow Models and Submodels* (CRWMS M&O 2000 [DIRS 122797]). Since the preparation of initial reports, additional flow fields have been generated to investigate the effects of a post-10,000 year climate (i.e., full glacial) and an expanded repository footprint.

Using different climate scenarios and conceptual models for flow, the simulated flow fields predict percolation distribution within the UZ system, components of fracture and matrix flow, probable flow paths below the potential repository, and groundwater travel times in the UZ. The flow model used to generate the three-dimensional steady-state flow fields provides parameters and bounding conditions for subsequent modeling studies and analyses, such as seepage into drifts and the TSPA.

Uncertainties associated with the three-dimensional flow fields are largely attributable to the limited data available to characterize the spatial and temporal distribution of net infiltration and the spatial variability of rock hydrologic properties. This also imparts uncertainty in conceptual models used to describe flow behavior, since these models are developed primarily from site data. The assumption of steady-state flow and the use of layer-averaged rock parameters are among these conceptual uncertainties. An additional source of uncertainty stems from the numerical techniques employed to simulate flow conditions, such as grid resolution, and the applicability of the van Genuchten relationships and the DKM approach. However, the impact of uncertainties associated with available data on model results for performance analysis is different depending on the type of data. For example, the net infiltration rate at Yucca Mountain has perhaps the most significant effect on repository performance (CRWMS M&O 2000 [DIRS 122797], Figure 6-57). For the current climate, this model boundary condition is believed to be well constrained as a result of decades of field and model calibration studies using measured data. Uncertainties associated with other data inputs will have a lesser impact on modeling results used for performance assessment because they affect only fluid distribution and flow paths, rather than net flow rates.

Through bounding and sensitivity studies, uncertainties in the three-dimensional flow fields can be identified, constrained, and perhaps quantified. Numerical simulations with the flow model have used 13 different infiltration maps to examine the effects of different climate scenarios on UZ flow. This helps bound model predictions of system response during potential future conditions. Different conceptual models, in particular those related to perched water below the potential repository horizon, have been developed and modeled to assess the sensitivity of model results to changes in fracture parameters (which are poorly constrained by site data) within the CHn.

Overall, the simulated flow-field results show the greatest sensitivity to the magnitude of net infiltration. Model results are also sensitive to grid resolution, seen particularly within the PTn unit (i.e., finer vertical resolution leads to greater lateral flow). Assumptions regarding the conceptualization and parameterization of fractures within the CHn unit and fault zones have large uncertainties as a result of limited or no data, yet these UZ features appear to have a significant impact on flow behavior below the repository. Additional sensitivity studies, using different conceptual models and a range of hydrologic parameters for fractures and faults, are

needed to assess the potential range of variability in flow behavior between the repository horizon and the water table. Furthermore, continual data collection from the existing underground tunnels and boreholes, and incorporation of these data into the modeling studies will significantly reduce the uncertainties associated with the model predictions.

3.3.5 Thermal-Hydrologic Effects on Unsaturated Zone Mountain-Scale Flow

3.3.5.1 Introduction

UZ flow (Sections 3.3.4 and 4.3) and transport (Section 11.0) will be affected by heat released from the decay of radioactive waste within emplacement drifts in the potential repository at Yucca Mountain. The effects of heat on UZ flow can be analyzed on different spatial and temporal scales. Mountain-scale TH response requires a model that includes the spatial variability of thermal and flow properties, infiltration, and physical features (such as faults) that may promote heterogeneous behavior.

This section summarizes the modeling and uncertainty studies performed to determine the effects of heat on mountain-scale UZ flow, liquid saturation, and temperature. Specifically this section summarizes work conducted since TSPA-SR to examine TH effects over a range of thermal loading by addressing both higher and lower-temperature operating modes for the repository. Section 4.3.5 will present an investigation of the evolution of near-drift TH conditions, on a much smaller scale, than the mountain-scale TH model, to more accurately determine the likelihood of seepage into an individual drift for a given set of thermal-loading conditions. The mountain-scale TH model presented in this section provides an analysis of temporal and spatial variability in UZ conditions under thermal load. Such variability may result from the temporal and spatial distribution of UZ thermal and flow properties, variation in infiltration, changes in lithology, and the presence of faults. In this analysis, the focus is on how the thermal-hydrologic coupled processes affect the magnitude and spatial distribution of mountain-scale liquid saturation, temperature, and the liquid flux at the repository horizon and the rest of the UZ.

Like any model, mountain-scale TH models are subject to uncertainties associated with the conceptual model, parameter selections, and data. These will be addressed in the following subsections and summarized in Section 3.3.5.8. Modeling studies discussed here include alternative thermal operating modes for below-boiling and above-boiling temperatures within the rock mass adjacent to the repository drift.

3.3.5.2 Goal of the Mountain-Scale Thermal Hydrologic Models

The mountain-scale TH simulations provide predictions for thermally affected liquid saturation, gas- and liquid-phase flux (together referred to as flow fields), and the distribution of temperature and saturation in the UZ. Of particular interest is the impact of thermal loading imposed by waste emplacement on water percolation at and near the repository host rock (e.g., drainage between pillars), and the potential flow barrier effects in the basal vitrophyre of the Topopah Spring Tuff and zeolites of the Calico Hills Formation underlying the repository horizon. These rock units impede the transportation of radionuclides from the repository to the water table because of their low permeability and/or high sorptivity.

The TH model therefore provides for qualitative and quantitative evaluation of repository-heat impact on the UZ and includes prediction of the following:

- Extent of the two-phase zone
- Liquid and gas flux in near and far field
- Moisture redistribution in the UZ
- Temperature near drifts and within pillars
- Drainage potential of the pillars
- Potential for flow and transport property changes in the PTn and CHn hydrogeologic units
- TH effects on the water table and perched water bodies
- Influence of climate and forced ventilation.

3.3.5.3 Discussion of Analysis Model Report Revision 00 Results

The *Mountain-Scale Coupled Processes (TH) Models* report (CRWMS M&O 2000 [DIRS 144454]) documents the development of the mountain-scale TH model used to support the TSPA-SR (CRWMS M&O 2000 [DIRS 153246]). The study reported in the above documents used the EDA II operating mode with an initial thermal load of 72.7 kW/acre (1.45 kW/m of drift) and a forced ventilation period of 50 years, during which 70 percent of the decay heat was assumed to be removed. The model evaluates the effects of heat on UZ flow and the distribution of liquid and temperature over a period of 100,000 years, and provides the necessary framework to test conceptual hypotheses of coupled heat and fluid flow in the UZ. The simulations were conducted using TOUGH2 V1.4.

The mountain-scale TH model (CRWMS M&O 2000 [DIRS 144454]) was developed from the UZ flow model and therefore retains geological and hydrologic properties of that model. The thermal and flow parameters used as input to the model were based on the calibrated property set (CRWMS M&O 2000 [DIRS 144426]) developed for the UZ flow model. The simulations were performed using a spatially varying mean-infiltration rate, which was altered according to the infiltration model climatic variation over the thermal-loading period.

Two-dimensional and three-dimensional simulations were conducted in the TH model (CRWMS M&O 2000 [DIRS 144454]). The two-dimensional simulations were based on two cross sections, NS#1 and NS#2, which contained local refinements to explicitly represent the 5-m diameter emplacement drifts. Figure 3.3.5-1 shows a plot of the two-dimensional cross section NS#2 with the location of the repository and the UZ hydrogeologic model units.

Sensitivity studies were performed to assess the model and parameter uncertainties. For the thermal input, two operation modes were defined: forced ventilation for the first 50 years (during which 70 percent of the decay heat generated by the emplaced waste was removed) and

no forced ventilation. To assess the effect of climate, simulations were also carried out with the present-day infiltration in effect for the entire 100,000 years and, alternatively, with present-day infiltration applied only for the first 600 years. This period was followed by monsoon infiltration from 600 to 2,000 years, after which glacial-transition infiltration was applied.

The primary objective of *Mountain-Scale Coupled Processes (TH) Models* (CRWMS M&O 2000 [DIRS 144454]) was to evaluate the effects of heat on mountain-scale flow. The simulations were therefore designed specifically to address large-scale flow issues such as the effects of faults, perched water bodies, the interface of the repository unit (TSw) with the overlying PTn and the underlying CHn hydrogeologic units. Because discretization for both the three-dimensional model and the NS#1 cross sections are coarse, the sensitivity studies were conducted only on the two-dimensional NS#2 cross section. In the local refinement of the two-dimensional NS#2 cross section, there are five lateral gridblocks between drifts spaced 81 m apart. This north-south section includes potential emplacement drifts located in the middle nonlithophysal and the lower lithophysal units of the Topopah Spring welded tuff.

As expected, simulation results predicted that at the repository horizon maximum temperatures occurred in the drift walls, and less elevated temperatures occurred in the pillars between adjacent drifts. For the operation mode with 50 years of forced ventilation, the temperatures in the pillars were predicted to rise to an average of 80° to 85°C. In the immediate vicinity of the drifts, the predicted temperature rose above boiling and reached 110°C at drifts with locally low ambient percolation flux (caused by spatially variable infiltration). The dryout in the fracture and matrix around the drifts was maintained for hundreds of years. Zones of increased liquid saturation appeared above the dryout zone, and liquid flow rates one to two orders of magnitude higher than the ambient flux, primarily through the fractures, were predicted for the first 100 years of emplacement. The liquid fluxes toward the emplacement drift are driven by capillary pressure gradients resulting from the drying around the drifts. However, the decay heat from the potential emplacement drifts easily vaporizes this enhanced liquid flux, so that in fact no liquid flux was predicted to reach the emplacement drift wall. That is, the coupled process models predict no flux crossing the drift during the thermal period when the rock mass temperatures are at or above boiling. As for the drainage of thermally induced liquid flux away from the emplacement drift, the simulations predicted that liquid flow through the pillars between the emplacement drifts mostly continued at a rate close to the ambient percolation flux for most of the thermal period.

For the operating mode with no provision for forced ventilation, simulated results pertaining to flux changes were qualitatively similar to those discussed above. Quantitatively, this case gave rise to higher temperatures, a larger degree of drying in the rock mass surrounding the drifts, and larger dryout zones that also persisted longer. For example, in the absence of forced ventilation for the first 50 years of waste emplacement, temperatures in the completely dry rock mass at the drifts were predicted to rise to 250°C, and temperatures within the pillars may rise to boiling (about 96°C) after 1,000 years of heating.

In the absence of ventilation, the two-phase boiling zone was predicted to extend 200 m above the drift, to the base of the PTn (about 1,270 masl at the center of the cross-section) (Figure 3.3.5-1). At the top of the CHn unit (about 910 masl), the predicted maximum temperature rose to 75° to 80°C. With ventilation, the models predicted a boiling zone that

extends to about 50 m above the drifts. Both models predicted little influence of perched water on UZ TH conditions at or above the drifts, because most perched water bodies are located 100 to 150 m below the potential repository, where temperatures did not rise to boiling conditions.

3.3.5.4 Model Development since Revision 00 of the Analysis Model Reports

Model development since the initial issue of *Mountain-Scale Coupled Processes (TH) Models* (CRWMS M&O 2000 [DIRS 144454]), which was based on the EDA II repository operating mode, involves studies of coupled processes for a range of operating modes (Section 2.3.2). The models use both the three-dimensional numerical model and the NS#2 cross-section model documented in the initial TH model. The models also use boundary and ambient conditions, and infiltration rates documented in the initial TH model. Even with forced ventilation, the initial TH models with the EDA II thermal load predicted above-boiling temperatures in the rock near the emplacement drifts for hundreds of years. TH simulations described in this study therefore focus on the lower-temperature options in which the rock temperatures are not expected to rise above boiling anywhere in the repository. To arrive at the lower-temperature case, a lower initial thermal load of 67.7 kW/acre (1.35 kW/m of drift, Section 2.3.2) is used with a forced-ventilation period of 300 years (during which 80 percent of the heat is removed). This areal thermal load is obtained by scaling the EDA II thermal-load of 72.7 kW/acre, with a drift lineal thermal-load of 1.45 kW/m, to the proposed drift loading of 1.35 kW/m. In this new TH analysis the 50-year, 70 percent forced ventilation operating mode is referred to as the higher-temperature case and the 300-year, 80 percent forced ventilation operating mode is referred to as the lower-temperature case. The initial study documented in *Mountain-Scale Coupled Processes (TH) Models* (CRWMS M&O 2000 [DIRS 144454]) is hereafter referred to as the EDA II Case.

These model developments focus on assessing uncertainties pertaining to thermally induced flux caused by a range of thermal load conditions. In this section, studies carried out to investigate TH conditions in both the higher-temperature (above boiling) and the lower-temperature (below boiling) repository are described using the new initial thermal load. Specifically, these model developments include:

- TH models for the higher-temperature (above boiling) case, in which 70 percent of the heat is removed for 50 years, using an effective drift thermal load of 1.35 kW/m. The equivalent three-dimensional areal load for this drift thermal load is then 67.7 kW/acre.
- TH models for lower-temperature (below boiling) operating mode, in which the effective drift thermal load is 1.35 kW/m and forced ventilation removes 80 percent of the heat for a 300-year period.
- TH models using a modified thermal conductivity and heat capacity of the rock mass, to account for the lithophysal porosity of the upper and lower lithophysal units in the matrix properties for both the lower-temperature and higher-temperature operating modes. Lithophysal cavities reduce the effective thermal conductivity and the thermal capacity of the matrix continuum in the upper-lithophysal (tsw33) and lower-lithophysal (tsw35) units. The justification and approach for incorporating the effect of lithophysal cavities in the TH models is presented in Section 4.3.5.4.

- Assessment of the impact of increased infiltration (resulting from uncertainty in the climate scenario) on seepage, particularly for the lower-temperature case.

Except for the modified thermal properties described above, the simulations presented in this study use the thermal and flow properties of the initial TH model. The revised PTn flow properties described in Section 3.3.3 are not used.

3.3.5.5 Mountain-Scale Thermal Hydrologic Results and Analysis

Table 3.3.5-1 summarizes the numerical model cases (cases 1 through 7) simulated to characterize the mountain-scale TH processes under thermal loading. All these simulations subsequent to the EDA II Case use a thermal load of 1.35 kW/m (67.7 kW/acre) as the initial thermal load. These simulations were conducted to evaluate the extent of the thermally disturbed zone and the mountain-scale predicted changes in temperature, saturation, and percolation flux. In particular, the TH model results that bound the uncertainty in performance issues are of interest. Therefore, several simulation cases are conducted to ascertain the effect of grid resolution, the emplaced thermal load, the period of forced ventilation, thermal properties, and the effect of uncertainty in effective net-infiltration rates. All the simulations use numerical grids, boundary and ambient conditions, and infiltration rates documented in *Mountain-Scale Coupled Processes (TH) Models* (CRWMS M&O 2000 [DIRS 144454]) and briefly discussed in Section 3.3.5.3.

Cases 1 and 2 in Table 3.3.5-1 provide the base-case UZ three-dimensional TH conditions for the lower-temperature repository operating mode, using the thermal properties for the EDA II Case and a set of the thermal properties modified to include lithophysal cavities associated with the upper-lithophysal (tsw33) and lower-lithophysal (tsw35) units (Figure 3.3.5-1). The three-dimensional model provides direct assessment of the application of UZ three-dimensional grid to model TH processes, so that changes in temperature and flux can be directly compared to the ambient-condition UZ flow-fields used in TSPA transport abstractions. However, the coarse grid and the planar (continuous heat-source) model used in the three-dimensional models prevent near-drift processes from being adequately resolved because temperature, saturation, and liquid flux are averaged over the large gridblocks that represent the repository. The coarse grids give rise to smaller changes in temperature, saturation, and flux than those given by the refined grid models. Cases 1 and 2 show no boiling and little change in liquid flux and liquid saturation, even near drifts. The predicted maximum temperature at the repository horizon is about 72°C for these coarse grids (Bodvarsson 2001 [DIRS 154669], Attachment 6, pp. 69 to 70). This was expected, because even the EDA II Case thermal load with ventilation showed no substantial changes in flux and liquid saturation (CRWMS M&O 2000 [DIRS 144454]).

Several two-dimensional refined grid (NS#2) TH simulations were conducted to give a more realistic estimation of expected mountain-scale and near-drift changes in temperature, saturation, and flux. Cases 3 and 4 provide predictions of two-dimensional TH conditions for the higher-temperature repository (including the effects of lithophysal cavities). Cases 5 and 6 provide similar predictions for the lower-temperature (below boiling) repository thermal load, in which forced ventilation removes 80 percent of the heat for 300 years. Case 7 provides an upper-bound scenario of the effect of a higher net infiltration on the lower-temperature operating mode. The results of TH simulations were evaluated using temperature and liquid saturation

contours for entire cross-section at selected times during thermal period. The results were also evaluated using temperature and liquid flux profiles at location #1 (Figure 3.3.5-1) at the center of the cross-section and by using temperature and flux distribution above the drifts (Bodvarsson 2001 [DIRS 154669], Attachment 6, pp. 83 to 103).

Temperature—Figures 3.3.5-2 and 3.3.5-3 show the distribution of temperature along the refined cross section NS#2 after 1,000 years. The results are for the higher-temperature case (Case #3, 70 percent forced ventilation for 50 years, Figure 3.3.5-2), and the lower-temperature case (Case #5, 80 percent forced ventilation first 300 years, Figure 3.3.5-3). The figures show that at lateral distances of 100 m or more from the potential repository, no substantial increases in temperature are predicted. This response suggests that the ambient percolation flux (predominantly vertical) controls the temperature changes outside the potential repository boundaries. In the lower-temperature case, modification of thermal properties to include lithophysal cavities (Case #6) has little effect on the mountain-scale TH conditions because boiling does not occur. In the higher-temperature case (Case #4), lithophysal cavities may lead to higher temperatures in the drift and in the UZ above the drift (Bodvarsson 2001 [DIRS 154669], Attachment 6, pp. 71 to 76, 99 to 101).

Figures 3.3.5-4 and 3.3.5-5 show the temperature profiles at location #1 at the center of the repository for the higher-temperature refined grid NS#2 case, without and with lithophysal cavities (Case #3 and Case #4 respectively). In these figures, the initial inclination of the temperature profile indicates the ambient temperature gradient with present day infiltration. The drift is at an elevation of about 1,070 meters above sea level where ambient temperature is about 24°C and the water table is at 730 masl where ambient temperature is about 32°C.

In both cases, the TH model predicts completely dry drifts with temperatures rising above-boiling to about 115°C for Case #3 and 118°C for Case #4 after 500 years. With lithophysal cavities (Figure 3.3.5-5, Case #4), a 50-m heat-pipe zone develops above the drift at 500 years. The heat pipe condition is represented by a near vertical temperature profile above the drift at this time. Vapor convection flow from the heat pipe raises temperatures 4°C to 5°C up to 150 m above the drift compared to the model with thermal properties of the initial TH model (Figure 3.3.5-4, Case #3). In both cases, the water table temperature rises from ambient (32°C) to 67° to 68°C after 10,000 years of thermal loading; the temperature at the top of the CHn (910 masl), on the other hand, rises to about 73° to 74°C after 5,000 years, and then declines to about 65°C by 10,000 years. Lithophysal cavities have little effect on temperature conditions below the repository. Units with lithophysal cavities predominantly occur at or above the elevation of the potential repository. Without lithophysal cavities, maximum temperature at the base of the PTn (Figure 3.3.5-4) is about 57°C after 1,000 years. With lithophysal cavities (Figure 3.3.5-5), the predicted maximum temperature at the base of the PTn rises to 70°C, due to increased vapor convection above the drifts. Similar to the model results documented for the EDA II case in *Mountain-Scale Coupled Processes (TH) Models* (CRWMS M&O 2000 [DIRS 144454]), the maximum temperature in the drift pillars is about 85° to 90°C in these higher-temperature cases (Bodvarsson 2001 [DIRS 154669], Attachment 6).

Figure 3.3.5-6 shows the predicted temperature profiles at the same location for the lower-temperature case without lithophysal cavities (Case #5). The predicted maximum drift temperature is about 90°C after 500 years. Lithophysal cavities raise maximum drift-wall

temperature to 95°C, with little impact on the rest of the profiles (Bodvarsson 2001 [DIRS 154669], Attachment 6, p. 74, Case #6). In both cases, the temperatures at the base of the PTn are predicted to rise by a maximum of about 24° to 27°C, to 44° to 47°C after 2,000 years. At the water table the predicted maximum temperature is 60° to 63°C after 10,000 years and at the top of the CHn, the maximum temperature is 65° to 67°C after 5,000 years. For these lower temperature cases, the maximum temperature in the drift pillars is about 70° to 75°C. The higher predicted temperatures above are for the TH model with lithophysal cavities. Much lower temperatures are predicted when five times the ambient infiltration rate is considered (Bodvarsson 2001 [DIRS 154669], Attachment 6, pp. 75 to 76, 102 to 103, Case #7).

Liquid Saturation and Flux—Figure 3.3.5-7 shows a contour plot of fracture liquid saturation at 1,000 years for the higher-temperature case using the nonlithophysal thermal properties (Case #3). After 100 years (Bodvarsson 2001 [DIRS 154669], Attachment 6), completely dry fracture conditions are predicted near the drifts and in a few isolated locations with low ambient percolation flux, and the fractures remain dry for nearly 1,000 years. At 2,000 years, the fracture saturation in most drifts recovers to above 90 percent of ambient saturation. After 5,000 years, the liquid saturation is primarily controlled by the prevailing climate, with little influence from repository heat. Saturation within the pillars remains at or above ambient levels throughout the simulated period. In the lateral direction, the liquid saturation more than 50 m away from the repository stays at near-ambient conditions.

Figures 3.3.5-8 and 3.3.5-9 show the predicted fracture liquid flux profiles at location #1 for the models without and with lithophysal cavities, respectively, for the higher-temperature operating mode (Table 3.3.5-1, Cases 3 and 4). The analysis presents only fracture flux, because for the UZ flow properties used in the TH models, more than 95 percent of the flow within the TSw units is through the fractures. Under ambient conditions fracture flux at drift elevation is about 4.5 mm/yr.

Qualitatively, the predicted flux is similar to the results presented for the EDA II Case (i.e., high flux above the drift), but zero or small below the drift. Most or all of the predicted enhanced liquid flux above the drift is vaporized by the repository heat and does not cross the drift boundary for up to 2,000 years. Without lithophysal cavities (Figure 3.3.5-8, Case #3), the predicted maximum liquid flux above the drift rises to about 120 mm/yr after 100 years, but drops to 40 mm/yr after 500 years. At 1,000 years, the liquid flux above the drift is 25 to 40 mm/yr (enhanced by climate), but again declines to less than 1 mm/yr below the drift. At 2,000 years, the flux above the drift is about 20 mm/yr, but drops to about 10 mm/yr below the drift. With lithophysal cavities (Case #4, Figure 3.3.5-9), the flux above the drift at 1,000 years is about 35 mm/yr, but declines to 0 mm/yr below the drift. In this case, at 2,000 years, the flux above the drift is about 15 mm/yr, but declines to about 8 mm/yr below the drift.

For the lower-temperature cases, the heat perturbation is not large enough, to completely dry up the fractures near the drifts. As a consequence, the model predicts reduced (but nonzero) fracture liquid flux through the drift at all times. Figures 3.3.5-10 and 3.3.5-11 show the predicted fracture liquid flux in the models without and with lithophysal cavities (Cases 5 and 6, respectively). Up to 500 years, average liquid flux above the drift is about 5 mm/yr, but rises to about 15 mm/yr immediately above the drift and declines to less than 2 mm/yr below the drift for Case #6 and to about 2-3 mm/yr for Case #5. In both cases, at 1,000 years, average liquid flux

above the drift is 20 mm/yr, declines to 7 mm/yr at the drift horizon and rises to 20 mm/yr below the drift. From 1,000 to 2,000 years, the flux above and below the drift is primarily controlled by the climate because the fracture network above and below the drift is almost completely resaturated. Results using the refined drift-scale TH model (see Section 4.3.5) show a complete drying up more than 5 m below the drift during this period. Thus, although the refined-grid mountain-scale model does not predict complete drying of the fracture network below the drift (because the grid is still too coarse), it is expected that the near-field drift environment will be dry, and little or no liquid will seep below the drift for 1,000 to 2,000 years.

Figure 3.3.5-12 shows the flux profiles for the upper-bound infiltration case (Case #7, that is, five times the mean of present-day ambient, monsoon, and glacial-infiltration flux), for the lower-temperature operating mode without lithophysal cavities. In this case, the model shows (as expected) that the impact of heat on flow is minimal under conditions of high-infiltration flux, except in the immediate vicinity of the drift where minor drying is predicted. The flux in this case is primarily controlled by the prevailing climate used in the model (0 to 600 years, 5 times present-day mean infiltration; 600 to 2,000 years, 5 times mean monsoon infiltration; and 2,000 to 10,000 years, 5 times mean glacial transition infiltration).

3.3.5.6 Abstraction for Total System Performance Assessment

Previous subsections describe the two-dimensional and three-dimensional TH process models that explore the effects of heat on mountain-scale temperature, liquid saturation, and percolation flux for the higher- and lower-temperature repository operating mode over 100,000 years of thermal loading. The three-dimensional model provides mountain-scale TH conditions that could be abstracted by the TSPA-SR (CRWMS M&O 2000 [DIRS 153246]) for direct comparison with UZ ambient flow-field data. However, because the 5-m diameter drifts are much smaller than the 81-m wide gridblocks used in the three-dimensional ambient and TH model, the results of the mountain-scale TH models based on the three-dimensional grid are averaged out (smeared) and show little change in flux due to heat, as similarly predicted in the TH models developed to support the TSPA-SR. The two-dimensional refined grid model, which traverses all 53 drifts, gives a more realistic prediction of temperature, saturation, and fluxes on the mountain scale, as well as near the drifts and within the drift pillars at the repository horizon. The ambient and thermally affected two-dimensional model will therefore give a more realistic indication of the effect of heat flux at the mountain-scale. A more detailed investigation of the near-drift changes in flux, temperature, and saturation is discussed in the drift-scale TH model (see Section 4.3.5). The drift-scale model predicted increased saturation and flux due to condensation above the drift. The models also predict reduced liquid saturation and flux in the drift shadow below each drift lasting 1,000 to 2,000 years, during which most of the drainage occurs within the pillars. TSPA-SR models that assume the enhanced liquid flux above drifts represents expected percolation flux through the drifts during the thermal period use a very conservative approach, because flux out of the drifts, as predicted in Section 3.3.5.5, is much smaller than flux above the drifts. A less conservative approach would use flux below the drifts to predict the effects of heat on transport. Although not used for TSPA-SR, this less conservative approach will be used in TSPA-LA analysis for license application.

3.3.5.7 Multiple Lines of Evidence

Numerical modeling of mountain-scale thermal hydrology provides insight into the performance of the potential repository under thermal loading. Approaches for development of the numerical model and the simulation of thermal-hydrologic processes are generally based on geothermal- and petroleum-reservoir simulation methods. Nonisothermal heat and fluid flow in unsaturated fractured geological media such as Yucca Mountain can be modeled in a similar manner. The justification for model approaches employed here, and the validity of the results, depends on the successful modeling of fluid and heat transport in large geothermal systems, for which an extensive volume of field data is available to provide model validation. A detailed literature survey of the application of the TOUGH2 family of codes to model coupled heat and fluid transport in geological media is presented in initial *Mountain-Scale Coupled Processes (TH) Models* report (CRWMS M&O 2000 [DIRS 144454]). This document discusses the similarity between these natural-analogue applications and the TH processes modeled here. Table 3.3.5-2 documents recent applications of TOUGH2 in modeling geothermal systems. These systems are supported by extensive data collected during exploration and production, which allow for development of a calibrated natural-state model. The natural-state model is then used for prediction of future performance based on production history. A similar approach is used to develop the UZ natural-state (ambient) model (CRWMS M&O 2000 [DIRS 144454]), which is then used to predict TH conditions discussed in this Section.

In modeling the impact of heat on the UZ, the only available validation data are from small-scale heating experiments that mostly provide near-field response (within a few meters of the drift wall) over a couple of months to a few years. These experiments include, for example, the Single Heater Test (a 9-month heating period) and the larger Drift Scale Test (a 4-year heating period). These tests give temporal and spatial variation in temperature and liquid saturation in the UZ near the drift when heat is applied. The small spatial and temporal scales of these tests limit their use for validation of the mountain-scale TH processes that are expected to last thousands of years and provide UZ response to heat over hundreds of meters.

Therefore, numerical modeling of mountain-scale TH will play a crucial role in understanding the impact of heat on the performance of the UZ. The validity of the mathematical and numerical approaches in modeling UZ isothermal (ambient) and nonisothermal processes has been demonstrated by field data and natural-analogue models and is extensively discussed in *Unsaturated Zone Flow and Transport Model Process Model Report* (CRWMS M&O 2000 [DIRS 151940]). Although the TH model incorporates the results of the small-scale heating experiments, it relies mainly on the conceptual and mathematical validity of the modeling approach for flow, selection of thermal properties, and construction of the numerical grids. Performance assessment TH models, based on numerical simulation of fluid and heat flow, include important physical processes affecting repository and host rock behavior.

3.3.5.8 Summary of Uncertainties and Their Treatment

The uncertainties in model parameters associated with the mountain-scale TH model development were considered and the impact on mountain-scale UZ flow evaluated. A key uncertainty results from using limited data to perform mountain-scale predictions in a fractured

heterogeneous system where the impacts of heterogeneity on the mountain-scale processes are uncertain.

Table 3.3.5-3 summarizes uncertainties by category (i.e., conceptual, data, or parameter). The primary uncertainty issue associated with each category is described, followed by possible methods for treating or addressing that uncertainty. Each of the uncertainties is representative of decisions that may impact the model goals.

3.3.5.9 Summary and Conclusions

This TH modeling study investigates the effects of higher- and lower-temperature thermal loads on the UZ of Yucca Mountain. This study uses two-dimensional and three-dimensional dual-permeability submodels of the three-dimensional UZ flow model and incorporates the calibrated model properties of the UZ flow model. The study also investigates the effect of UZ lithophysal cavities on TH response. Detailed investigation of the UZ response to thermal loading, using both the higher-temperature operating mode (thermal load 1.35 kW/m, ventilation 70 percent for 50 years) and the lower-temperature operating mode (thermal load 1.35 kW/m, ventilation 80 percent for 300 years) is conducted using refined two-dimensional cross-sectional models that include explicit representation of the drifts of the repository. The models include expected future climatic changes in infiltration rate. The numerical grids are sufficiently refined to depict mountain-scale, long-term TH behavior resulting from thermal load within the drifts, but do not explicitly include detailed heat-transfer processes within the drifts.

This study indicates that the heat source and its distribution, the thermal and flow properties of the rock, and the infiltration rates control boiling and rewetting TH processes at the repository. In the higher-temperature cases (1.35 kW/m 70 percent ventilation for 50 years), temperatures are predicted to rise to boiling conditions only within the immediate area of the drifts. The temperatures may rise above 110°C at some drifts. Temperatures in the pillars are predicted to rise to an average of 85° to 90°C. The higher temperature is likely when the effects of lithophysal cavities on thermal properties are modeled. For the lower-temperature cases, (1.35 kW/m 80 percent ventilation for 300 years) predicted maximum temperature at the drifts is 90°C without lithophysal cavities and 95°C with lithophysal cavities. Therefore, no boiling is predicted even when the effects of lithophysal cavities on thermal properties are included. The lower-temperature operating mode also predicts little potential for temperature-induced property changes in the PTn (1270 masl), CHn (910 masl), and the water table (730 masl) where predicted maximum temperatures are 44° to 47°C, 65° to 67°C, and 60° to 63°C, respectively.

For the higher-temperature cases, thermal loading at the repository results in significant changes in temperature, moisture distribution, and flux at the repository and in zones directly above and below the repository. The increase in liquid flow occurs only at early times (less than 100 years). This liquid does not enter the drifts because the heat within the potential repository drifts easily vaporizes this liquid flux. The model predicts that vertical liquid flow in the pillars between the drifts continues at a rate close to the ambient percolation flux for most of the thermal-loading period. In some locations, the flow may be enhanced by condensate drainage lasting for several hundred years. For these higher-temperature cases, localized dryout of the fracture and matrix continua at the repository is predicted, particularly below areas with low infiltration. This dryout zone may extend tens of meters into the drift shadow below each

potential repository drift. The temperature of the repository drifts rises to above boiling conditions. The temperature of the pillars rises to a maximum of 85° to 90°C. With lithophysal cavities, temperatures are predicted to rise to 70°C at the base of the PTn, and to 73°C at the top of the CHn and 67°C at the water table, again showing little potential for temperature-induced property changes. Without lithophysal cavities predicted maximum temperature is 57°C at base of the PTn, 73°C at the top of the CHn and 67°C at the water table. Lithophysal cavities therefore, primarily influence temperatures at or above the drifts.

For the lower-temperature cases, the TH models predict little change in UZ liquid flux except in the immediate vicinity of the potential repository drift (Section 3.3.5.5). Because boiling conditions do not occur, and the fractures are not completely dry, the mountain-scale TH model predicts reduced (but nonzero) flow crossing the repository horizon throughout the thermal-loading period. Within the first 2,000 years, average liquid flow crossing the drifts is less than 25 percent of the prevailing ambient flux, because repository heat is not large enough to vaporize all the percolation flux. In the lower-temperature case, the TH model still predicts substantial drying of the fractures in the drift shadow below the drifts, drying that lasts up to 2,000 years. The low fracture saturation in the drift shadow implies reduced potential for flow and transport below the drift for up to 2,000 years. The drying of the fractures below the drift is better resolved by TH simulations using a refined (about 1-m grid spacing) drift-scale grid (Section 4.3.5).

Lithophysal cavities reduce the effective thermal conductivity and the thermal capacity of the matrix continuum in the upper-lithophysal (tsw33) and lower-lithophysal (tsw35) units. For the same thermal load, explicitly accounting for the effects of lithophysal cavities leads to an increase in temperature caused by heat released over the same period. The three-dimensional model predicts a maximum increase of 1° to 2°C. In the refined model, the maximum temperature at the drift increases from 115° to 118°C for the higher-temperature cases. The models predict that at 1,000 years, temperatures up to 150 m above the drift are 1° to 5°C higher when thermal effects of lithophysal cavities are included. For the lower-temperature operating mode, the model still predicts a below-boiling-temperature scenario, even when the effects of lithophysal cavities are included. In this case, the predicted maximum temperature increases from about 90°C to about 95°C at the drift after 500 years. This increased temperature results in more drying of fractures near the drifts and the development of drier fractures in the drift shadow below. Therefore, lithophysal cavities, although not contributing to boiling at the drifts for this lower-temperature operating mode, may lead to further lowering of liquid flux below the drift and enhanced drainage flux through the drift pillars.

When a higher infiltration flux (5 times mean) is applied, the TH model for the lower-temperature case predicts little or no drying of the fracture network, even near drifts. Therefore, heating in the lower-temperature case may have a minimal effect on percolation flux throughout the thermal cycle.

The mountain-scale TH model is designed to predict the scale of thermal disturbance to the hydrologic setting of the emplacement drifts outside the near-field, which is considered in Section 4.3.7. The initial TH model is based on the EDA II design with a thermal loading of 72.7 kW/acre and a 70 percent heat removal by ventilation for 50 years. Subsequent modeling considers seven cases, using the same thermal load (67.7 kW/acre) in all cases. The temperature

profile is varied in the latter modeling by changing the rate of heat removal and the duration of ventilation (two sets of rates). In addition, rock thermal properties are varied (lithophysal/non-lithophysal). Percolation flux is varied spatially and temporally. The results of modeling are predictions of change of temperature at key locations such as the top of the CHn and at the water table, the extent and process of two-phase flow due to boiling and the impact of drying on fracture flow around the drift. Liquid and gas flux and local temperature histories are important intermediate steps. In the higher-temperature case of the initial TH modeling, completely dry drift wall temperatures reach 250°C, and pillar temperatures may locally rise to 97°C. In the lower temperature case the drift wall temperatures may exceed 110°C with maximum temperatures in the pillars averaging 85° to 90°C. Percolation flux is found to be the primary control, at the mountain scale, of the boundary of the two-phase flow region, boiling front position, and the rate of recovery of flow to ambient flow conditions. Heat flow above the repository is by heat pipes, which do not significantly alter the ambient flow around the repository and little effect is expected on cooling and post cooling percolation flux.

The more recent modeling was not strictly based on the EDA II repository design. Thermal loading has been adjusted, rock properties and ventilation rates varied so that none of the drift rock temperatures are expected to rise above boiling for the lower temperature cases (Table 3.3.5-1). Infiltration rates and resulting percolation fluxes are varied in accord with predicted climatic variation from the Climate Model (Section 3.3.1). None of the cases predicts temperatures in the CHn high enough to alter the hydrologic or sorptive properties of this unit.

None of the expected effects of waste heat predicted by the mountain-scale TH model permanently change the hydrologic character of the site. The predicted short-term changes are over (in 1,000-2,000 years) before any releases are expected from the emplacement drifts and all of the short-term hydrologic changes at the mountain scale are conservative in their influence on UZ flow and transport. At higher percolation fluxes associated with wetter climates modeling implies there may be no significant TH effects. The consideration of seven cases with varying heat input (two thermal loads, two ventilation scenarios), variation of rock properties and changes in recharge/percolation flux, is more than adequate to identify any heat driven anomalies in the site and repository hydrologic behavior over a very wide range of temperatures. However even with the coarse grids, predicted drift wall temperatures may rise up 10°C above the desired goal of 85°C for “waste-package” surface at some locations. Additional ventilation may be required to meet “waste-package” surface temperature goals.

3.3.6 Thermal-Hydrologic-Chemical Effects on Unsaturated Zone Flow and Geochemistry

3.3.6.1 Introduction

This section summarizes the modeling and uncertainty studies performed for the evaluation of THC effects on flow and geochemistry in the UZ at the mountain scale. The major THC processes important for the UZ are (1) mineral precipitation/dissolution affecting flow and transport to and from the potential repository and (2) effects on the compositions of gas and liquid that may seep or flow into drifts. THC processes at the mountain scale affect the flow and sorption properties of rock units within the UZ. Modification of these properties through hydrothermal alteration of zeolitic and vitric tuffs and mineralization of fractures may influence

the amount of lateral flow that may divert water, thus reducing the percolation flux to the potential repository and the transport time to the saturated zone. Alteration may also affect the transport of radionuclides from the repository to the saturated zone. Uncertainties in the TSPA-SR (CRWMS M&O 2000 [DIRS 153246]) that the work in this section addresses are: (1) mountain-scale effects of THC processes on flow and transport, (2) mountain-scale THC effects on the variability of water chemistry entering drifts under thermal loading conditions. Natural analogue studies can be utilized to constrain the potential impact of THC processes on total repository performance and validate predictive models for Yucca Mountain.

The mountain-scale THC model is a new two-dimensional model developed after the TSPA-SR (CRWMS M&O 2000 [DIRS 153246]) that is based on the mountain-scale TH model documented in *Mountain-Scale Coupled Processes (TH) Models* (CRWMS M&O 2000 [DIRS 144454]), and the conceptual models and data for THC processes documented in *Drift-Scale Coupled Processes (DST and THC Seepage) Models* (BSC 2001 [DIRS 154677]). Many of the uncertainties in the conceptual models and data used for input and model validation are identical to those discussed in the latter AMRs. However, the drift-scale THC models are focused primarily on processes that affect seepage (and the chemistry of potential seepage) into drifts. Therefore, the effect of THC processes on flow in the Paintbrush hydrogeologic unit (PTn), the basal vitrophyre of the Topopah Spring Tuff, and the vitric and zeolitic zones in the Calico Hills hydrogeologic unit below the potential repository are not of particular concern for the drift-scale THC models.

The purpose of the mountain-scale THC model is to reduce the uncertainties associated with coupled THC processes that are caused by variations in geology (structure and lithology), infiltration rate, and temperature at a mountain or repository scale. Because these variations are larger than that of mineralogical variations in the welded units they are the most important to capture. These are processes that affect the percolation flux at the potential repository horizon (relevant to seepage) and flow below the potential repository (relevant to radionuclide transport in the UZ). Small-scale and localized processes, such as mineral precipitation in the boiling zone, can only be captured in finely gridded drift-scale models. Thus, the mountain-scale THC model is focused on larger-scale changes in chemistry and flow that are not localized to very small regions adjacent to the drift. Large-scale gas-phase convection and lateral flow are not represented in the THC Seepage models, and therefore, the mountain-scale THC model can address uncertainties in phenomena that may not arise in the drift-scale "chimney" models. However, these effects are prominent on the edges of the repository and do not invalidate the results of the THC Seepage models because they do consider local gas convection effects. The Mountain-Scale THC model provides a more heterogeneous set of results for a given time but is essentially modeling the same processes as the THC Seepage models.

Three main types of uncertainty are discussed in the section: data uncertainties, uncertainties arising out of features, events, and processes, and conceptual uncertainties. Because the results in this section are from a new model, with limited analyses performed, the results should be considered as preliminary. In addition, long-term impacts have not yet been assessed.

The methods used to evaluate THC effects on flow and geochemistry include the estimation of thermodynamic and kinetic parameters, model development, testing and model validation using large-scale thermal test and laboratory experiments, and predictive process modeling. This

approach was chosen because it provides the means to test the appropriateness of the conceptual model, to evaluate uncertainties in different conceptual models, and to provide predictions of potential effects on water and gas chemistry, as well as changes in hydrologic properties that result in changes in flow. Uncertainties in some thermodynamic and kinetic parameters were evaluated using sensitivity studies and comparisons to data from the Drift Scale Test and laboratory experiments, which are discussed in Section 4.3.6. Remaining unquantified uncertainties were addressed in *Features, Events, and Processes in UZ Flow and Transport* (BSC 2001 [DIRS 154826]). Unquantified conceptual uncertainties were assessed in analogue studies and other corroborating observations (CRWMS M&O 2000 [DIRS 141407]).

The conceptual model for THC processes provides a framework for modeling the pertinent mineral-water-gas reactions in the host rock, under thermal loading conditions, as they influence the chemistry of water and gas in the mountain and associated changes in mineralogy. The data incorporated in the model include hydrologic and thermal properties from the calibrated property sets, geologic layering from the UZ three-dimensional flow and transport model, geochemical data (fracture and matrix mineralogy, aqueous geochemistry, and gas chemistry) derived from various sources, thermodynamic data (minerals, gases, and aqueous species), data for mineral-water reaction kinetics, and transport data. Simulations of THC processes included coupling among heat, water, and vapor flow; aqueous and gaseous species transport; kinetic and equilibrium mineral-water reactions; and feedback of mineral precipitation/dissolution on porosity, permeability, and capillary pressure for a dual-permeability (fracture-matrix) system.

The effect of coupled THC processes on the evolution of flow fields and water and gas chemistry in the UZ is evaluated in this section for a higher-temperature thermal operating mode based on the thermal loading and properties used in *Mountain-Scale Coupled Processes (TH) Models* (CRWMS M&O 2000 [DIRS 144454]). Because this is a new model, a higher-temperature baseline analysis was performed first, which may bound the upper limit of THC effects on mountain-scale flow and chemistry that may be expected under above-boiling conditions. Effects of THC processes at the drift scale under the lower-temperature operating mode are evaluated in Sections 4.3.6 and 6.3.1.5.

3.3.6.2 Goal of the Mountain-Scale Thermal-Hydrologic-Chemical Model

The goals of the model used for prediction of mountain-scale THC processes are:

- Provide a conceptual basis and methodology for developing a mountain-scale THC model to assess uncertainties in the modeling results. Use the results to assess uncertainties in the drift-scale THC models (as well as other UZ flow and transport models)
- Predict large-scale changes in hydrologic properties resulting from mineral precipitation/dissolution and associated THC effects on UZ flow
- Predict large-scale mineralogic changes that could impact UZ transport (i.e., effects on glassy and zeolitic units below the potential repository) (see Section 11.3.5)

- Predict large-scale changes in water and gas chemistry that can be used to extend the variability predicted by drift-scale models.

The important mountain-scale coupled THC processes are illustrated schematically in Figure 3.3.6-1. Some UZ processes, such as the distribution of net infiltration, may strongly affect THC processes by modifying the fluxes and concentrations of components in waters that migrate to the repository horizon. The effect of THC processes on UZ flow may include modification of the percolation flux beneath the nonwelded tuffs in the Paintbrush hydrogeologic unit (PTn) and alteration of flow paths (lateral flow) below the potential repository in the vitric and zeolitic layers of the Calico Hills hydrogeologic unit (CHn) and on the basal vitrophyre of the Topopah Spring Tuff. In addition, small-scale hydrologic processes, such as fracture-matrix interaction, have a strong effect on the chemical evolution of the system and the distribution of mineral precipitation in fractures and the matrix.

3.3.6.3 Basis of Mountain-Scale Thermal-Hydrologic-Chemical Model and Simulation Results

3.3.6.3.1 Description of the Mountain-Scale Thermal-Hydrologic-Chemical Model

A cross section was chosen from the UZ three-dimensional flow and transport model grid that follows a roughly north-south trend through the potential repository and runs perpendicular to the trend of the potential waste emplacement drifts (Figure 3.3.6-2). This orientation allows for the effects of THC processes on flow between drifts to be evaluated. The two-dimensional grid, geological layering, infiltration rates, and hydrologic and thermal properties were derived from *Mountain-Scale Coupled Processes (TH) Models* (CRWMS M&O 2000 [DIRS 144454]). Each drift is represented as an individual grid block. The purpose of the model is to evaluate processes in the UZ; however, the grid includes an extension of several hundred meters below the water table to provide a far-field constant-temperature boundary, but without any flow into or within this saturated region.

Mineral abundances were assigned to each hydrogeologic unit based on data from the three-dimensional mineralogical model V3.0 (DTN: LA9908JC831321.001 [DIRS 113495]) (for a single column taken near the center of the potential repository footprint) and from fracture data as described in *Drift-Scale Coupled Processes (DST and THC Seepage) Models* (BSC 2001 [DIRS 154677], p. 32, Section 4.1.2.1). Therefore, each model layer is characterized by uniform mineralogical abundances, although some layers may change from zeolitic to vitric along strike. Fault mineralogy was approximated by the average of the mineral abundances for each major hydrogeologic unit. The minerals, aqueous and gaseous species in the model geochemical system are listed in Table 3.3.6-1, and are the same as those in the extended-case geochemical system described in *Drift-Scale Coupled Processes (DST and THC Seepage) Models* (BSC 2001 [DIRS 154677], pp. 67 to 69, Section 6.1.7). Although the base case geochemical system captured more closely the pH and gaseous carbon dioxide concentrations in samples collected from the DST, silica concentrations were better in the extended case system simulations and therefore effects on flow owing to mineral precipitation may be more realistic. The initial and infiltrating water chemistry was set to that from the matrix pore water collected from the Topopah Spring middle nonlithophysal unit (Ttpmn) in Alcove 5, near the ongoing Drift Scale Test, as documented in *Drift-Scale Coupled Processes (DST and THC Seepage) Models* (BSC

2001 [DIRS 154677], Table 3). All other geochemical input data are derived from the latter report. Although this water may not be characteristic of all pore waters in the UZ, it has been used successfully in validation studies with the Drift Scale Test, as described in the AMR and also summarized in Section 4.3.6. Side boundaries taken far from the repository edges (see Figure 3.3.6-2) were set to be no-flux for flow, heat, and chemical transport. Details of the model simulations and parameters are described in Bodvarsson (2001 [DIRS 154669], Attachment 10, pp. 8 to 20)

Simulations were run under the higher-temperature design option using the mean infiltration rate for the modern climate. TOUGHREACT V2.3 was used for the simulations. Although the effects of other climate states imposed at later times have not been evaluated, the range in infiltration rates in this cross section is from nearly 0 to almost 50 mm/year. The simulations investigated the main thermal period up to the early post-thermal period (about 7,000 years). In addition to investigating the effects of above-boiling temperatures on THC processes, the higher-temperature option was chosen for consistency with the majority of the THC Seepage simulations, as discussed in *Drift-Scale Coupled Processes (DST and THC Seepage) Models* (BSC 2001 [DIRS 154677]). Climate effects were evaluated in this AMR and showed qualitatively the same behavior, with somewhat greater amounts of mineral precipitation under higher infiltration rates.

To assess uncertainties associated with mineral reaction rates, some of which were shown to have a strong effect on water and gas chemistry in the drift-scale THC simulations (BSC 2001 [DIRS 154677], p. 97), two simulations were performed that used alternative values for the reaction rate of anorthite. Anorthite (an endmember in the plagioclase feldspar solid solution series) has a strong effect on pH through its dissolution to form calcic zeolites. The lower rate (by three orders of magnitude) resulted in a smaller deviation in the chemical evolution of the initial water under ambient temperatures (corroborating evidence for effective reaction rates), with the model infiltration rate and initial and boundary gas-phase carbon dioxide concentrations. This simulation will be referred to as "Extended Case 1" and that with the higher rate for anorthite as "Extended Case 2." Some additional parameters were modified that have a less substantive effect on the simulation results, such as the initial precipitation rate of new secondary phases.

3.3.6.3.2 Effects of Thermal-Hydrologic-Chemical Processes on Hydrologic Properties and Mineralogy

Some of the more important indicators for the effect of THC processes on hydrologic properties and mineralogy are shown in Figure 3.3.6-3 after about 1,400 years of heating (Extended Case 1) and in Figure 3.3.6-4 after 5,000 years (Extended Case 2). The main difference in the results for the two cases was in the gas-phase carbon dioxide concentrations and pH. The differences were not great enough to markedly change the mineral abundances and distributions. Longer time periods were not considered in these simulations; however, two-dimensional drift-scale THC simulations have shown that amorphous silica precipitation during the boiling period occurs in the first few thousand years (BSC 2001 [DIRS 154677], p. 168). Later changes occurred slowly over the next several tens of thousands of years as a result of calcite precipitation. For reference, Figure 3.3.6-3a shows the distribution of net infiltration imposed along the top model boundary.

After 1,400 years, the temperatures around the repository are below boiling everywhere (Figure 3.3.6-3b), and the isotherms show some slight localized depression owing to focusing of the percolation flux near the center of the region having higher infiltration. These zones of focused flow are also the areas where there is a small fracture porosity reduction, in contrast to the majority of the area above the potential repository (where porosity increased in the large condensation zone). TH effects on the percolation fluxes at the mountain scale are discussed in Section 3.3.5. The porosity reductions are generally much less than 1 percent, similar to that seen in areas where the temperatures are still at their ambient value. Porosity reductions in the Tiva Canyon Tuff (TCw) are elevated relative to the ambient system as a result of increased calcite precipitation (Figure 3.3.6-3c). As can be seen in the latter figure, areas of calcite dissolution above and below the plane of the drifts is responsible for much of the porosity increase observed in Figure 3.3.6-3b. The distribution of amorphous silica is generally confined to boiling areas very close to the drifts, but larger regions are evident below the edges of the potential repository (Figure 3.3.6-3d). These areas are characterized by very low fracture saturation that developed in part from gas convection at the edges. At the northern edge, there is also a fault acting as a conduit for gas flow out of the heated zone.

Effects of THC processes below the repository are strongest in the zeolitic Calico Hills unit, where the zeolite minerals clinoptilolite, heulandite, and mordenite are initially stable and precipitating in the ambient system. They are also dissolving as the heat pulse migrates into the zeolitic units (Figure 3.3.6-3e). In this model simulation, the zeolites are being replaced by feldspars in the heated region, whereas the reverse reaction is taking place slowly in the unheated parts of the zeolitic zones. The effect on glassy units is notably small (Figure 3.3.6-3f), with very slow dissolution in the Paintbrush nonwelded unit (PTn) occurring equally in heated and unheated regions.

After 5,000 years, most of the region above and directly below the repository (in the TSw) shows a small net reduction in fracture porosity of less than 1 percent (Figure 3.3.6-4a). Above the northern edge, there persists a region of small porosity increase related to enhanced convection and condensation. Temperatures become more irregular as a result of diversion of water into the approximate center of the potential repository, combined with topographic effects (the deepest part of the potential repository that is also away from edges is warmest). Precipitation of fracture calcite is ubiquitous, with increases in both heated and unheated areas (Figure 3.3.6-4b). The areas that show the most effect as a result of heating are in the TCw and below in the zeolitic units, where calcic zeolites (clinoptilolite, heulandite, and mordenite predominantly) are dissolving to produce Na- and K- feldspars and increasing the calcium in the associated waters. A small increase in amorphous silica is evident below the northern edge of the potential repository (Figure 3.3.6-4c), where gas convection has kept this area very dry. However, amorphous silica has generally stopped precipitating and is slowly dissolving into the percolating cooler waters.

The distribution of precipitation and dissolution of clinoptilolite (Figure 3.3.6-4d) shows dissolution in the heated region of the Calico Hills Unit, with dissolution also progressing into zeolitized regions of the TCw, above the PTn. In general, the ambient temperature zeolitic units show precipitation, driven by the dissolution of remaining feldspars in these rocks. It is not known how rapidly such reactions are currently taking place in the mountain under the present conditions, but it is likely that changes on the order of 1 percent (volume of the rock) over

5,000 years are too large because the minerals are still present after several million years. Thus, it can be expected that the reverse reactions in the heated zone are also taking place more rapidly in the simulation than would occur in the actual system. The causes of the increased reaction rates can be due to several model parameters and processes, such as the effective reactive surface area, kinetic rate laws and parameters, inhibition caused by mineral coatings, thermodynamic stabilities of aluminosilicates, local initial water and gas chemistry, and rates of transport via diffusion and fracture-matrix interaction (matrix imbibition). Because the major precipitating zeolite is clinoptilolite, which is the major zeolite mineral seen in these rocks, the thermodynamic relations for the minerals appear to give the observed mineral paragenesis. Therefore the effective surface areas of the feldspars in the altered rocks may be much lower due to the alteration that has already taken place. Some of these uncertainties are discussed further in Sections 3.3.6.6, 4.3.6.8, and 6.1.3.8.

Changes in UZ flow due solely to mineral precipitation/dissolution above the potential repository are small, but qualitatively show diminishing fracture porosity over time with slight but increased flow diversion and focusing. Below the potential repository, the increased porosity in the zeolitic units could lead to somewhat higher percolation fluxes through these units and the interbedded vitric units. The result of this would be reduced lateral flow, and it could lead to increased travel times for radionuclide transport because of sorption in the zeolitic units and matrix diffusion in the vitric units. However, there are uncertainties regarding alteration rates of the basal vitrophyre so that if the rates were higher, the result could be increased lateral diversion below the potential repository.

The higher-temperature operating mode simulations cover a range of thermal conditions that bracket the expected response for a lower-temperature operating mode. For example, in mountain-scale simulations, temperatures are at a maximum near the center of the potential repository, with cooler regions at the margins due to enhanced heat loss, and grading into regions at the ambient geothermal gradient. Temperature-dependent reactions such as the breakdown of clinoptilolite are greatest where maximum temperatures persist for the longest period of time near the center of the potential repository and decline toward the margins. Simulations employing a lower-temperature design option would exhibit maximum changes in zeolite alteration similar to those at equivalent temperatures near the repository edges. A lack of boiling temperatures and reduced gas convection also would result in less precipitation of amorphous silica around the potential repository.

3.3.6.3.3 Effects of Thermal-Hydrologic-Chemical Processes on Water and Gas Chemistry

Effects on water chemistry are most pronounced during the early thermal period, when condensation and dryout/boiling are driving dilution and evaporative concentration. Also, at this time, elevated temperatures result in greatly enhanced reaction rates and shifts in the thermodynamic stabilities of coexisting minerals. Another important process is the exsolution of carbon dioxide out of the water and transport in the gas via diffusion and advection. The latter process, in turn, has a large effect on pH, and therefore on mineral-water reactions and reaction rates. The effect of these varied coupled processes on pH after 1,400 years of heating is shown in Figure 3.3.6-5a. The initial ambient pH in the model is about 8.3 at the repository horizon and 7.8 in the surface infiltrating water. The area in the center of the potential repository shows a

distribution similar to that observed in the drift-scale THC models (CRWMS M&O 2001 [DIRS 154677]), with somewhat higher pH waters (up to about 8.8) forming above and around the drifts owing to carbon dioxide loss and reactions with aluminosilicates. However, at the edges of the repository, the strong gas convection effects and the migration of carbon dioxide from the central region outward (Figure 3.3.6-5b) have resulted in lower near-neutral pH waters (down to about 7). Areas of enhanced dilution as a result of condensation and subsequent drainage in fractures are evident in the distribution of chloride shown in Figure 3.3.6-5c. Areas of very high chloride below the potential repository edges and in a fault at the northern edge are the result of strong convection of gas drying out these areas and condensing in areas above. The fracture liquid saturations in these high concentration areas are nearly zero.

Under a lower-temperature operating mode, the edge effects seen in higher-temperature operating mode simulations would be reduced because of smaller temperature gradients and the absence of boiling, thus leading to smaller spatial differences in gas and water chemistry. A lack of boiling temperatures and reduced gas convection also would result in less precipitation of amorphous silica around the repository.

3.3.6.4 Abstraction for Total System Performance Assessment

Although the results are based on a very limited analysis of possible scenarios (e.g., climate, geochemical conceptual models, thermodynamic data, and kinetic data), the small changes in porosity are a basis for not performing TSPA abstraction of the THC effects on flow. Therefore, results described in this section reduce uncertainties associated with assumptions made for model abstractions supporting the TSPA, since the effects of mountain-scale THC processes on flow were assumed to be negligible in the TSPA-SR. However, as discussed in Section 3.3.6.6, there are many unquantified uncertainties associated with mountain-scale THC processes. Therefore, conditions, parameter ranges, or both, may exist such that there are significant effects of THC processes on flow and transport that may make TSPA assumptions non-conservative.

3.3.6.5 Multiple Lines of Evidence

3.3.6.5.1 Yucca Mountain Self-Analogue

A good analogue for understanding future THC reactions at the mountain scale is the fossil hydrothermal system at Yucca Mountain itself (Bish and Aronson 1993 [DIRS 100006]). Detailed mineralogical examination of Yucca Mountain Tuffs showed that most zeolitic alteration occurred from 13 to 11.6 Ma, shortly after tuff emplacement. After formation of the major zeolitic horizons, deep-seated hydrothermal activity persisted until about 10 Ma. The preservation of low-temperature zeolites (clinoptilolite and mordenite) suggests that this activity was limited to temperatures of up to 90 to 100°C.

Conceptual models for mineral evolution at Yucca Mountain (Carey et al. 1997 [DIRS 101323]) suggest that the most likely mineralogical reactions caused by repository heating would include dissolution of volcanic glass and precipitation of clinoptilolite, clay, and opal-CT (i.e., opal with cristobalite- and tridymite-type stacking); dissolution and precipitation of silica polymorphs (cristobalite, opal-CT, tridymite, and quartz); alteration of feldspars to clays; and reactions involving calcite and zeolites. Present-day temperatures in drill hole G-3 compare closely to

paleotemperatures inferred from mineralogical data. In contrast, an increasing abundance of clays and zeolites, along with a decreased abundance of glass, indicate higher paleotemperatures for drill holes G-1 and G-2, which are closer to the center of the Timber Mountain caldera source of eruption (G-2 being the farthest north).

In addition to temperature, the water saturation also has a strong impact on water-rock reactions, as kinetically controlled reactions proceed much more rapidly under saturated conditions. Zeolite reactions are likely to proceed more slowly in the Yucca Mountain UZ (excluding perched water zones) than below the water table (Carey et al. 1997 [DIRS 101323]). The persistence of opal-CT below the water table indicates that kinetically controlled silica reactions at Yucca Mountain are slower than suggested by laboratory studies.

Thin coatings of calcite and silica polymorphs found on fractures and lithophysal cavities in the ESF record chemical and isotopic changes in the UZ over the past 10 million years (Marshall and Whelan 2000 [DIRS 154415]). In the Topopah Spring Tuff, uranium-lead ages of opal and chalcedony coatings can be used to constrain the ages of associated calcite. Strontium isotope ratios in calcite increase from the base to the outermost surface of the coatings, recording a systematic change in pore water isotopic composition due to water-rock interaction (Marshall and Whelan 2000 [DIRS 154415]). Marshall and Whelan (2000 [DIRS 154415]) constructed a one-dimensional advection-reaction model to predict the evolution of strontium isotope ratios in the water, which can be used to estimate approximate ages for precipitated calcite. The $\delta^{18}\text{O}$ values of the calcite samples gradually increase with decreasing model strontium age, suggesting a cooling trend with time, with elevated temperatures restricted to prior to 6 Ma.

3.3.6.5.2 Geothermal Systems

Many processes that are expected to take place under repository conditions are the same as those that occur in geothermal fields. These include evaporation, boiling, condensation, single- and two-phase fluid flow, mineral reaction, precipitation and dissolution, and consequent potential changes in fracture-matrix interaction. Coupled processes related to geothermal systems have been observed, measured, and simulated for more than two decades in the geothermal industry. Geothermal analogues are one of the major ways of building confidence in understanding the thermal-hydrologic behavior of the repository system as it is coupled to chemical processes over long time periods. Data from geothermal fields can be used to test coupled process modeling codes used by the project to match observations (e.g., chemical reactions and occurrence of heat pipes) in geothermal fields with those predicted by the code.

The versatility of geothermal reservoir simulators has made possible their application to a wide range of fluid and heat flow problems. To produce an adequate model, numerical codes must be able to handle processes of heat transfer; two-phase flow under nonisothermal conditions in one, two, and three dimensions with varying degrees of non-linearity; coupling of fluid and heat flows; and complex boundary conditions. Modeling of geothermal systems has provided major advances toward this goal, which adds confidence in numerical models for Yucca Mountain. For a detailed discussion of geothermal analogues and modeling, see Section 4.3.6.7. A brief discussion follows.

Bruton et al. (1995 [DIRS 117033]) reviewed literature and data for many geothermal fields as a means of selecting a field-analogue site for THC studies. Some of these fields were considered unsuitable because they occurred in rock types dissimilar to Yucca Mountain, a few lacked sufficient data or had access problems, and others were entirely liquid- or vapor-dominated fields. The geothermal system at Wairakei was selected as the site most amenable to study of THC processes because it possessed the greatest number of features similar to Yucca Mountain (Bruton et al. 1995 [DIRS 117033], p. 8).

Mineral-fluid relations in Wairakei and other New Zealand geothermal fields were simulated (Glassley and Christenson 1992 [DIRS 109923]; Bruton et al. 1993 [DIRS 109901]). The goal of these simulations was to validate the thermodynamic database used for Yucca Mountain THC models through comparisons between observed mineral assemblages and model simulations of equilibria for the Wairakei system. The Wairakei geothermal system provided the opportunity to demonstrate that the Yucca Mountain Project EQ3/6 thermodynamic database and associated model could simulate observed mineral-water compositions for a specific example within the possible range of temperatures and water conditions anticipated in a Yucca Mountain repository system. The results of these modeling studies were generally consistent with observed vein and matrix mineral equilibria at Wairakei for fluids at temperatures greater than 240°C. Field data and model results indicated that stable mineral assemblages could be significantly impacted by small differences in fluid chemistry, temperature, or pressure. Comparison of laboratory data with field data from natural hydrothermal waters at Wairakei for amorphous silica precipitation showed that significant discrepancies exist between results obtained with different test conditions (Carroll et al. 1998 [DIRS 124275]). Silica precipitation rates measured in the field were 400 times faster than those obtained in laboratory measurements. Silica precipitation under repository conditions at Yucca Mountain could exhibit rate behavior somewhere in the range between the laboratory and field experiments.

3.3.6.6 Summary of Uncertainties and Their Treatment

As is the case for all coupled process models, there are many uncertainties in the results of the Mountain-Scale THC model. However, the model results address the goals outlined (see Section 3.3.6.2) and are therefore considered acceptable, given the intended purpose of the model and the use of its results for downstream users. It is important to note that the primary conceptual models and data for coupled THC processes are derived from the drift-scale THC models (BSC 2001 [DIRS 154677]), which have undergone extensive validation to measured data from the DST and from laboratory experiments. To further reduce the uncertainty in the predictions of large-scale THC effects on mountain-scale flow and transport (if such a reduction were required by downstream users of the THC model results), the following sources of uncertainty could be examined:

- Uncertainties in three-dimensional TH processes at a mountain scale and their effect on THC processes (i.e., gas convection, focused flow)
- Uncertainties in thermodynamic data (i.e., relative stabilities of feldspars, clays, and zeolites) that relate specifically to vitric and zeolitic horizons

- Uncertainties in kinetic data (i.e., aluminosilicate rate laws and parameters and rates of nucleation) also related specifically to vitric and zeolitic horizons
- Uncertainties in geochemical conceptual models (e.g., mineral solid solutions, precipitating mineral assemblages, reactive surface area estimation)
- Uncertainties in the effective mineral-water reactive surface areas in heterogeneous unsaturated fractured rock, which is being addressed through continuing and new laboratory studies, the planned Cross-Drift Thermal Test, and sensitivity studies
- Uncertainties in fracture and lithophysal hydrologic parameters (i.e., fracture and lithophysal porosity and unsaturated hydrologic properties)
- Uncertainties in the distribution of water and gas chemistry in the UZ and in infiltrating water.

Table 3.3.6-2 summarizes the key conceptual and parametric uncertainties that are specific to the prediction of mountain-scale THC processes. Many general THC issues, and those related to seepage chemistry or localized mineral precipitation adjacent to drifts, are discussed in Sections 4.3.6 and 6.3.1.5.

3.3.6.7 Summary and Conclusions

The uncertainties associated with the effects of THC processes on flow and chemistry in the UZ at the mountain scale were outlined in this section. This new work involved two-dimensional simulations to address uncertainties that relate to the modification of UZ flow paths and fluxes, water and gas chemistry in the UZ, and the transport of radionuclides in the UZ. The results of these simulations, based on a limited range of input parameters, indicate that mineral precipitation/dissolution will not significantly affect the hydrologic properties and, therefore, the percolation flux compared to TH changes above the potential repository in the thermal and early post-thermal period. For comparison, TH effects on the percolation flux at the mountain scale are discussed in Section 3.3.5. Edge effects owing to gas convection produce mineral precipitation below the drifts (as a result of enhanced dryout) at the potential repository edge that is not observed in drift-scale THC simulations, as presented in *Drift-Scale Coupled Processes (DST and THC Seepage) Models* (BSC 2001 [DIRS 154677]). The ranges in water and gas compositions are wider than those predicted by the drift-scale THC models at a given time as a direct result of the edge effects. Whereas the range may be greater at a given time, the overall range in chemistry is comparable to that observed in the different drift-scale THC simulations over a longer time period. The range in pH of about 7 to 9 is strongly linked to changes in gas-phase carbon dioxide concentrations (relative to the ambient system away from the repository) that are much smaller in the higher-temperature potential repository center (and pH is higher) compared to the edges (which have somewhat elevated values and pH values down to approximately 7).

The important issues associated with the prediction of mountain-scale coupled THC processes have been summarized and their status assessed in this section; however, many uncertainties at the mountain-scale over extended time periods have yet to be addressed in a systematic fashion.

THC model validation, discussed in Section 4.3.6, encompasses some of the uncertainty issues, but large-scale issues related to conceptual model and data uncertainties (i.e., climate, infiltration, saturated zone effects, fault properties and conceptual models, and mineralogical and water chemistry variations) must be treated by simulating a range of possible conditions and by analysis and validation through study of natural analogues. THC processes at the drift-scale and at the laboratory-scale have been validated as discussed in Section 4.3.6. This work validates many aspects of the Mountain-Scale THC Model, but does not address the latter-mentioned parameters and processes. Uncertainties that arise out of ranges in parameters that have not been assessed can be further reduced through additional field thermal testing, laboratory experiments, and modeling. It should also be noted that the incorporation of new features or processes, such as heterogeneity, carry additional uncertainty to the simulations, even if they reduce other aspects of the uncertainty.

3.3.7 Thermal-Hydrologic-Mechanical Effects on Mountain-Scale Permeability

3.3.7.1 Introduction

This section presents a scoping simulation of the impact of THM processes on permeability at the mountain scale. This scoping work is documented in Bodvarsson (2001 [DIRS 154669], Attachment 9, pp. 1 to 78). The THM effect around the potential repository has largely been ignored in simulations of mountain-scale flow and was not included in the TSPA-SR (CRWMS M&O 2000 [DIRS 153246]). The uncertainty introduced by the assumption that THM processes have little impact on mountain-scale flow is addressed in this section.

3.3.7.2 Goal of Thermal-Hydrologic-Mechanical Model for Flow on the Mountain Scale

THM model studies are being conducted to provide insight into how mechanical stresses arising from the decay heat of the repository will affect rock mass permeability. These studies are intended to allow an assessment of how the permeability changes caused by THM coupled processes will affect the flow on the mountain scale from the land surface to the water table.

3.3.7.3 Model Development

The coupled THM study was performed using a joining of two codes: TOUGH2 V1.5 and FLAC 3D V2.0. This joint code is referred to as the "TOUGH-FLAC" code (Bodvarsson 2001 [DIRS 154669], Attachment 9, pp. 1 to 43). The two well-established codes were joined through three carefully designed linkage routines (Delb.dat V1.0, Gpzones.dat V1.0, and tin.dat V1.0). The first code is TOUGH2 V1.5, which incorporates the dual-permeability (fracture and matrix continua) approach. It has been proven successful in predicting the temperature and moisture distribution of field experiments at Yucca Mountain, including the Single Heater Test (CRWMS M&O 1999 [DIRS 129261], Section 12) and the Drift Scale Test (CRWMS M&O 2000 [DIRS 151964], Section 7). The second code is the industry-standard FLAC3D V2.0, which calculates fractured rock and soil mechanical processes in a continuum model.

The general conceptual model for THM processes may be described as a multiphase, non-isothermal and deformable medium where voids of the rock skeleton are filled partially with liquid water and partially with gas. Thus, it is a three-phase system (gas, liquid, and solid) where each of the fluid phases has two components (water and air). The gas phase is modeled as an

ideal gas mixture composed of dry air and water vapor, and the liquid phase consists of water and dissolved air. The mechanical behavior of the porous and fractured media responses to changes in temperature, skeletal effective stress, and strain is modeled with accompanying porosity and permeability changes. Coexisting fluid and solid components are assumed to be in local thermal equilibrium (i.e., locally they are at the same temperature). While a few main fractures may be discretely defined within a rock matrix, the main part of the fractured porous rock is treated as a single continuum or dual continuum (fracture system and matrix blocks). In a dual-continuum model, the temperature and pressure may be different in the matrix and fractures, while the total stress (as opposed to the effective stress) is assumed to be same in both continua. Four types of conservation equations are needed to fully describe such systems, including two mass-balance equations for the two fluid components, one energy-balance equation, and one momentum-conservation equation of rock deformation forces.

The fluid mass-balance equation of a coupled hydraulic and mechanical system can be rigorously derived by combining the fluid mass-conservation equation with the solid mass-conservation equation, considering the relative motion of the fluid to the moving solid, according to Rutqvist et al. (2001 [DIRS 154587]). In such a case, the volumetric strain in the mass-balance equation is coupled to the force-balance equation through Biot's storage and effective stress parameters (Biot 1941 [DIRS 121082]), and the final equations are solved simultaneously in a fully coupled model. In general, a reservoir engineering approach can be used by accounting for rock deformation changing the porosity. However, in the current application, a simpler approach of estimating change in porosity, and hence permeability, from a change in stress is used by adopting an empirical nonlinear relationship. Such an approach implies that the TOUGH2 V1.5 and FLAC3D V2.0 codes can be used in their standard versions, but linked together through numerically calculated porosity, permeability, and effective stress changes. The codes are executed iteratively, with transfer of data through external linking modules. Through various iterative schemes, either explicit or implicit sequentially coupled solutions can be achieved.

The model has been calibrated and partly validated against hydromechanical and thermomechanical data from the niche tests, and the Drift Scale Test. The thermomechanical responses (displacements caused by thermal expansion of rock) in the early time of the drift scale models simulation are within the range of measurements at the drift scale heater test (Bodvarsson 2001 [DIRS 154669], Attachment 9, p. 64). A calibration of the relationship between stress and permeability for the drift scale calibrated hydrogeological properties is described in Section 4.3.7.4.3. A similar calibration of the stress-permeability relation was conducted for this mountain scale model as described in the next section.

3.3.7.4 Application and Results on Mountain-Scale Flow

The model domain is designed by first taking a multiple-layered column extending vertically from the ground surface down to the water table. The vertical layering for the model is chosen to correspond to the vertical contacts at the Nevada State Plane Coordinates 170572.39 m (Easting) and 233194.536 m (Northing) used in *Development of Numerical Grids for UZ Flow and Transport Modeling* (CRWMS M&O 2000 [DIRS 114277], Attachment VI; DTN: LB990701233129.001 [DIRS 106785]). These coordinates represent an interior point near the center of the potential repository location. The layers are extended horizontally to form a two-dimensional section that runs along the northwest direction exactly normal to the

emplacement drifts in the TSPA-SR UZ site-scale model (CRWMS M&O 2000 [DIRS 114277]). The cross-sectional length of the repository along this section is approximately 4.2 km, and the section contains 53 emplacement drifts. The left boundary of the two-dimensional model domain is at the center of the repository, which has a half-symmetric length of 2,106 m (26.5 canisters spaced 81 m apart). This left boundary is closed to heat and fluid flow by symmetry and is allowed zero normal displacement mechanically (i.e., on rollers). The right boundary is set at a distance of 3,000 m from the right edge of the repository. At this boundary, a constant stress is maintained with a gradient according to Table 3.3.7-1, and no heat or fluid flow can cross it. The top boundary is the land surface at constant temperature and free to move mechanically, while the bottom boundary is at the water table, which is at constant temperature and on rollers mechanically.

The input hydraulic and thermal parameters for the layers are based on the mountain-scale calibrated property set presented in *Calibrated Properties Model* (CRWMS M&O 2000 [DIRS 144426], Section 6.1.4). The model input thermal parameters are modified to include effects of lithophysal cavities in the tsw33 and tsw35 hydrogeologic units, as shown in Table 4.3.5-1. Mechanical and thermal-mechanical (TM) parameters for TM rock mass units are extracted from *TBV-332/TBD-325 Resolution Analysis: Geotechnical Rock Properties* (CRWMS M&O 1999 [DIRS 126475], Section 7.2.3). In the present simulation, the below-boiling thermal operation mode is studied (Bodvarsson 2001 [DIRS 154669], Attachment 9, pp. 1 to 78). This is effected by imposing an initial thermal load of 67.7 kW/acre (1.35 kW/m of drift) with a forced ventilation period of 300 years, during which 80 percent of the heat is assumed to be removed. The thermal load is imposed on 26.5 drift elements located 81 m apart along the 2,106-m long repository at level 1080.3 m in the tsw35 hydrogeologic unit (the lower lithophysal unit of the Topopah Spring welded tuff). The half drift is located at the mid-symmetry line on the left side of the model.

THM-related parameter data used and their sources are shown in Table 3.3.7-1. These parameters are the same as those used for the drift scale model in Section 4.3.7, except that the parameters b_{max} and α have been re-calibrated for a higher mountain scale rock mass permeability. In this simulation conservative values of b_{max} and α were assumed corresponding to the strongest permeability increases observed at the niche experiment and to the strongest permeability decreases observed at the Drift Scale Test (Bodvarsson 2001 [DIRS 154669], Attachment 9, pp. 45 to 49). Thus, this model simulation does not cover the entire uncertainty range of hydromechanical properties, but is a conservative one.

Results of this simulation show that temperatures peak at about 800 to 1,600 years after emplacement, depending on locations and input conditions. The temperature distribution at 1,000 years is shown in Figure 3.3.7-1. As expected, temperature contours center around the repository. Figure 3.3.7-2 shows the horizontal stress distribution at 1,000 years. In this figure, a contour line marked by an arrow, separates a region of thermal compression (negative values) near the repository and a region of tension (positive values) near the land surface. The result is caused by the interaction between the horizontal stress imposed on the right boundary at 5,000 m and the mechanically free boundary at the land surface. Vertical stress distribution, which is not shown, has horizontal contours indicating stress variation due to the thickness of overburden.

Corresponding to the calculated stress distributions, Figures 3.3.7-3 and 3.3.7-4 show the changes in vertical and horizontal permeabilities caused by the THM effects. There is a decrease in permeability near the repository by a factor of about four and an increase in permeability in the layers near the land surface. Table 3.3.7-2 shows the changes in permeability for the various hydrostratigraphic layers. They are different for the different layers because the permeability change is a function of the initial permeability of each layer. The percentage change is larger for a layer with lower initial permeability. A calibration study related to this behavior using ESF niche test data is discussed in Section 4.3.7.4.3.

Overall, the permeability changes (Table 3.3.7-2) are moderate, ranging from a factor of 0.28 to 2.75 except for part of the most shallow layer near the land surface, where a factor of 38 was found. This latter value may be highly uncertain due to the vicinity of the free land surface. However, layers near the land surface do not play a critical role in the flow pattern at the mountain scale.

The modeled changes in permeability in the far field are due to elastic deformation and therefore are reversible upon cooling. Inelastic deformation and permanent changes in permeability may occur near the drifts as discussed in Section 4.3.7.5. Permeability changes due to rockfall are discussed in Section 4.3.7.4.

3.3.7.5 Abstraction of Total System Performance Assessment

The work reported in this section is devoted to evaluating process model simulations and uncertainties. Simulation results for this study are not yet used to support any abstraction models for the TSPA. The results obtained so far show changes of permeability resulting from THM processes below one order of magnitude, and are different for different hydrostratigraphic layers.

3.3.7.6 Multiple Lines of Evidence

The impact of THM processes on the performance of a potential high-level radioactive waste repository has been assessed through field studies at a variety of underground sites. At the Nevada Test Site, a series of TM/THM experiments were conducted in the G-tunnel in Rainer Mesa. Results show a direct relationship between thermal input and fracture permeability changes. Thus, increasing temperature on a rock block under triaxial confinement lowered the apparent permeability of a single fracture from 234 to 89 microdarcies (Hardin and Chesnut 1997 [DIRS 100534], pp. 4 to 6). Further, THM effects were also observed in experiments at the Stripa mines in Sweden. Fracture closure and reduction in permeability were confirmed by observation of diminished water inflow to heater and instrument boreholes (Nelson et al. 1981 [DIRS 150092]).

In addition to these experiments, corroborative results on coupled THM effects may be found in the geothermal literature. A survey of geothermal reservoir properties worldwide (Björnsson and Bodvarsson 1990 [DIRS 154606]) showed a correlation between permeability and temperature for various geothermal systems (Figure 3.3.7-5). The values are scattered, but they indicate a trend of decreasing permeability with increasing temperature. The low permeability at temperatures around 300°C and above is more likely caused by geochemical effects. The THM effects may be present at lower temperature. The straight-line fit through the points has a

regression coefficient of 0.5 (Bodvarsson 2001 [DIRS 154669], Attachment 4, p. 36) and shows a half-an-order decrease of permeability with a 100°C rise in temperature.

3.3.7.7 Summary of Uncertainties and Their Treatment

Table 3.3.7-3 provides a summary of the uncertainty issues related to THM effects on mountain-scale flow and their treatment.

3.3.7.8 Summary and Conclusions

A coupled THM continua code, which is a linkage of the TOUGH2 V1.5 and FLAC3D V2.0 codes through carefully designed interface routines, has been applied to the simulation of permeability changes in a region around a potential repository from the ground surface to the water table. Prior to this set of calculations, no fully coupled THM modeling had been done for the conditions at Yucca Mountain (i.e., unsaturated, highly fractured rock with heat input). Therefore, the uncertainty is unbounded. The results of the present study indicate compression near the repository and expansion from the land surface above the repository down to an elevation of 1,290 m. These cause corresponding changes in permeability. Table 3.3.7-2 shows the calculated changes in vertical and horizontal permeability values for the lower-temperature operating mode. The calculation was conducted with hydromechanical properties, conservatively calibrated against the geologic layers near the land surface that do not play a critical role in the flow pattern at the mountain scale. These changes are moderate, probably without significant impact on the TSPA for the potential repository. However, uncertainties remain for the higher-temperature operation mode and for more realistic geometries, as indicated in Table 3.3.7-3. The uncertainties will be further bounded as new heater test data become available and the model is updated.

INTENTIONALLY LEFT BLANK